AMERICAN UNIVERSITY OF BEIRUT

TECTONIC EVOLUTION AND SEISMIC HAZARD ANALYSIS OF THE DAMOUR-BEIT ED DINE FAULT SYSTEM.

by
ABDEL HALIM MOHAMMAD KHEIR
YASSINE HAJJ CHEHADEH

A thesis
submitted in partial fulfillment of the requirements
for the degree of Master of Science
to the Department of Geology
of the Faculty of Arts and Sciences
at the American University of Beirut

Beirut, Lebanon
Januaray, 2015

AMERICAN UNIVERSITY OF BEIRUT

TECTONIC EVOLUTION AND SEISMIC HAZARD ANALYSIS OF THE DAMOUR-BEIT ED DINE FAULT SYSTEM.

by

ABDEL HALIM MOHAMMAD KHEIR

YASSINE HAJJ CHEHADEH

Approved by:

Dr. Ata Elias, Assistant Professor
Geology — Advisor

Dr. Abdel-Fattah Abdel-Rahman, Professor
Geology — Member of Committee

Dr. Ali Haidar, Assistant Professor
Geology — Member of Committee

Date of thesis/dissertation defense: January 29, 2015

AMERICAN UNIVERSITY OF BEIRUT

THESIS, DISSERTATION, PROJECT RELEASE FORM

Student Name: Yassine Hajj Chehadeh Abdel Halim Mohammad Kheir
Last First Middle

◯ Master's Thesis ◯ Master's Project ◯ Doctoral Dissertation

☐ I authorize the American University of Beirut to: (a) reproduce hard or electronic copies of my thesis, dissertation, or project; (b) include such copies in the archives and digital repositories of the University; and (c) make freely available such copies to third parties for research or educational purposes.

☐ I authorize the American University of Beirut, **three years after the date of submitting my thesis, dissertation, or project,** to: (a) reproduce hard or electronic copies of it; (b) include such copies in the archives and digital repositories of the University; and (c) make freely available such copies to third parties for research or educational purposes.

_____

Signature Date

ACKNOWLEDGEMENT

I would like to greatly thank Dr. Ata Elias for his guidance, support and constructive criticism. No words can express how grateful I am for the generous time he spent teaching me. What I learned from him is more than just geology; I learnt a wide range of skills such as objectivity, critical thinking, organization, writing and a whole range of virtues among which I would like to emphasize on patience and passion for research.

I would like to greatly thank Prof. Abdel-Fatah Abdel-Rahman and Dr. Ali Haidar not only for their constructive criticism for this work. Prof. Abdel-Rahman provided continuouslearning, guidance and support ever since I joined the Geology Department here at the American University of Beirut in 2005. Dr. Haidar was generous in providing precious tools, out of his wide knowledge that will help us everywhere we go.

Special thanks are also due to Mr. Maroun Ijreiss, Miss Nisrine Lababidi and Mrs., Huda Nisr Abdel-Sater as they were always there ready to help and assist in many of the tasks we worked on. They can be best described as the unkown soldiers behind every work in our Geology department.

To my father Mohammad: I owe you the biggest gratitude and respect. You were always here for us, providing us with all the support needed through your wise guidance and vision. I love you Baba, you will always be my role model and I am sure you are proud of us.

To my mother Yaldez: the dearest to my heart. You were a containing mother and provided us with all the love and tenderness, while growing up. You also took great care of us and stayed awake during long nights to insure our well-being. I love you Mama, you will always be my angel and I am sure you are proud of us.

To my little brother Ahel: We have shared a wonderful childhood together. I love you bro and I want you to know that I am always there for you.

To a special person and a great influence “P.R.M.T.”. Sometimes good things happen by coincidence. You have contained me and taught me valuable stuff. Being thankful is not enough.

Finally to my dear friends among whom I would like to specially thank, Mr. Wissam Timani with whom I spent very long hours working together each on his dissertation. He witnessed the funny reaction after I got block rotation idea, I also learned a lot about bad driving in Lebanon from him. To thank also Mr. Liwaa Aridi, Mr. Bilal Dirani and Miss Rasha Koudsi dear friends who gave me company several times to the field. This work wouldn’t have been fulfilled without your support.

AN ABSTRACT OF THE THESIS

Abdel Halim Yassine Hajj Chehadeh for Master of Science
Major: Geology

Title: Tectonic Evolution and Seismic Hazard Analysis of the Damour-Beit ed Dine Fault System.

Tectonic deformation accommodated by rotating parallel faults is known as bookshelf faulting. Several examples from around the world show that it is an efficient mechanism in accommodating part of the strain generated from shearing on overlapping parallel transform faults. The Mt. Lebanon Range is dissected by several E-W faults, most likely activated as counter-clockwise (CCW) dextral bookshelf structures during the Cenozoic. Yet their kinematic evolution seems more complex due to the presence of an older, Mesozoic, normal component on many of these structures. Here we show that the 25Km long Damour-Beit ed Dine Fault, the southernmost of the E-W old Mesozoic normal faults in Lebanon, reactivated most-likely as a CCW, dextral bookshelf structure during the Cenozoic which translates into seismic hazard for the surrounding area. We also show that the Southern Central Mt. Lebanon (SCML) is characterized by WSW-ENE shortening responsible for the uplift of this area in the Cenozoic. Using morphotectonics and seismicity analysis we prove that the DBF is an active structure. The drainage pattern in the area readjusted to the active growth of the structures leaving wind gaps. Structural mapping show ~2Km of cumulative dextral displacement associated with the Late Miocene-present CCW bookshelf reactivation of the DBF, induced by the sinistral shear on the Lebanese Restraining Bend. The smaller scale NW-SE faults mapped north of the DBF, have similar Mesozoic-Cenozoic evolution. Their reactivation in the Cenozoic as CW, sinistral bookshelf faults resulted in their 10°-18° CW rotation relative to similar structures south of DBF. We also measured at least 3% shortening in a 22Km distance along an E-W direction in the SCML. We suggest that folding in the SCML is also compatible with overall shortening and thrusting in Lebanon. Also, we compiled instrumental and historical seismicity catalogs of the area, converted to a uniform coda magnitude scale. We assessed the accuracy of earthquakes' location for the instrumental seismicity data of 2006-2010 provided by the local network. The seismic activity during that period shows a net clustering of M_C <3.4 earthquakes along a narrow, planar zone mimicking the DBF, to depths of around 30km, strongly suggesting the crustal extent of the structure. Using deterministic and probabilistic methods, we show that this area is susceptible of $5.0 \leq M_{Wmax} \leq 6.8$ earthquake, though more likely to be on the lower side of the estimation range. We speculate that the frequent mass movements observed in the area are related to rupturing of the DBF in the past. These results suggest that other E-W faults in Lebanon can also have similar crustal extent accommodating ongoing, CCW, dextral bookshelf faulting and represent an important contribution to the seismic hazard of the country.

CONTENT

ILLUSTRATIONS

LIST OF TABLES

ABBREVIATIONS

1. CCW: Counter-clockwise
2. CNRS: Centre National de Recherches Scientifiques.
3. CW: Clockwise
4. DBF: Damour-Beit ed Dine Fault.
5. DEM: Digital Elevation Model.
6. DSTF: Dead Sea Transform Fault.
7. GRAL: Geophysical Research Array of Lebanon.
8. LFS: Levant Fault System.
9. LRB: Lebanese Restraining Bend.
10. MLT: Mount Lebanon Thrust.
11. NASA: The National Aeronoautics and Space Administration.
12. NCGR: National Center of Geophysical Research.
13. RMS: Root Mean Square.
14. SCML: Southern Central Mount Lebanon.
15. SRTM: Shuttle Radar Topography Mission.

To my parents and teachers

CHAPTER 1

INTRODUCTION

This research deals with the structural setting of the Damour-Beit ed Dine fault (DBF), the southernmost E-W structure mapped in the Mt. Lebanon area.

Several research studies have addressed these E-W structures (e.g. Hancock & Atiya, 1979; Ron, 1987; Gedeon, 1999; Homberg et *al.*, 2010…). Thus many ideas are suggested regarding their inception age, the main deformation mechanisms through which they accommodate the strain arising from the major tectonic phases in the area and their recent activity. These ideas are associated with serious limitations like:

- The large scale of the conducted studies, which may have lead to disregard some important details.
- The need to review these ideas in light of the recent geologic understanding/discoveries in the area.
- The lack of significant morphotectonic indications to better depict recent tectonic activity.

In order to better understand the structural setting of DBF, and to assess the associated seismic hazard, we revisited the mophotectonics and the seismicity of the DBF and surrounding area.

In this chapter we review the morphotectonics and historical seismicity of the regional plate boundary, the Levant Fault System (LFS). We focus on its Lebanese

segments and the associated secondary structures. We also review the historical seismicity of the LFS and set the framework for this study.

1.1. Morphotectonics of the Levant Fault System Region

Lebanon is located over the sheared NW margin of Arabia. The imposing mountainous relief of this country is very different from its surroundings that are characterized by subdued relief and lower topography. The main structuring element of this margin is an active plate boundary materialized by the Levant Fault System (LFS), also known as the Dead Sea Transform Fault (DSTF). This active fault system separates the Arabian plate from the Levantine-Sinai plate (Quennell, 1958; Freund, 1965). It extends from the Gulf of Aqaba in the south to the Taurus mountain ranges in the north (Fig. 1.1), covering a distance of ~1000 Km (Quennell, 1958).

The LFS is a sinistral strike-slip plate boundary along which left-lateral shear is believed to have initiated (18-15 Ma) in Middle Miocene (Eyal et *al.*, 1981) in parallel to the (30-25 Ma) initiation of rifting in the Red Sea in Oligocene (Courtillot et *al.*, 1987).

The trace of this fault system is in fact a series of strike-slip fault segments separated by step-overs, either transtensive or transpressive structures depending on the direction of their step relative to the sinistral strike slip shear (Daëron, 2005).

The morphotectonics of this margin can be subdivided into three distinct regions from south to north where Lebanon occupies the central part (Fig. 1.1). The classic south to north description of these segments will be adopted.

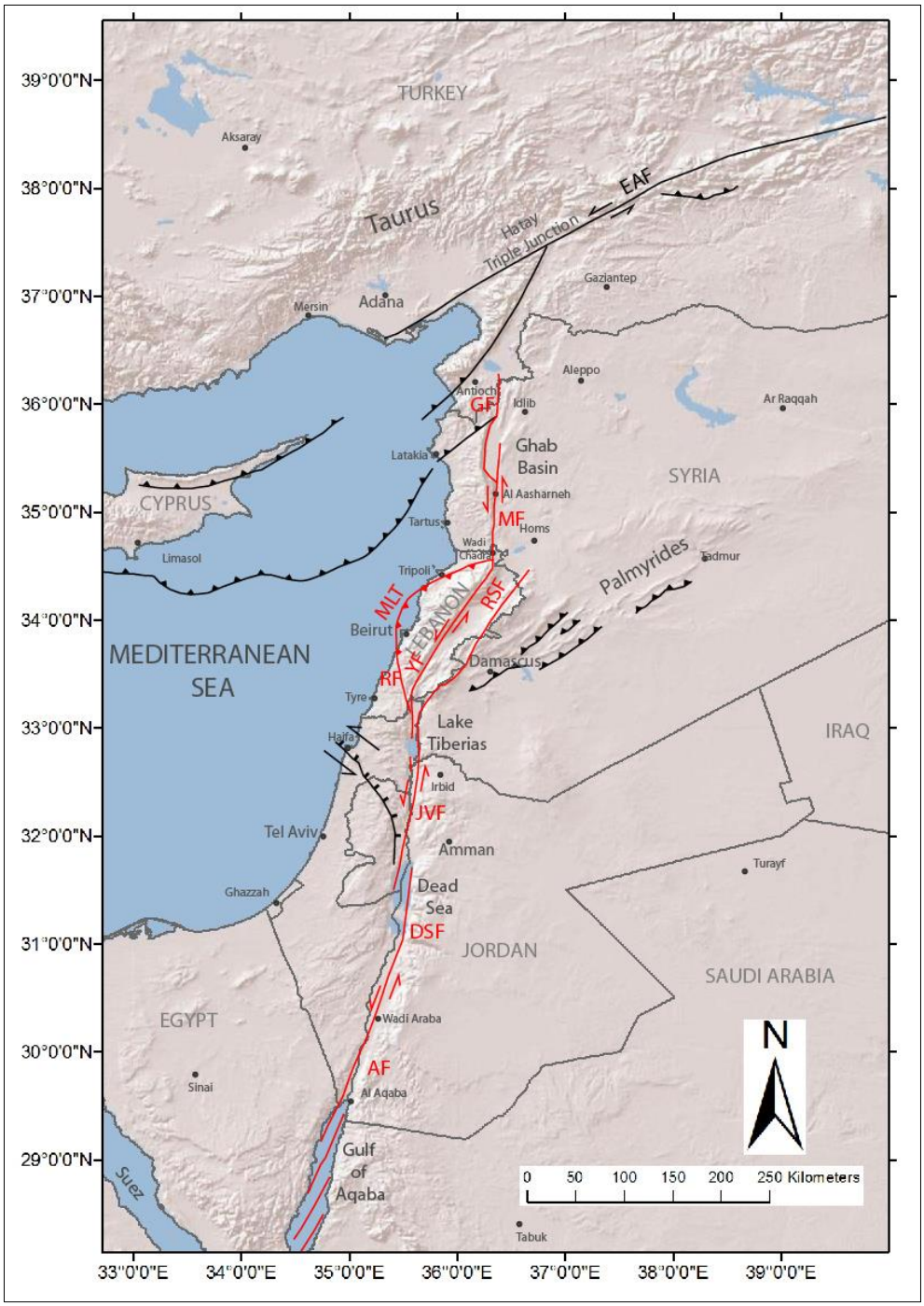

Figure 1.1: Map of the major segments of the LFS
(AF: Araba Fault, DSF: Dead Sea Fault, JVF: Jordan Valley Fault, RF: Roum Fault, MLT: Mount Lebanon Thrust, YF: Yammouneh Fault, RSF: Rachaya-Serghaya Fault, MF: Missyaf Fault and GF: Ghab Fault. Other Faults are in Black.)
(Modified from Girdler (1990); Daëron (2005); Elias et *al.* (2007); Le Beon et *al.* (2008); and Mahmoud et *al.* (2012)).

1.1.1. The LFS South of Lebanon (Southern Levant Area)

South of Lebanon, different segments of the LFS (Fig. 1.1) are mapped and identified in details (Girdler, 1990; Le Beon et *al.*, 2008) in the Palestine-Jordan area. These are:

1. Northwards, from the Gulf of Aqaba in the South extends the Araba fault reaching Wadi Araba.
2. The Dead Sea fault is a left-stepping segment of the Araba fault. It extends from Wadi Araba to slightly north of the Dead Sea, striking ~N-S. This releasing step creates in the Dead Sea basin, a typical pull-apart structure (Garfunkel, 1981; Girdler, 1990).
3. The Jordan Valley Segment extends northward, from the Dead Sea to Lake Tiberias, striking N-S.

This fault system is about 450 Km in length and comprises a series of left-stepping faults, which show minor overlaps in the step-over areas (Garfunkel, 1981; Daëron, 2005). Pull-apart basins, illustrated as rhomb-shaped grabens (Fig. 1.2) are formed in the areas of overlap, as a result of the kinematics of this active fault system (Garfunkel, 1981; Girdler, 1990).

Kinematically, the LFS system is a sinistral strike-slip plate boundary almost striking N-S to the south of Lebanon. A total of 105-107 Km of left-lateral displacement is constrained in this area (Freund, 1965).

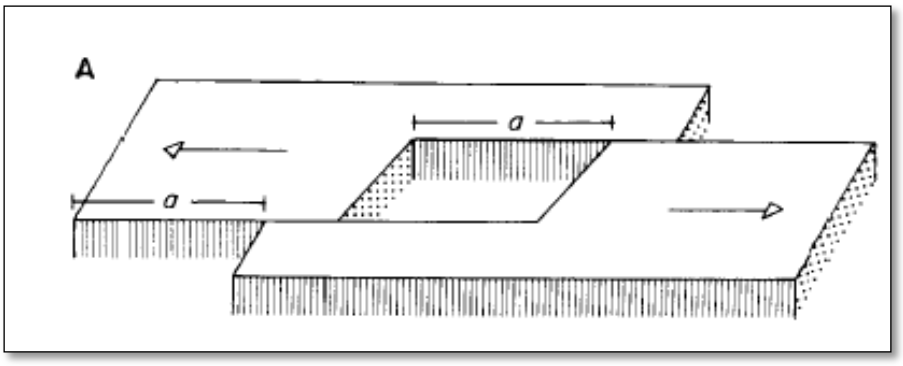

Figure 1.2: The concept of the formation of pull-apart basins in relation with sinistral strike-slip motion (Garfunkel, 1981).

LFS activity to the south of Lebanon started in Late Oligocene-Early Miocene and is still active. The displacement along this fault took place in several phases among which 30- 45 Km are attributed to Plio-Pleistocene times, the time of generation of the pull-apart basins (Quennell, 1958; Quennell, 1959; Freund, 1965; Garfunkel, 1981; Joffe & Garfunkel, 1987; Girdler, 1990).

Slip rates on the southern LFS are estimated by Freund et *al.* (1970) to be 0.35-0.6cm/a average for the past 12-7Ma. Garfunkel (1981) reports a 0.7-1cm/yr slip rate on the southern LFS for Plio-Pleistocene till present times (5-2 Ma). Westaway (1994) estimates the overall slipping rate of the entire LFS system to be ~ 0.6-0.8cm/yr for the past ~ 5Ma. These values are based on the dating of offset geologic features. A recent geodetic investigation of slip rates on the southern LFS conducted by Le Beon et *al.* (2008) shows a slip rate of 0.49 ± 0.14cm/yr (measured using GPS) for the modern activity of the fault system.

1.1.2. The LFS in Lebanon

Figure 1.3: Structural Map of Lebanon showing the LFS segments in Lebanon and the majority of E-W striking secondary faults (after Elias et *al.*, 2007).

In Lebanon, the LFS splays into four main branches (Figs. 1.1 and 1.3); the Roum fault, the Mount Lebanon Thrust (MLT), the Yammouneh fault and the Rachaya-Serghaya fault (Dubertret, 1955).

The Roum fault extends from the western tip of the Hula basin in the south of Lebanon to the Bisri River in the north for about 35Km (Figs. 1.1 and 1.3), where its trace is subdued in the topography and replaced by the NE-SW striking Jabal el Mazraa flexure, also known as the Chouf Monocline (Heybroek, 1942; Nemer & Meghraoui, 2006). Recent studies show the connection between the N-S striking Roum fault and the offshore MLT (Elias et *al.*, 2007; Carton et *al.*, 2009). The Roum fault is a sinistral strike-slip structure, which accommodated 5-10Km of displacement (Walley, 2000) since its initiation in Mid-Miocene time.

The Mt. Lebanon Thrust is a ~90Km long thrust belt that extends for about 30Km offshore Lebanon (Figs. 1.1 and 1.3). It connects directly with a left-stepping segment of the Roum fault (the Saida fault) near al Damour where it bends to a ~NE-SW direction parallel to the Yammouneh. In the north the MLT merges with the (~E-W) oblique Aabde thrust ramp (Elias et *al.*, 2007; Carton et *al.*, 2009). The MLT consists of east dipping thrust faults with an average Slip rate of ~0.1-0.2cm/yr as estimated by Elias et *al.* (2007). This complex fault system accommodates shortening from the active transpression along the LRB. Thrusting is dominant on NE-SW directed faults (Akkar, Tripoli, Qartaba, MLT faults for example) although a minor strike-slip component is more pronounced on other faults (Roum, Saida, Abdeh) with different strike directions (Elias et *al.*, 2007).

The Yammouneh fault is the direct connection between the LFS segments in south and north of Lebanon (Daëron, 2004). This fault striking ~N25°E extends from the Hula basin in the south to Wadi Chadra in the north, where it changes its direction to ~N-S extending in Syrian territories (Figs. 1.1 and 1.3). Its overall length is 160Km and it exhibits left-lateral strike slip kinematics, where offsets up to 48Km are constrained along

this structure in northern Lebanon (Walley, 2000). The Yammouneh fault is the most active strike-slip structure in Lebanon with slip rates of 0.51 ± 0.1cm/yr for the Late Pleistocene-Holocene times as estimated by Daëron (2004) using cosmogenic ^{36}Cl dating of offset features in alluvial fans. Another slip rate of 0.8cm/yr is estimated by Westaway (1994). Gomez et *al.* (2007) estimate a slip of 0.4-0.5cm/yr from a GPS survey conducted over a 5 year period.

Finally, the Rachaya-Serghaya faults are a system of ~N25°E striking right-stepping en-echelon faults. The Rachaya fault extends from the Hula basin in the south to Rachaya in the north for a distance of around 40Km (Figs. 1.1 and 1.3) while the Serghaya fault runs to the east of the Rachaya fault from the east of the latitude of Rachaya in the south to the east of the latitude of Baalbeck in the North for around 60Km (Dubertret, 1955). These faults are parallel to Yammouneh and show similar sinistral strike-slip motion. Walley (2000) estimated a 20Km offset on the Serghaya fault.

1.1.3. The LFS North of Lebanon (Northern Levant Area)

To the north of Lebanon, the LFS re-adjusts itself in the ~N-S striking left-stepping geometry it has to the south of the latitude of Lebanon (Fig. 1.1). In fact two segments are distinguished: the Missyaf fault and the Ghab fault.

The Missyaf fault is the northward continuation of the Yammouneh fault. It extends over a distance of ~74Km between Wadi Chadra in the south and north of al Aasharneh in the north, bounding the eastern side of Ghab, where it steps to the left (Fig. 1.1).

West of the Ghab basin, extends the Ghab fault northward (Fig. 1.1), in a segmented geometry, to meet with the East Anatolian fault (EAF) and the Taurus thrust belt at the Hatay triple junction (Chorowicz et *al.*, 2005).

The Ghab basin is interpreted as a pull-apart resulting of left-stepping on the sinistral strike-slip LFS in Syria. Results from Brew et *al.* (2001), imply an Early Pliocene age of the Ghab basin, suggesting a relatively young age of the LFS in Syria.

In addition, Meghraoui et *al.* (2003) estimate the slip rate on the Missyaf fault at 0.69 ± 0.1cm/yr for the last 2000 years, while Chorowicz et *al.* (2005) estimate a rate of 0.33cm/yr left-lateral motion using measured offsets in volcanic features (shield volcano) younger than 6Ma.

1.2. Morphotectonics of Mt. Lebanon

The clockwise change in strike from ~N-S in the south of Lebanon, to ~ N 25°E in Lebanon, resulted in transpression along the Lebanese segment of the LFS. These transpressive stresses are expressed by two NNE-SSW oriented mountain chains (the Mt. Lebanon to the west and the Anti-Lebanon to the east) separated by the Bekaa depression (Beydoun, 1981). The following discussion deals with the morphotectonics of Mt. Lebanon.

1.2.1. General Morphology of Mt. Lebanon

The Mt. Lebanon chain is a NNE-SSW elongated mountain range that extends for ~160Km from Marjayoun -where the Litani River changes its direction from NE-SW to ~ E-W- in the south to Wadi Chadra in the north, running parallel to the Lebanese coast (Fig.

1.4). The Eastern boundary of this mountain chain is the Yammouneh Fault and the Bekaa Valley (Fig. 1.3). On the other hand, its western boundary is more complex. From Nahr el Damour northward, the main bounding element is the Eastern Mediterranean margin hosting narrow alluvial covered coastal plains interrupted by rocky headlands (Fig. 1.4). To the south of Nahr el Damour the western bounding element of Mt. Lebanon is materialized by a flat lying terrain, the Tyr-Nabatiye plateau (Fig. 1.4).

The backbone of Mt. Lebanon extends at a great proximity to the Yammouneh fault mimicking the direction of this structure. It culminates at Qornet es Sawda (3084m.a.s.l), Jabal Sannine (2630m.a.s.l) that consists of dolines rich Cenomanian rocks (Sannine Formation) and at Jabal el Barouk (1980m.a.s.l) covered by highly karstified and deformed Jurassic carbonates (Bikfaya formation), thus showing a southward decrease in topographic relief. The crest of Mt. Lebanon hence acts as a water divide, shedding rain water toward the Mediterranean Sea or toward the Bekaa, via seasonal streams that do not traverse this barrier (Fig. 1.4).

The eastern flank of Mt. Lebanon -located between the Backbone of this mountain and the Bekaa Valley- is a steep and narrow surface that shows rapid decrease in relief from 2500m.a.s.l to ~1000m.a.s.l over a concise geographic area.

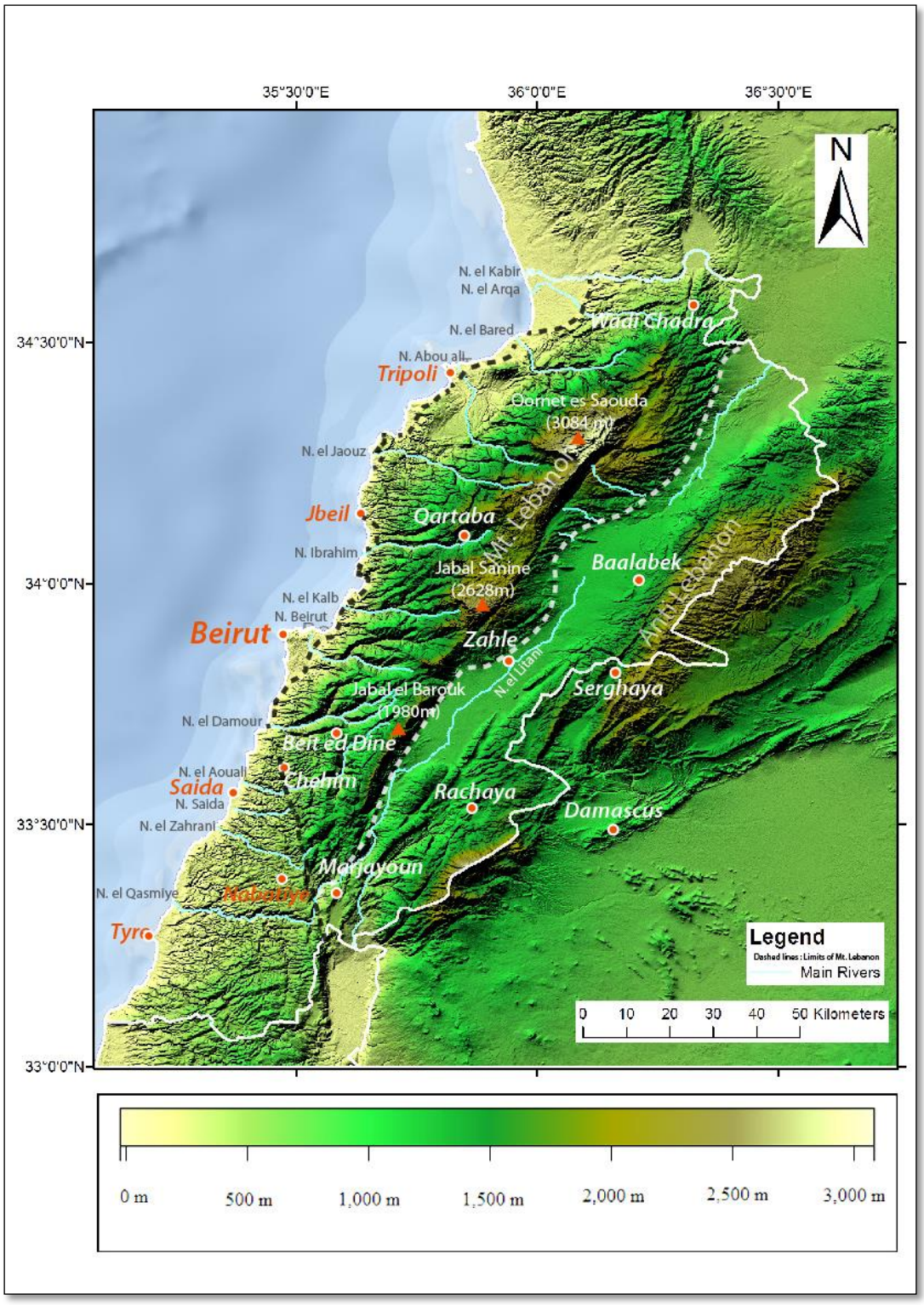

Figure 1.4: Topographic Map of Lebanon plotted based on the NASA SRTM elevation files and showing the main geomorphologic features of the country. The dashed white and black lines are the western and eastern limits of Mt. Lebanon.

The western flank of Mt. Lebanon -located between the backbone of Mt. Lebanon and the coastal area- emerges from the Eastern Mediterranean through a zone consisting of flat lying abandoned marine terraces that descend toward the coast in a step-like geometry (Sanlaville, 1977), connecting the western tip of Mt. Lebanon with the Lebanese coastal zone. To the east of this domain lies a higher landscape (~1500m.a.s.l) consisting of gently sloping terrains with sometimes accentuation of inclination, thus forming a larger step-like plateau geometry.

1.2.2. General Tectonics of Mt. Lebanon

The Mt. Lebanon is a coastal range consists of a mega-anticline like structure whose western forelimb is a NNE-SSW steeply dipping monocline, the Mt. Lebanon Flexure that disappears at the latitude of Chehim. The eastern back limb of this mega-anticline dips steeply toward the Bekaa valley and is cut by the Yammouneh fault. The area in between is relatively tabular consisting of very broad wavelength, low amplitude folds hosting intermittently smaller scale tight folds; the major strike orientation for these structures is NNE-SSW, parallel to the Yammouneh Fault.

Further complexity is added to the large structure of Mt. Lebanon by a set ~E-W striking faults, extending between Deir el Qamar in the south and Chekka in the north (Fig. 1.3). These dissect the central and northern parts of this mountain range into a set E-W elongated blocks bound by these secondary structures (Freund, 1965; Freund & Tarling, 1979; Hancock & Atiya, 1979; Ron, 1987...).

The geomorphologic and structural features of Mt. Lebanon are in genetic relation with the tectonics of the Levant Fault System, which is associated with the left-lateral slip

of the Levantine plate past the Arabian plate. In Lebanon this plate motion is portrayed by slip-partitioning on the LRB (Elias et *al.*, 2007). The Yammouneh fault is accommodating the biggest sinistral strike-slip component of the plate motion (Daëron et *al.*, 2004; Daëron, 2005; Daëron et *al.*, 2007) while compression responsible for the uplift of Mt. Lebanon is taken by thrusting on the east dipping Mt. Lebanon Thrust system (Elias et *al.*, 2007). A part of the missing 105 Km left lateral offset witnessed to the south of Lebanon is thus taken by compression and uplift of Mt. Lebanon (Elias et. *al.*, 2007) and probably Anti-Lebanon, which is not studied in details yet in Lebanese territories.

The sinistral strike-slip kinematics of the Yammouneh fault induced a synchronous dextral strike slip motion on the smaller scale ~E-W faults, accommodated by a counter-clockwise rotation of the E-W elongated blocks (Freund & Tarling, 1979; Ron, 1987). This Cenozoic block rotation kinematics has probably overprinted the initial normal kinematics of the E-W faults, which are believed to originally date back to a Mesozoic extensional phase, the inception time of these structures (Walley, 1988; Homberg et *al.*, 2010).

1.3. Historical Seismicity of the Levant Region

Tectonic activity along the LFS since Middle Miocene resulted in many earthquakes of varying magnitudes. Those that struck the region during the past 3000 years are recorded by historians in the time of absence of instrumental seismicity.

The occurrence of $M > 6$ tremors was quite frequent during this time span. The sources of these major earthquakes are believed to be different branches of the LFS, which we described in section 1.1.

Such large earthquakes are good indicators of the activity of this plate boundary. For this reason few of these events will be briefly discussed, adopting the same south to north order as in section 1.1, keeping in mind that many other large earthquakes took place during this period.

1.3.1. The Southern LFS Historical Seismicity

The Southern LFS in all its branches generated large earthquakes during mankind history. Few examples of the most noticeable events that took place in this Holly Land region are:

- In year 31 B.C a large earthquake with a $M_L \sim 7$ destroyed Jerusalem and surrounding cities (Daëron, 2005). This event is believed to be located on the Jericho Fault also known as the (JVF) Jordan Valley Fault (Reches & Hoexter, 1981).
- In year 749 A.D an $M_S > 7$ earthquake (Marco et *al.*, 2003) resulted in the destruction of Jerusalem and landsliding in Mount Tabor in the Gallile area (Sbeinati et *al.*, 2005). Uncertainty lies on the exact year of occurrence of this event which is believed to have occurred on January 18, somewhere between 746 A.D and 749 A.D (Ambraseys, 2009). Reches & Hoexter (1981) and Marco et *al.* (2003) locate this event on the Jordan Valley fault.
- In 1068 A.D a $M_L = 7$ earthquake (Ben-Menahem, 1991) struck Palestine, destroying Elat and Ramla and damaging Jerusalem. This earthquake, which was

located on the Araba fault, was accompanied by a tsunami that hit the Southern Levant coast (Daëron, 2005).

- On July 11, 1927 the first large earthquake to be recorded by seismic instruments struck the Holy Land area with a local magnitude M_L = 6.3 (Ben-Menahem, 1991). This tremor lead to destructions in several cities such as Jerusalem, Nablus, and Amman… and was accompanied by a 1m high tsunami wave in the Dead Sea. Its epicenter is believed to be located on a fault located in the Dead Sea area (Plassard & Kogoj, 1981; Ambraseys, 2001; Avni et *al.*, 2002; and Shapira et *al.*, 2000-2007).
- On November 22, 1995, an M_W = 7.2 (Shapira et *al.*, 2000-2007) earthquake struck Palestine and Israel. The epicenter of this earthquake was located on the Araba fault near the Gulf of Aqaba (Ambraseys, 2001; Shapira et *al.*, 2000-2007).

1.3.2. The Lebanese Restraining Bend Historical Seismicity

Large earthquakes are also abundant throughout the history of Lebanon. Among the many events that struck this country only a few will be mentioned as examples. These are:

- On July 9, 551 A.D. struck Lebanon causing great damage to Beirut, Jbeil, Tripoli, and Saida… Elias et *al.* (2007) reported an M_W = 7.4 - 7.5 (Elias et *al.*, 2007) for this tremor.This event burnt Beirut to ground, and generated a Tsunami wave along the coastal area and landsliding in Wejj el Hajjar near Chekka and Batroun (Plassard & Kogoj, 1981; Darawcheh et *al.*, 2000; Sbeitani et *al.*, 2005;

Amiran et *al.*, 1994…). The Epicenter of this earthquake is located on the offshore Mount Lebanon Thrust (Fig. 1.3) where fault rupture created escarpments in the bathymetry (Elias et *al.*, 2007).

- In the early morning of May 20, 1202 A.D. an M_S = 7.5 earthquake hit Lebanon (Ambraseys & Melville, 1988). This tremor lead to catastrophic destruction in several cities of the region (Beirut, Tripoli, Safed, Nablus…) and resulted in many casualties. Some reports exist on tsunami waves that trailed this shaking, which hit the Levant coast especially in Cyprus; however those reports may be associated to another event. Shaking during this event triggered landsliding in several places. Reports also exist on a series of aftershocks that followed this main shock (Plassard & Kogoj, 1981; Ambraseys & Melville, 1988; Sbeinati et *al.*, 2005; Amiran et *al.*, 1994). The epicenter of this event is located on the Yammouneh fault on which evidence of co-seismic slipping is constrained (Daëron et *al.*, 2005).
- The year 1759 A.D. was seismically active. Two events hit the area in the same year. The first took place on October 30; it had an M_S = 6.6 (Ambraseys & Barazangi, 1989). The epicenter of this event is located on the Rachaya fault. Subsequent important damage and destruction are reported in Safed and Qneitra (Plassard & Kogoj, 1981; Ambraseys & Barazangi, 1989; Daëron et *al.*, 2005; Nemer et *al.*, 2008). Another main shock following this one took place on November 25 of the same year with an M_S= 7.4 (Ambraseys & Barazangi, 1989), destroying and killing people in the Chouf area, Baalbeck where three of the nine

pillars of the temple fell and in north Syria. The epicenter of this earthquake is believed to be located on the Serghaya fault (Plassard & Kogoj, 1981; Ambraseys & Barazangi, 1989; Sbeitani et *al.*, 2005; Daëron et *al.*, 2005; Nemer et *al.*, 2008).

- On January 1, 1837 an $M_S > 7$ earthquake hit the region (Ambraseys, 1997). The epicenter of this event is most probably located on the Roum fault (Daëron, 2005). This tremor resulted in destruction in several cities; however those located in South Lebanon and its surroundings were the most affected (Chehim, Saida, Marjayoun, Safed and Tiberias…). Furthermore, a seismic wave in Lake Tiberias accompanied this quake (Plassard & Kogoj, 1981; Ambraseys, 1997; Sbeinati et *al.*, 2005).

1.3.3. The Northern LFS Historical Seismicity

The neotectonic/seismic activity of the LFS is also imprinted in the history of Syria, where an important number of large historical earthquakes destroyed many of its main cities and resulted in an immense number of casualties. As examples, we will mention few of these events that happened within the Syrian territories. These are:

- In year 65 B.C a large earthquake with $M > 7$ struck the region resulting in intense destruction in Antioch and thousands of casualties. The epicenter of this earthquake is believed to be located somewhere on the northern segment of the LFS (Plassard & Kogoj, 1981; Sbeinati et *al.*, 2005; Daëron, 2005).
- On December 13, 115 A.D. a great part of Antioch was destroyed by a large earthquake that was accompanied by a tsunami on the Lebanese coast. This event

is believed to have a M > 7 and an epicenter located on the northern segment of the LFS. (Plassard & Kogoj, 1981; Sbeinati et *al.*, 2005; Daëron, 2005).

- On June 29, 1170 an $M_W \sim 7.7$ (Guidoboni et *al.*, 2004) earthquake located on the Missyaf fault, hit Syria and the surrounding region. Important destruction in Aleppo, Damascus and Tripoli arose from this event, which was also felt in Egypt. Reports on several aftershocks that followed the main shock are also found in the literature (Plassard & Kogoj, 1981; Guidoboni et *al.*, 2004; Sbeinati et *al.*, 2005).

1.4. Summary and Methodology

1.4.1 Summary

The LFS is a complex fault system extending for around 1000 Km from the Gulf of Aqaba in the south to the Hatay triple junction in the north, acting as the plate boundary between the Arabian and Levantine plates.

This sinistral strike-slip faults system instigated in Miocene time with the inception of the Red Sea rift. Ever since, the LFS has been the major structural control for the sheared Eastern Mediterranean margin.

Lebanon is located on a right-stepping restraining bend segment of this transform boundary. This dictated slip partitioning of the pure left lateral shear of the LFS to the south and the north of Lebanon, along several splaying faults in this country. The main players are the Yammouneh fault undertaking the major strike-slip component, the Rachaya-Serghaya fault and the Roum fault undertaking the remaining strike-slip component (Nemer

et *al.*, 2006). The offshore Mt. Lebanon Thrust (MLT) is accommodating the major compressive component that produces the uplift of Mt. Lebanon (Elias et *al.*, 2007).

To the north and the south of Lebanon left-stepping releasing bends (Garfunkel, 1981; Girdler, 1990; Brew et *al.*, 2001) resulted in the formation of pull-apart basins (Dead Sea, Lake Tiberias and Ghab Basin…).

The neotectonic activity of this fault system is imprinted in ~3000 years history through several $M_W > 7$ destructive earthquakes located along the various segments of the LFS. The latest event took place in 1995 in the Gulf Aqaba area.

This information summarizes the main guidelines for the regional neotectonism and seismic hazard of the eastern Mediterranean, and represents the general framework for the understanding of smaller scale deformation in smaller zones within this region, particularly the southern central Mt. Lebanon (SCML) our study area.

1.4.2 Methodology

This study integrates field investigation and aerial photography/satellite imagery interpretation of the southern central Mt. Lebanon (SCML), from a morphotectonics and structural perspective to understand better the structural evolution and activity of the Damour-Beit ed Dine fault system, in the context of the tectonic evolution of Lebanon and the Levant Fault System.

Geologic observation acquired and old geologic observations made by previous geologists and authors are reviewed and re-interpreted in framework of the modern understanding of Lebanon's tectonic setting.

Fault offsets are constrained using three marker cliffs -that will be depicted in chapter 2- of different ages to see time variation in fault activity. Additionally thickness estimates and calculations of all formations' exposures are estimated in order to understand the age and evolution of study area faults.

This geologic data is integrated in cross sections that illustrate the structures of the study area and in a geologic model for the tectonic evolution of the southern central Mt. Lebanon (SCML) area and Damour-Beit ed Dine fault system.

Instrumental and historical seismicity data is also implemented in order to better understand the active tectonic traits of the Damour-Beit ed Dine Fault (DBF) and the SCML, and the potential seismic hazard arising from this activity.

CHAPTER 2

REVIEW OF THE STRATIGRAPHY, GEOMORPHOLOGY AND STRUCTURAL EVOLUTION OF THE SOUTHERN CENTRAL MT. LEBANON.

In this chapter we define the southern central Mt. Lebanon (SCML) geographically. We also review the available literature for its stratigraphy, and geological structure and evolution.

2.1. Location of the Study Area

The SCML is located on the Western flank of the Mt. Lebanon range between longitudes E035˚20'00'' and E035˚43'00'' and latitudes N33˚50'00" and N33˚35'00" (Figs. 2.1-2.2).

It is a mountainous region that emerges eastward from a coastal zone oriented NNE-SSW, extending between ~Beirut and Saida (Fig. 2.2). To the east, however, it is bound by the backbone of the Barouk Mountain, which extends between Ain-Zhalta and Niha (Fig. 2.2). Subsequently, the area covered by this study is approximately A = 567Km^2, as calculated with Geographic Information System (GIS) tool.

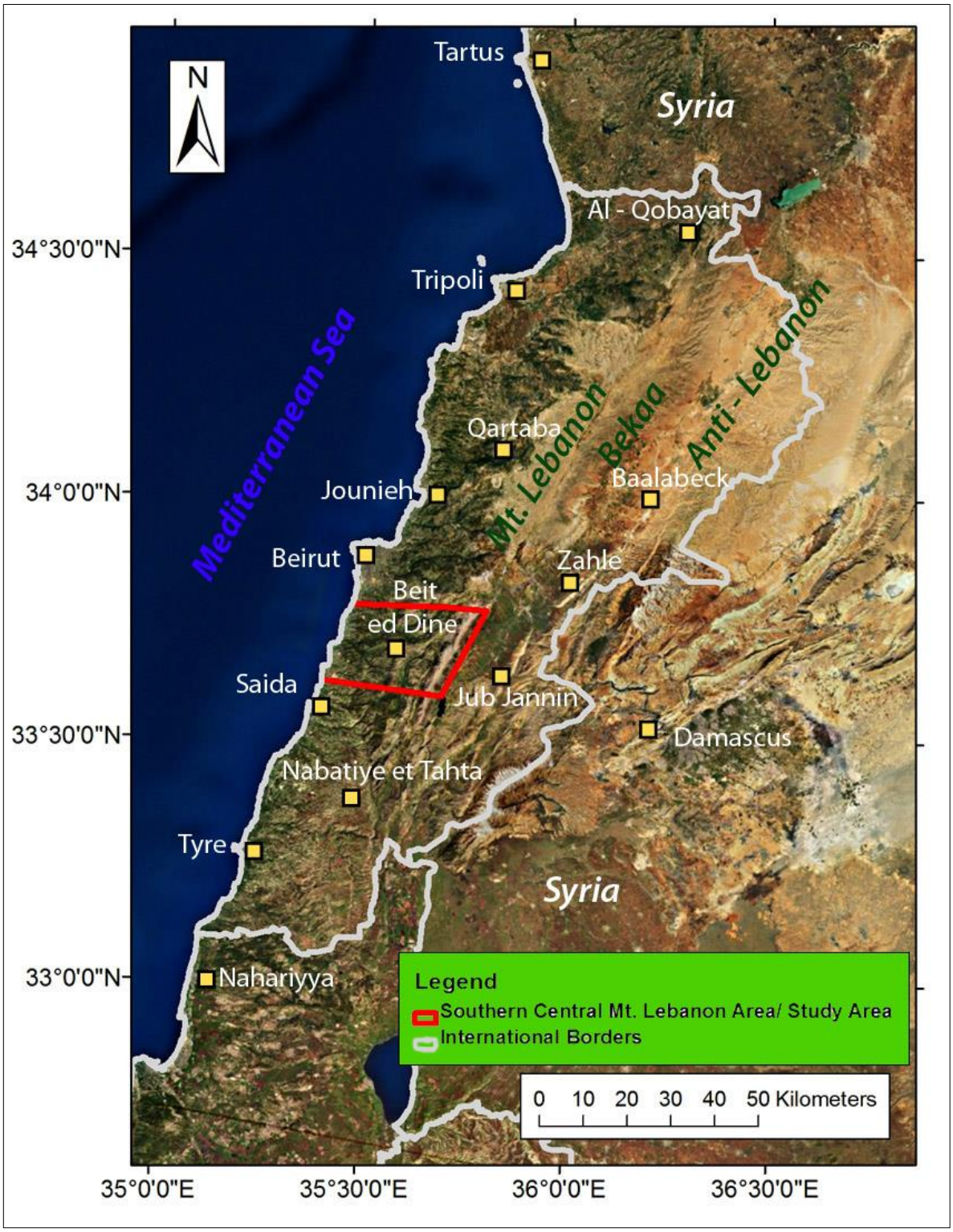

Figure 2.1: Satellite Image of Lebanon showing the location of the Study Area.

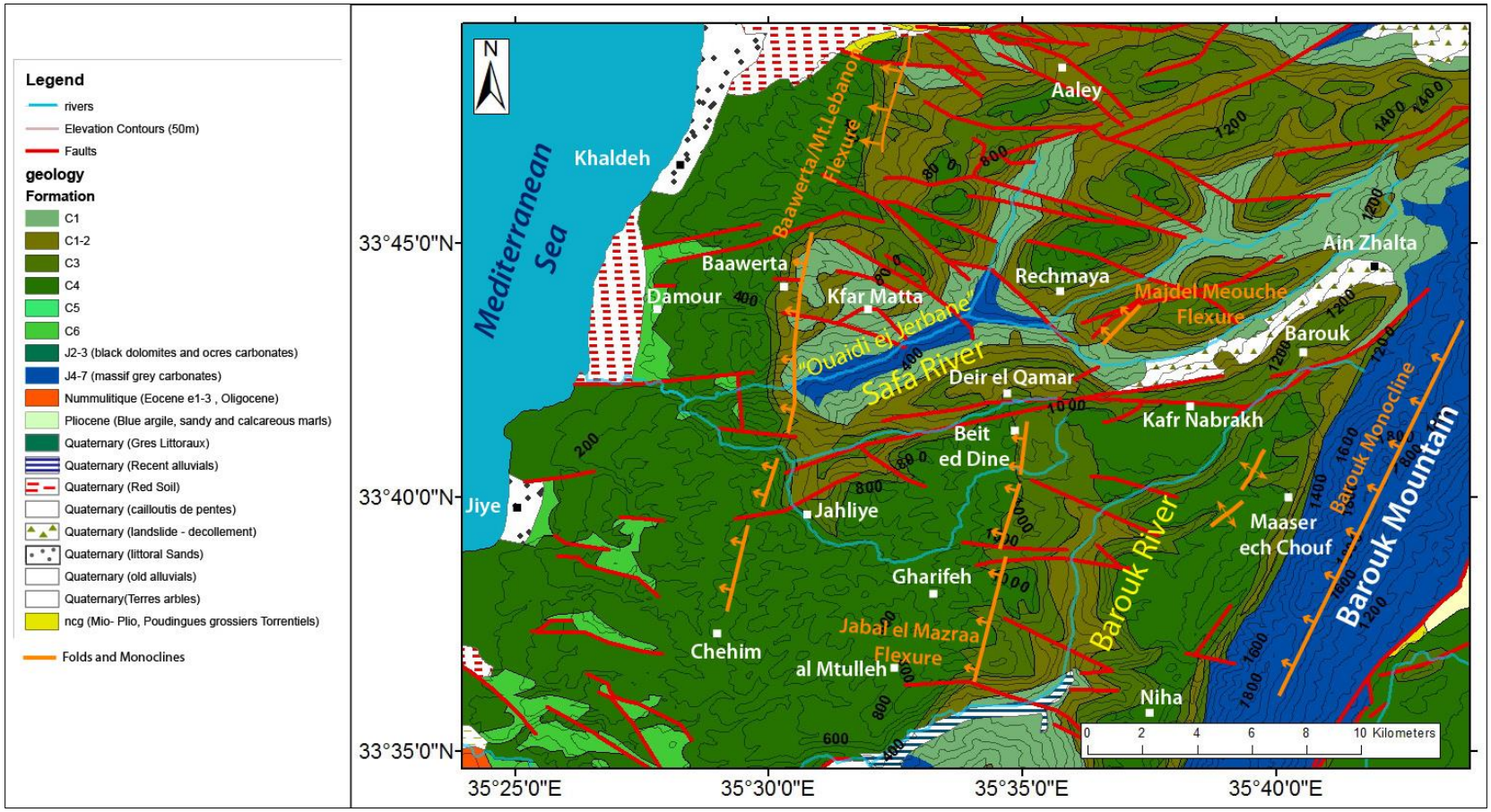

Figure 2.2: Geologic Map of the Study Area. Modified from Dubertret (1955).

2.2. Stratigraphy of the Southern Central Mt. Lebanon

The Upper Jurassic-Lower Cretaceous formations are the dominant outcropping rocks in the SCML, like in most of central Mt. Lebanon. They exhibit a various range of marine facies that reflect their Mesozoic sedimentary environment. Also some minor volcanic members are present among these formations. In contrast, the Cenozoic is almost totally absent from the area - no Paleogene or Neogene deposits can be found here unlike elsewhere in Lebanon (Fig. 2.2). The only Neogene occurrence is represented by Quaternary terrestrial deposits, distributed as patches over the SCML geologic map (Fig. 2.2).

In this section we review the exposed formations seen in the SCML, emphasizing on their lithology, ages, geographic exposures, thicknesses and other characteristics.

2.2.1. The Jurassic Formations

Two Jurassic formations outcrop within the study area: The Bikfaya and the Salima Formations.

2.2.1.1. The Bikfaya Formation (J6)

The J6 (Dubertret, 1945) or Bikfaya formation (Walley, 1997) consists of massive micritic limestone, grey in colour. It deposited during Kimbridgian-Middle Tithonian time - around 155-150Ma- in a mid-shelf to near shore environment (Walley, 1997).
This formation is mapped in two localities within the SCML:

1. It entirely covers the Barouk Mountain, located in the eastern part of the SCML (Fig. 2.2).

2. It is also observed, along the channel bed of Ouadi ej Jerbane (Fig. 2.2), where its cliffy nature forms a corniche that channelizes the Safa River (Fig. 2.3). This cliff is called in literature “Falaise de Djisr el Qadi” (Heybroek, 1942).

Figure 2.3: The Jurassic sequence of the study area as seen on the north bank of the Safa River. In this locality the J6 is cliff forming. Heybroek (1942) called this Jurassic cliff the “Jisr el Qadi Cliff”. The dark blue dashed line represents the upper boundary of the Jisr el Qadi Cliff which forms a part of the J6 formation; the light blue dashed lines represent the uncertain upper (top) and lower boundaries (bottom) of the J7 formation.

2.2.1.2. The Salima Formation (J7)

The J7 (Dubertret, 1945) or Salima formation (Walley, 1997) is composed of brown to yellow marly and oolithic limestone rich in iron. It deposited during late

Tithonian time -around 150-145Ma- in a high energy shallow marine environment (Walley, 1997).

The exposure of the Salima formation within the study area is confined to the banks of Ouadi ej Jerbane (Figs. 2.2 and 2.3), where it reaches a thickness of 50m (Dubertret, 1945).

2.2.2. The Cretaceous Formations

Several formations, lower to middle Creataceous in age are distinguished within the SCML. From oldest to youngest these are: Chouf, Abeih, Mdeirej, Hammana, Sannine and Chekka formations.

2.2.2.1. Chouf Formation (C1)

The C1 (Dubertret, 1945) also known as the Chouf Formation (Walley, 1997) consists of beige to white coloured sandstone sometimes rich in Iron oxide (Figs. 2.4 and 2.5). It is composed of fine to coarse sand grains intercalated with fine clay particles. Its early sedimentary units locally host a volcanic member consisting of basalts and volcanic tuff (Walley, 1997), which is clearly observed in the SCML.

The Chouf sandstone deposited in Early Cretaceous time (Barremian = 140-130Ma) in shallow marine, fluvial and lacustrine environments following an earlier magmatic phase (Walley, 1997).

Figure 2.4: The Cretaceous stratigraphic sequence of the study area, as seen in the vicinity of el Bire. The formations shown here are (from bottom to top): the C1 Chouf Sandstone fm, the C2a Abeih fm, the C2b Mdeirej fm and the C3 Hammana fm.

Figure 2.5: The Chouf sandstone observed in Maaser ech Chouf area. Around 4m of the entire thickness of the C1 formation which may reach 300m in the study area, are shown in this picture. Notice the presence of greyish to bleuish coal intercalated in this formation.

The prevalence of the C1 is confined mostly to the northern SCML - the area located north of Beit ed Dine- where this formation is seen flanking the Safa River and its major tributaries (Fig. 2.2). Here the Chouf sandstone forms an important depocenter that reaches a thickness of 300m. Another important exposure of the C1 is also seen flanking the western foot of the Barouk Mountain, mimicking the crest of this structural high (Fig. 2.2).

In this locality the C1 is in direct contact with J6 strata and exhibits an anomalous reduced thickness of tens of meters (Heybroek, 1942).

2.2.2.2. Abeih Formation (C2a)

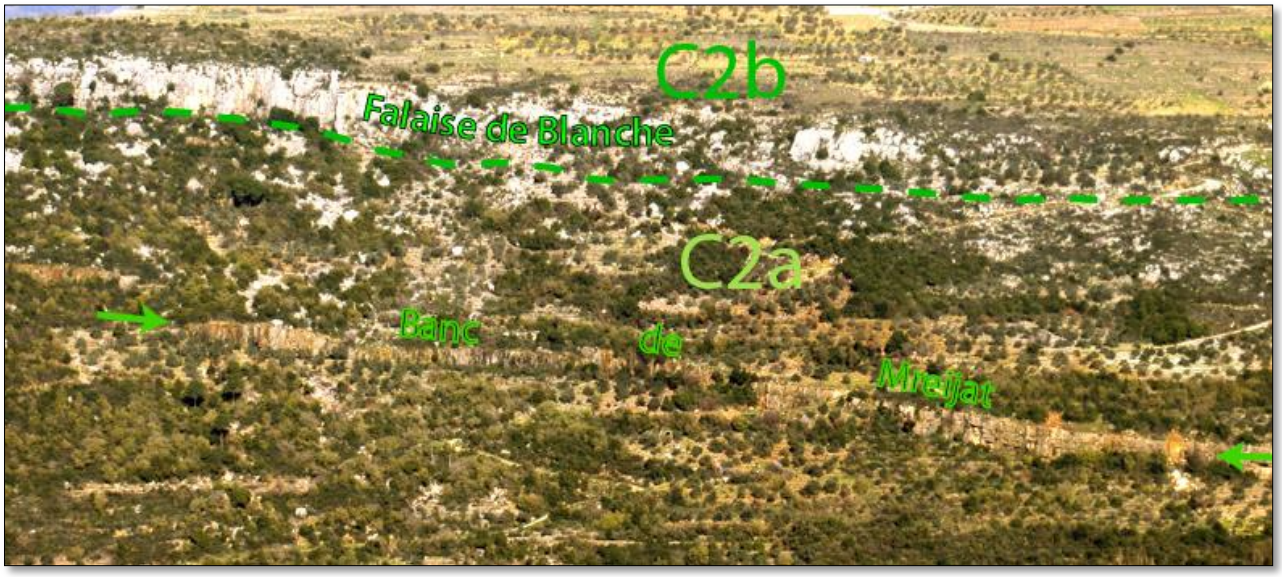

Figure 2.6: The Banc de Mreijat, a cliffy member of the Abeih formation, which stands out in the topography.

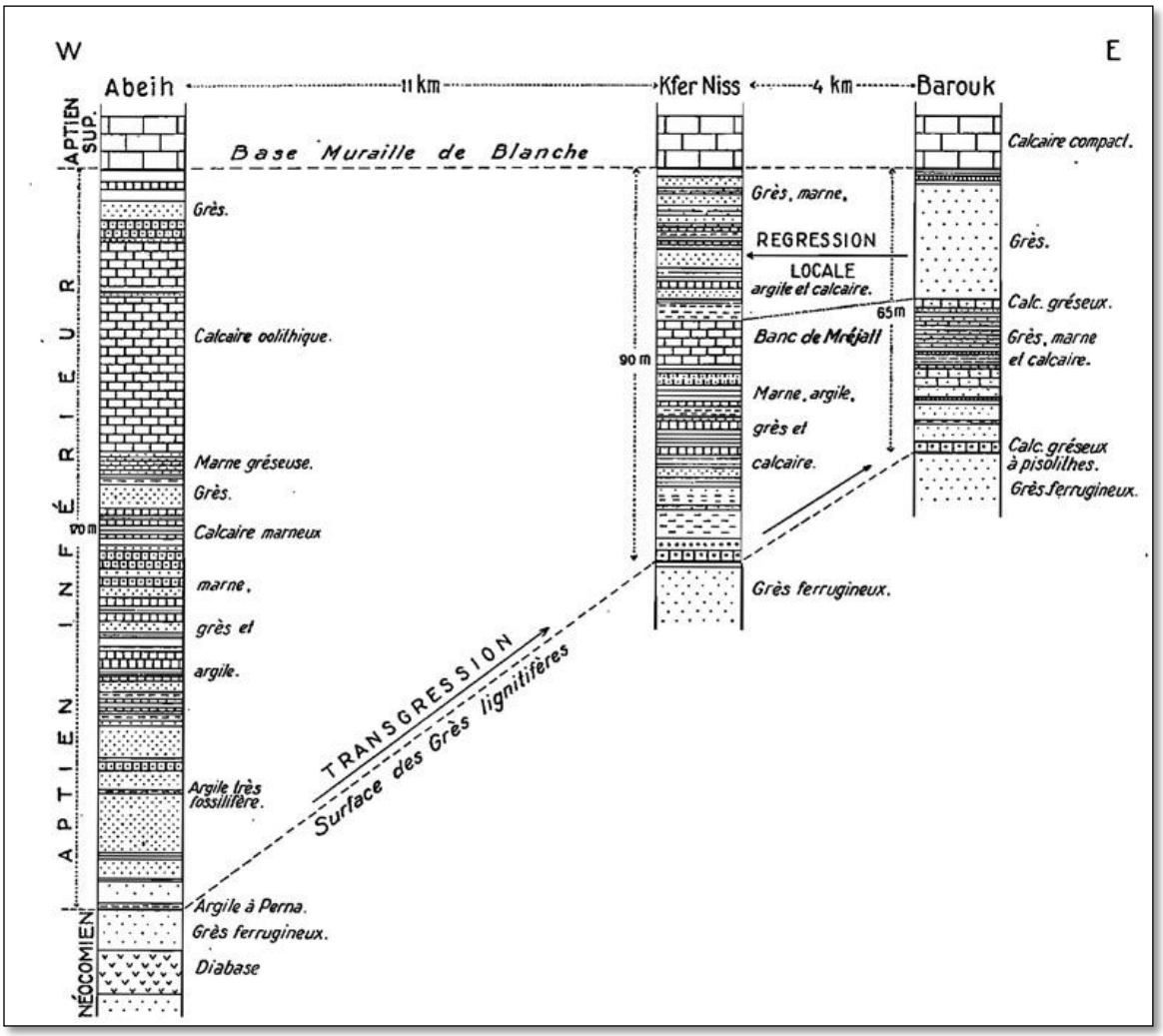

Figure 2.7: Westward thickening of the Abeih formation in lower Aptian time, constrained from stratigraphic logging, suggesting an eastward marine transgression (after Heybroek, 1942).

The C2a (Dubertret, 1945) -also known as the Abeih formation (Walley, 1997) - consists of ochre yellow to brown rock units (Fig. 2.4). It deposited during lower Aptian times around 130-125Ma (Dubertret, 1945) in a high energy, storm dominated shoreline environment, indicated by its gastropod and bivalve rich stratum consisting of terrigenous and marine detrital material, mainly sand, limestone and marl (Dubertret, 1945; Walley,

1997). In the SCML, the Abeih formation is the host, in its upper part, to an exclusive cliffy marker bed, the “Banc de Mreijat” (Figs. 2.4-2.7), well expressed in the Mreijat area (Heybroek, 1942) ~5Km to the east of Rechmaya (Fig. 2.2). It consists of detrital and oolithic limestone strata and varies in thickness between 2-10m (Heybroek, 1942).

To the north of Beit ed Dine the C2a is vastly exposed (Fig. 2.2) and thickens from 65m in the Barouk area, to 170m at Abeih, suggesting therefore an eastward marine transgression (Heybroek, 1942) during lower Aptian times (Fig. 2.7).

In the southern part of the SCML, the C2a is seen in the vicinity of the Barouk Mountain as well as in the Moukhtara-Maaser ech Chouf region, where the Barouk River incises deeply and exposes this formation along its channel bed (Fig. 2.2).

2.2.2.3. Mdeirej Formation (C2b)

The C2b (Dubertret, 1945) -also known as the Mdeirej Formation (Walley, 1997) - deposited during the Upper Aptian around 125Ma, in a shelf marine environment (Walley, 1997). Its lower part consists of the “Falaise de Blanche”: a 50-60m thick, pale grey and cliff forming rock unit (Figs. 2.4-2.8) composed of micritic limestone (Dubertret, 1945). Its upper part, on the other hand, includes "Orbitolines" rich, marly limestone layers that reach 55m in thickness (Fig. 2.4); Heybreok (1942) refers to these layers as the “Couches à Orbitolines”.

Figure 2.8: The Falaise de Blanche, a massive thick cliff forming unit of the Mdeirej formation. Picture was taken near Majdel Meouche-Bire, looking north and showing ~30m thick and horizontal Falaise de Blanche.

In the northern SCML (North of Beit ed Dine), the C2b is vastly exposed and is mapped on the banks of the Safa River (Fig. 2.2). However, in the south it is confined to two localities (Fig. 2.2):

– The area located between Maaser ech Chouf and Gharife hosting the incision of the Barouk River.

– The foot of the Barouk Mountain.

2.2.2.4. Hammana Formation (C3)

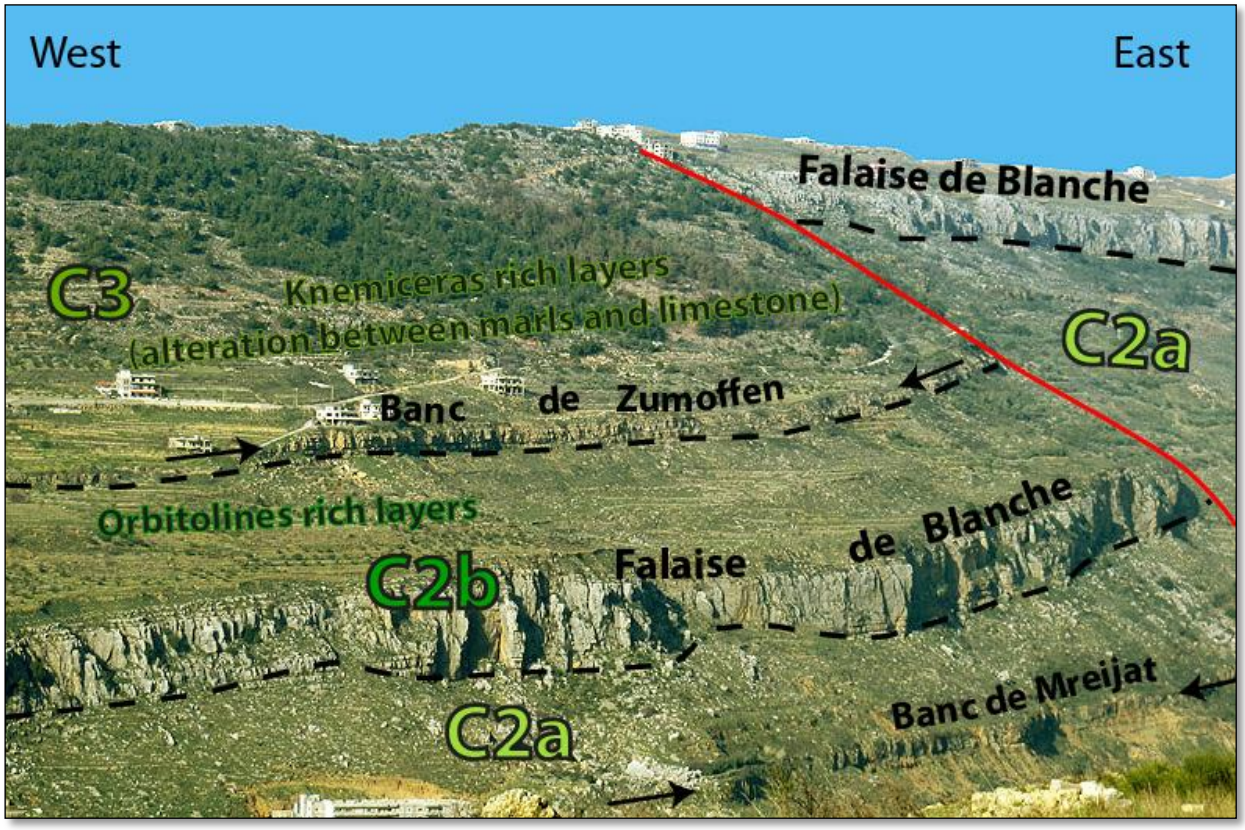

Figure 2.9: The Banc de Zumoffen, a cliff forming unit marking the boundary between the C2b and the C3 in the southern central Mt. Lebanon area. The Red line indicated to the Btater fault located midway between Richmaya and Btater.

The C3 (Dubertret, 1945) -also known as the Hammana Formation (Walley, 1997)- deposited in Albian (118-112Ma) in a shoreline to outer marine shelf environment.

A particularity of the stratigraphy of our study area, is the occurrence towards the base of the Hammana Formation of a ~10m thick cliff (Fig. 2.9) - the "Banc de Zumoffen"- composed of fossil rich, oolithic and detrital limestone (Dubertret, 1945) and not

represented elsewhere in the country. This cliff is overlain by ~110m thick alternation of chalky limestone beds and marls (Fig. 2.9), rich in Knemiceras fossils (Heybroek, 1942).

The surface exposure of the Hammana Formation is vast to the north of Beit ed Dine, where these Albian rocks cap the hills entrenched by the fluvial activity. To the south of this locality the C3 exposure is confined to the flanks of the Barouk River and to the foot of Jabal el Barouk (Fig. 2.2).

2.2.2.5. Sannine Formation (C4)

The C4 (Dubertret, 1945) - also known as the Sannine formation (Walley, 1997) - consists of thick, massive and pale grey rock units (Fig. 2.10) composed mainly of chalky limestone (Walley, 1997) that is rich in chert nodules and poor in fossils (Heybroek, 1942). It deposited during the Cenomanian around 100-94Ma, in a shelf marine environment (Walley, 1997).

In the northern SCML (North of Beit ed Dine) the Sannine formation mainly covers (Fig. 2.2):

- The coastal area between Damour and Baawerta (Fig.2.2).
- The top of the hills incised by the Safa River in the area between Baawerta and Ain-Zhalta.

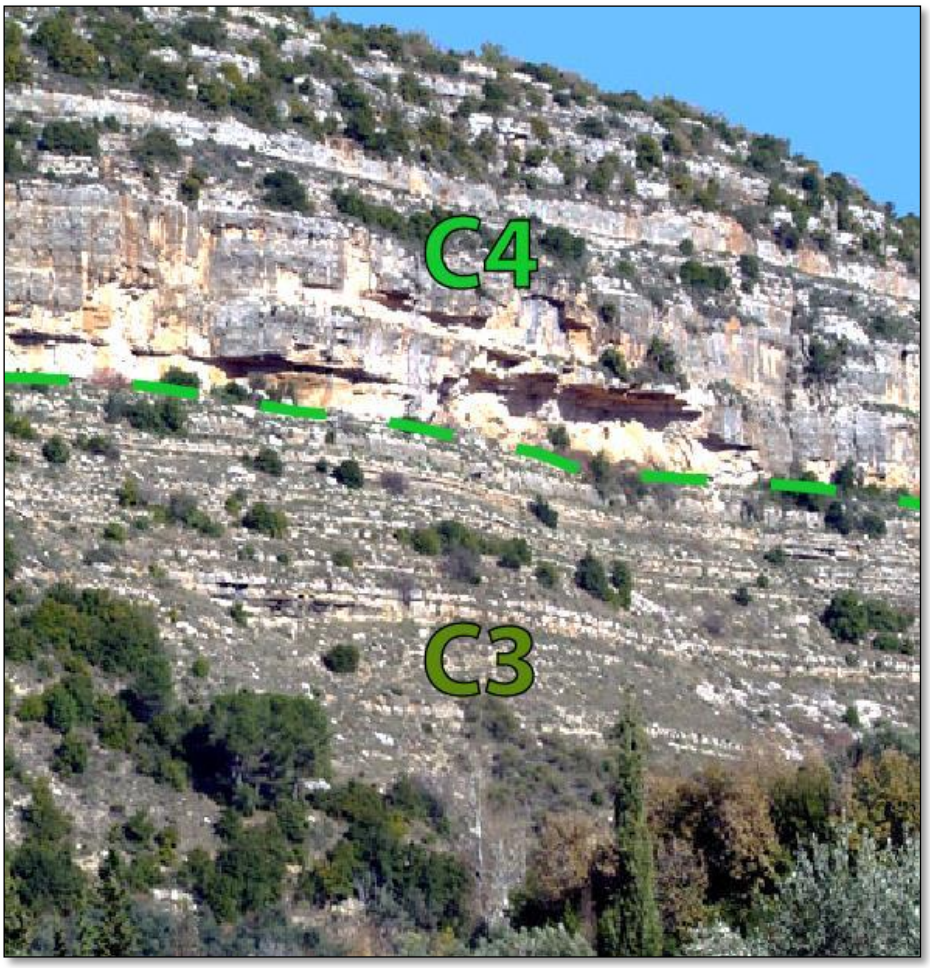

Figure 2.10: The C3-C4 boundary separating the massive chalky Sannine formation from the marly limestone layers of the Hammana Formation as seen in the Moukhtara area.

To the south, on the other hand, the C4 covers almost entirely the area between Maaser ech Chouf and Jiye (Fig. 2.2).

2.2.2.6. Chekka Formation (C6)

The C6 (Dubertret, 1949) -also known as the Chekka Formation (Walley, 1997)- is composed mainly of white chalk and marls, rich in microfossils, which deposited in

Coniacian to Maastrichtian (formerly known as Senonian) time (~93-64Ma), in a shelf marine environment (Walley, 1997).

In the SCML the C6 is highly eroded and is distributed as small patchy outcrops in the coastal zone extending between Damour and Jiye (Fig. 2.2), where it reaches a thickness of 200m (Dubertret, 1949).

2.2.3. Quaternary Deposits

Several types of Quaternary deposits are distinguished within the SCML (Dubertret, 1945):

- Quaternary alluvials: these consist of river sediments varying in size from clay to coarse pebbles showing cyclic graded bedding. They cover the Damour coastal plain (Fig. 2.2) and the banks of the Safa River as it incises in the Damour area.
- Quaternary beach deposits: brown coloured sand (Dubertret, 1945) mapped in the coastal area in the vicinity of Damour (Fig. 2.2).
- Quaternary mass wasting: consists of a chaotic mixture of sediments, with no obvious layering that originate from slope failure in pre-existing deposits. In the SCML these are located on the flanks of the Safa River, slightly to the north of Kafr Nabrakh, where formations with weak lithologies (such as the C1 and the C3) are exposed (Fig. 2.2).

2.3. Structural Geology of the Southern Central Mt. Lebanon

The geologic structures in Lebanon and in the study area in particular, are the end result of several tectonic phases witnessed by the whole region throughout time.

The mapping of these structures in the study area has been conducted first by Zumoffen (1926) on the 1:200000 geologic map of Lebanon. The geologic observations located within the study area have been later refined by Heybroek (1942) and by Dubertret (1945) in their 1:50000 geologic maps of Jezzine and Saida respectively.

In this section, the southern central Mt. Lebanon structural *geology* is reviewed; as a start the geologic observations provided by previous geologists are presented from west to east. Then this will be followed by a highlight on the generally accepted ideas related to the structural evolution of the southern central Mt. Lebanon, within the context of the Levant area.

2.3.1. Folding in the Southern Central Mt. Lebanon

The geology of the SCML area is shaped by a series of four, NE-SW trending large flexures, all asymmetric, with steep western limbs compared to relatively gently dipping to almost tabular eastern limbs. They are distributed on the northern and southern side of the Damour-Beit ed Dine fault. The later seem to be a major structuring element as it offsets some of these flexures or represents a limit to their extension. The limited observations we have in the Barouk area suggest that the Barouk Monocline is not affected by the fault but forms the eastern backstop of deformation in the area.

Other anticlines (Maaser ech Chouf and Jahliyeh anticlines) of smaller extent are also present and have a smaller impact on the structuring of the area.

2.3.1.1. The Baawerta Flexure

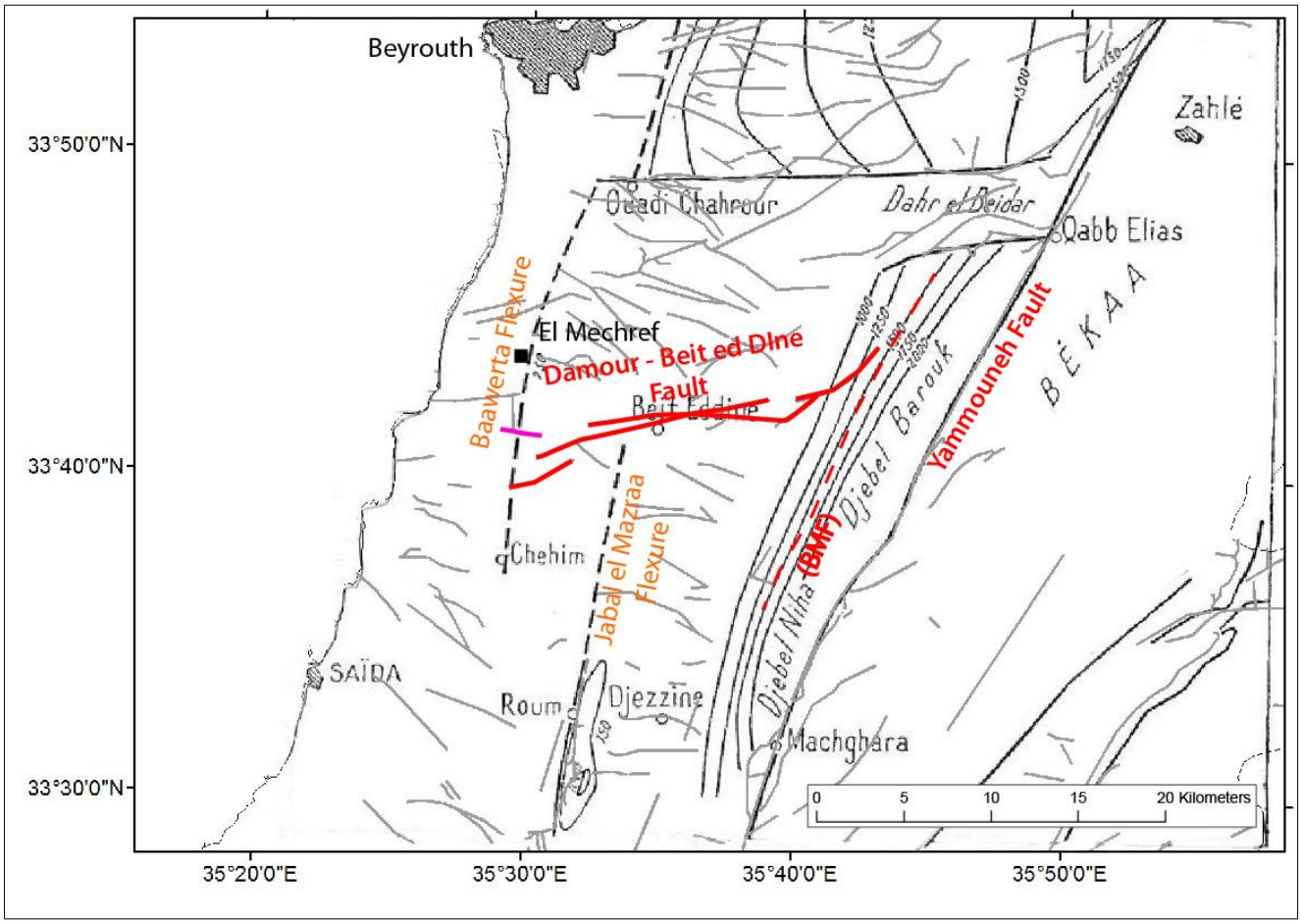

Figure 2.11: Simplified structural map of the southern central Mt. Lebanon area, showing the main structural elements of this region as mapped by Dubertret (1945). Grey lineaments are secondary faults digitized from Dubertret (1955) 1:200000 Geologic Map of Lebanon. The Red line is the Damour-Beit ed Dine fault system and the purple line is the Nahr el Hammam Fault (Modified from Dubertret (1945)).

The Baawerta flexure is the southernmost segment of the Mt. Lebanon Flexure, lying west of the SCML, parallel to the coastline (Heybroek, 1942; Dubertret, 1945). It is a

NNE-SSW striking and west, steeply dipping monocline of the Mesozoic limestone cover, abruptly terminating at Chehim (Figs. 2.11 and 2.12). A remarkable 2-3Km dextral offset of this flexure seen near Baawerta/Ouadi Chahrour (Fig. 2.11) is associated with shearing on the ~E-W striking Dahr el Baidar Fault, located slightly north of the study area (Dubertret, 1945).

Figure 2.12: Field view of the Baawerta Flexure as it deforms the Falaise de Blanche (C2b) in the Mechref area. (See Fig. 2.11 for a map view of the structure).

2.3.1.2. Jabal el Mazraa Flexure

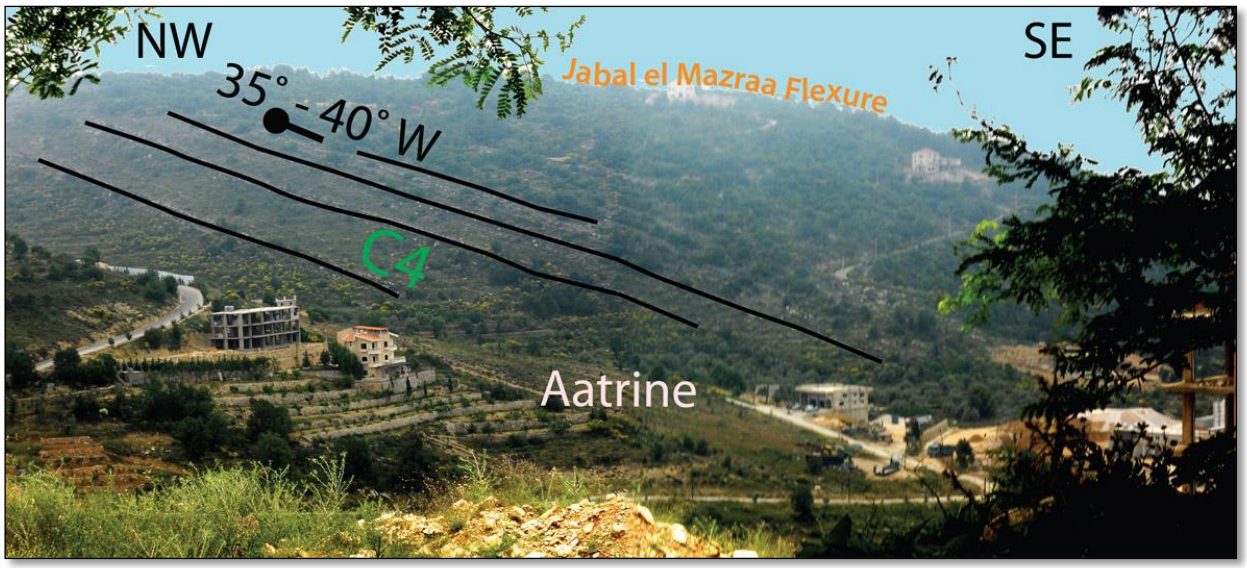

Figure 2.13: The Jabal el Mazraa Flexure as seen from Aatrine. (See Fig. 2.11 for a map view of this structure).

The "Jabal el Mazraa Flexure" (Heybroek, 1942) is located east of the Baawarta Flexure, 5-6Km east of Chehim. It is also known as the Roum Flexure (Dubertret, 1945) or Chouf Monocline (Nemer & Meghraoui, 2006). It is a second order west dipping monocline extending in a ~NNE-SSW direction between Roum and Beit ed Dine (Fig. 2.13), where it abruptly terminates northwards along the ~E-W Beit ed Dine fault (Fig. 2.11).

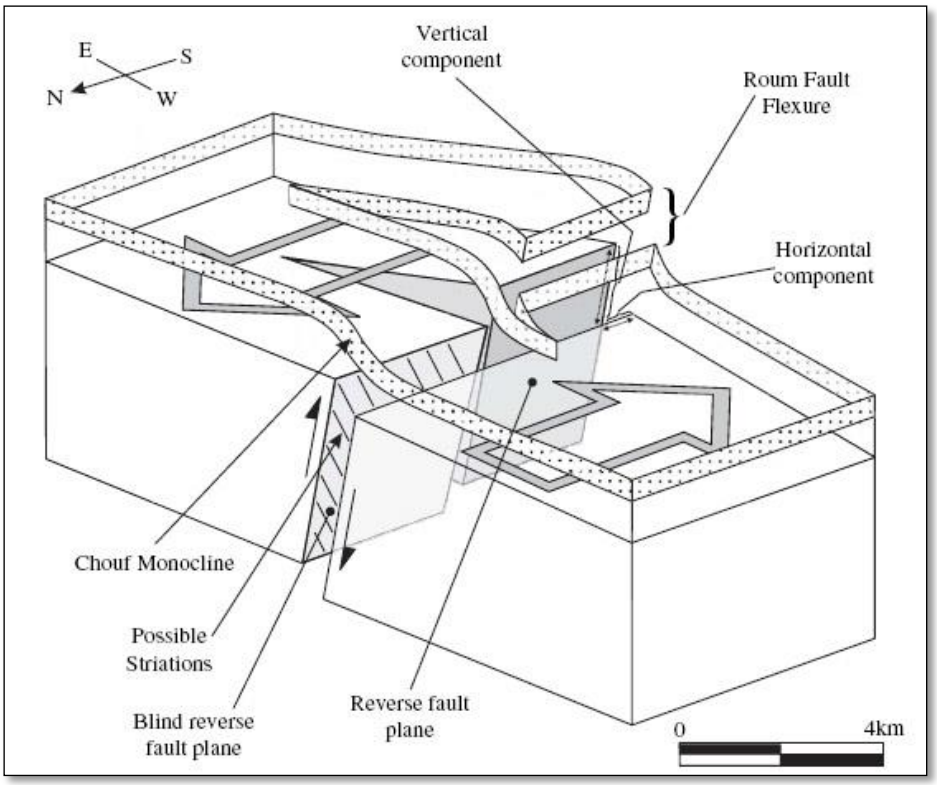

Figure 2.14: Sketch of the Chouf Monocline (also known as the Jabal el Mazraa Flexure) showing the blind reverse segment of the Roum Fault responsible for its formation as suggested by Nemer & Meghraoui (2006).

At depth, this structure is underlain by a blind thrust fault (Heybroek, 1942; Dubertret, 1945; Khair, 2001; Nemer & Meghraoui, 2006) that likely represents a secondary branch of the Roum Fault (Fig. 2.14).

2.3.1.3. The Majdel Meouche Flexure

In the vicinity of Rechmaya (Figs. 2.2 and 2.15) and at a distance of ~1Km west of Majdel Meouche lies the Majdel Meouche Flexure (Heybroek, 1942). It is a ~60˚W dipping

and NNE-SSW striking monocline with an overall length of ~3Km, therefore being a smaller structure compared to the Mt. Lebanon and Jabal el Mazraa Flexures.

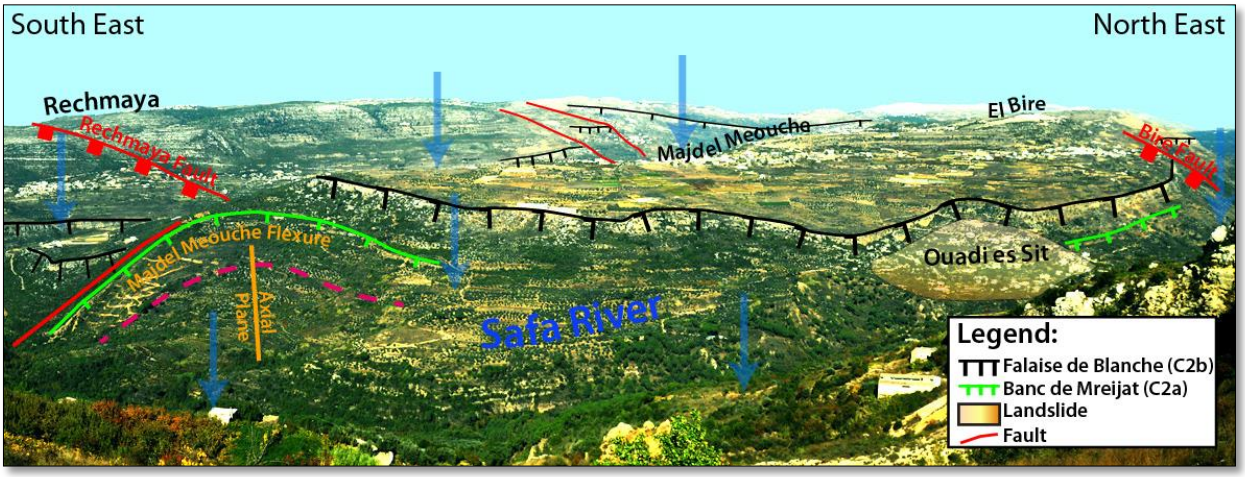

Figure 2.15: Panoramic view of Majdel Meouche-Rechmaya area, showing the Majdel Meouche flexure. (See location on Fig. 2.2).

2.3.1.4. The Barouk Monocline

The eastern part of the SCML consists of Jurassic strata (Fig.2.2) and lower Cretaceous rocks that dip ~40°W (Fig. 2.16), forming the Barouk Monocline (Heybroek, 1942; Dubertret, 1945). The hinge of this structure coincides with the backbone of the Barouk Mountain, which rises at an elevation of 1800-2000m a.s.l (Fig. 2.2). The NNE-SSW striking Yammouneh Fault truncates Barouk Monocline (Fig. 2.11) slightly to the east of its hinge line (Heybroek, 1942; Dubertret, 1945).

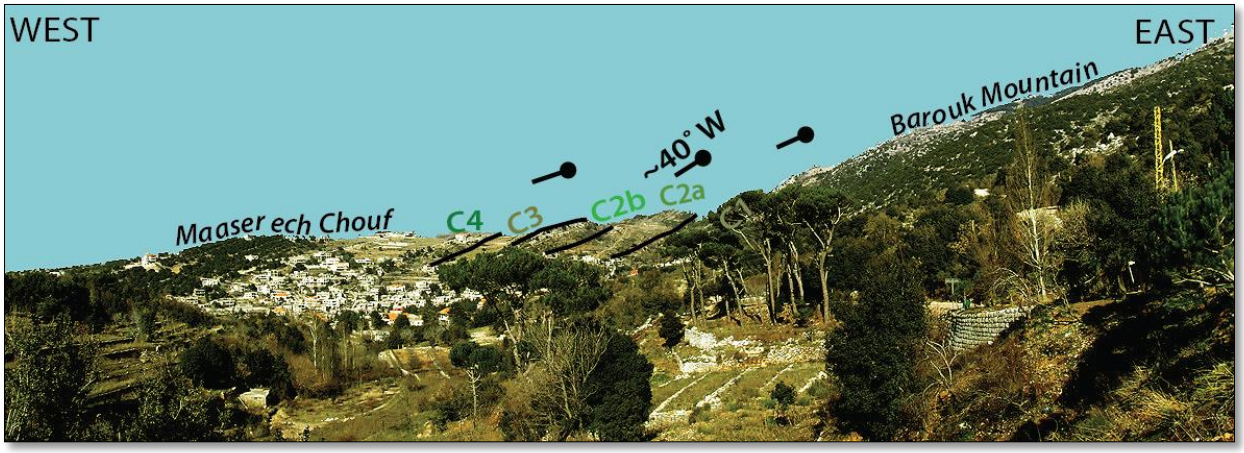

Figure 2.16: A panoramic view of Maaser ech Chouf showing the steeply dipping strata of the Barouk Monocline.

2.3.1.5. The Maaser ech Chouf Anticline

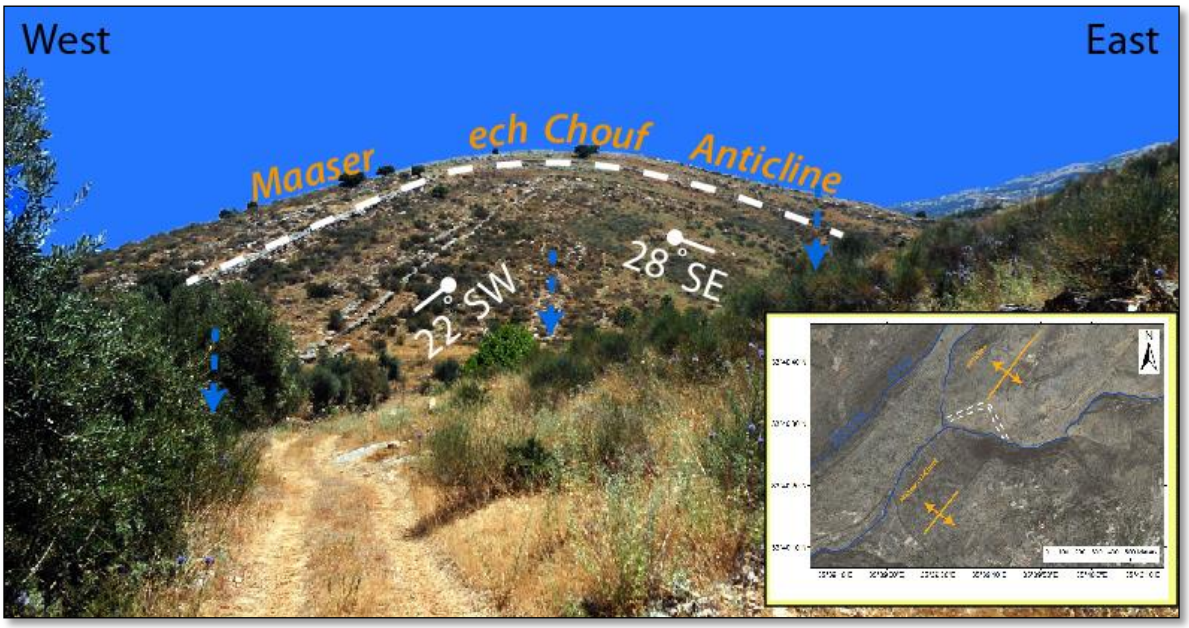

Figure 2.17: The Maaser ech Chouf anticline as seen on the field. The inset map shows the location of this structure.

In the Maaser ech Chouf area (Check Fig. 2.2 for location) small scale NE-SW striking folds are mapped. These are roughly parallel to the larger folds mapped in the area (Heybroek, 1942), yet they are tighter and more symmetrical as it is observed for the Maaser ech Chouf anticline (Fig. 2.17).

2.3.2. Faulting in the Southern Central Mt. Lebanon.

The western flank of Mt. Lebanon is dissected by numerous intermediate to small scale faults. The most prominent of these fault sets is the group of latitudinal E-W trending faults that run between the Yammouneh fault in the east and the coastline in the west. The southernmost of these faults is the (1) Damour-Beit ed Dine fault, mapped by Dubertret (1945) and other authors as a series of discontinuous E-W segments between Barouk and Damour. (2) The Dahr el Baidar fault is another E-W fault that bounds the SCML to the north. A dense network of smaller scale faults mostly with NW-SE strike is also visible in the area (Fig. 2.2).

2.3.2.1. The Damour-Beited Dine Fault System

The Damour-Beit ed Dine fault extends over ~25Km, from the Brouk Mountain in the east to the Jahliye area in the west. The available 1:50000 geological maps of the area show a discontinuous trace of the fault. It is mapped as a series of smaller scale NNE-SSW braided and stepping segments (Fig. 2.2). Namely the Beit ed Dine and Deir el Qamar Faults are the main splays of this fault, running parallel to each other (Heybroek, 1942). Its termination to the east is the curved NE striking Barouk fault that disappears in the Jurassic strata. To the west, smaller scale, discontinuous fault segments cut and offset Mid- to

Upper Cretaceous layers. These coastal segments interrupt the continuity of the shoreline trace bringing Quaternary deposits in touch with older Cenozoic material.

The Damour-Beit ed Dine fault is the southernmost sub-latitudinal fault observed along Mt. Lebanon. For Dubertret (1945) the E-W faults in general and the Damour-Beit ed Dine fault system in particular are subordinate structures that stop at the major Yammouneh fault. Walley (1998) speculated that it also has an offset paleo-continuation east of the Yammouneh Fault in the Bekaa Valley. He suggested that this structure is the boundary between northern and southern Mt. Lebanon characterized by two different structural styles: high elevated, thick-skinned, broadly folded northern Mt. Lebanon and lower lying, thin-skinned, closely folded southern Mt. Lebanon.

No geologic study has dealt specifically with this structure; however some ideas have been suggested concerning the kinematics and evolution of the E-W faults and the broader geologic structural evolution of Lebanon and the Levant area.

Homberg et *al.* (2010) conducted a field-based meso-scale structural assessment of Mt. Lebanon and concluded that the E-W faults were initiated in the Mesozoic, during a N-S to NNE-SSW extensional tectonic episode associated with the opening of the Neo-Tethys. The tectonic activity of the faults ceased prior to Cenomanian (Homberg et *al.*, 2010).

Gedeon (1999) suggested that the E-W faults located north of Beirut are active antithetic Riedel shears (R') created as a result of Cenozoic left-lateral shearing on the Yammouneh Fault. According to this model these E-W structures show only right-lateral shearing with no distinct evidence of bookshelf faulting.

A geometrical model was proposed by Ron (1987), based on paleo-magnetic measurements in order to explain the kinematics of the E-W faults of Lebanon. It suggests that left-lateral shear on the Yammouneh fault is accommodated by the E-W faults through a counter-clockwise bookshelf faulting mechanism (Fig. 2.18) characterized by:

- Right-lateral shear on these parallel, present day sub-latitudinal faults
- 61˚CCW rotation of the blocks bound by these structures, from their initial NW-SE orientation (Ron, 1987), constrained by paleomagnetic measurements.

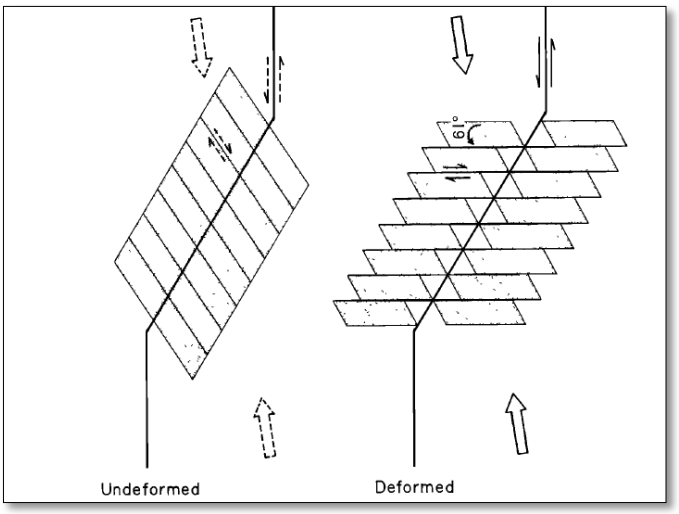

Figure 2.18: The CCW bookshelf faulting mechanism of the E-W faults in Lebanon (after Ron, 1987).

According to this model, these E-W faults have reached their maximum rotation allowed by the direction of the principal stresses in the region; thus they are inactive and being replaced by younger NW - SE right lateral faults.

The Nahr el Hammam segment of the DBF (Fig. 2.11) dextrally offsets the Mt. Lebanon by around 1Km (Arnaud, 1969). Thus the DBF is considered to post-date the folding observed within the SCML (Walley, 1998).

2.3.2.2. The Barouk Mountain Fault

One of the main differences observed when comparing the 1:50000 Jezzine maps of Heybroek (1942) and Dubertret (1945), is materialized by the Barouk Mountain Fault that discarded by Dubertret. This structure, mapped by Heybroek (1942), is a west dipping, SSW striking normal fault located at the foot of the Barouk Mountain, where an unconformable contact between Portlandian (J6) and Baremian (C1) is observed.

Heybroek (1942) includes this structure to explain the abnormal thickness of C1 in this area, and considers this normal structure to be the west bounding fault for the Barouk structural high, considered as a horst.

2.3.2.3. The NW-SE Striking Faults of the SCML

A series of NW-SE striking faults, smaller in scale compared to the DBF are observed on the geologic maps of the SCML (Heybroek, 1942; Dubertret, 1945). These are more abundant and longer to the north of the Damour-Beit ed Dine Fault compared with the south (Figs. 2.2 and 2.11). They also clearly offset the Lower Cretaceous formations in the area (C2a, C2b, C3 and C4), and seal downward in the C1 sandstone formation (Dubertret, 1955).

The structural setting of these steeply dipping normal faults is debatable. For Hancock & Atiya (1979) the NW-SE faults of Mt. Lebanon are sinistral strike-slip

structures, conjugate to the dextral E-W faults. Ron (1987) claims that the NW-SE faults seen in Lebanon are new right-lateral bookshelf faults replacing the ~E-W inactive ones. Others (i.e. Walley, 1988; Walley, 1998; Homberg et *al.*, 2010), considered these structures as Late Jurassic-Early Cretaceous extensional structures created during the Mesozoic, Neo-Tethian rifting. For Homberg et *al.* (2010), their activity ceased in Cenomanian.

2.4. Summary

Several opposing structural models were suggested in the literature, to discuss the timing and mechanisms responsible for the evolution of the main structures (E-W striking Damour-Beit ed Dine Fault, NNE-SSW striking folds and NW-SE striking faults) within our study area. Some models suggested that structures in the SCML are Mesozoic extensional features that are inactive in present time; other models suggested that these are associated with shear on the LRB and thus are Cenozoic.

Earliest literature on the area (i.e. Heybroek, 1942; Dubertret, 1945) considered the SCML structure as a horst, bound to the east by the Baawerta Flexure and to the west by the Yammouneh Fault, and structurally controlled by rifting (vertical motion) along the Dead Sea Rift zone. The geologic fabric of this area was described as tabular and little importance was given to folds that were interpreted as secondary tangential structures associated with the prevalent extensional tectonics along the Dead Sea Fault System (Heybroek, 1942).

It wasn't until the ~1960's that the idea of transform, left-lateral shear along the plate boundary was considered the dominant mechanism controlling the structural setting of the Eastern Levant area. Subsequently transpression was considered on the LRB (Quenell,

1958; Freund, 1965) since Miocene (Eyal et *al.*, 1981). Thrusting/folding seen in Lebanon were therefore given a primary role in the Cenozoic structural evolution of the country (Elias, 2006; Elias et *al.*, 2007), to which the compressive structures observed in the SCML can be attributed (Elias, 2006; Nemer & Meghraoui, 2006; Elias et *al.*, 2007).

In this study, we will investigate the structural setting of the SCML and in particular the evolution and tectonic activity of its main structures, in order to understand the ages and mechanism through which deformation is happening. The geomorphologic, stratigraphic and structural ideas suggested by several researchers concerning this study area, set the framework for our research. In the next chapter, which will include our own observations, interpretations and structural model for the evolution of the southern central Mt. Lebanon, we either adopt some of these ideas, or re-interpret/ put to question others.

CHAPTER 3

MORPHOTECTONIC AND STRUCTURAL GEOLOGY OF THE SOUTHERN CENTRAL MT. LEBANON REGION

In this chapter, we present our geologic observations in the southern central Mt. Lebanon area (SCML) acquired through field work, satellite imagery/aerial photographs interpretations and elevation profiles/contours maps data analysis. In addition we measure thicknesses for the exposed formations in the area. We finally present these data, along with previous observations as synthetic geological cross sections of the region.

The outcome of this chapter is a geologic model of the southern central Mt. Lebanon area showing its evolution through Mesozoic-Cenozoic.

3.1. Morphotectonics of the Southern Central Mt. Lebanon

The Southern Central Mt. Lebanon -as defined earlier (Chapter 2, section 2.1)- is a mountainous coastal region located between the coast and the Bekaa plain and culminating over the Barouk Mountain ridge to the east. Its western flank stretches over 25Km between a narrow coastal plain to the West and the ~ 1900m high Barouk Mountain (Fig. 3.1). The saw-like shoreline has rightward steps along its length, where rocky headlands interrupt narrow stretches of alluvial and beach deposits along the coast.

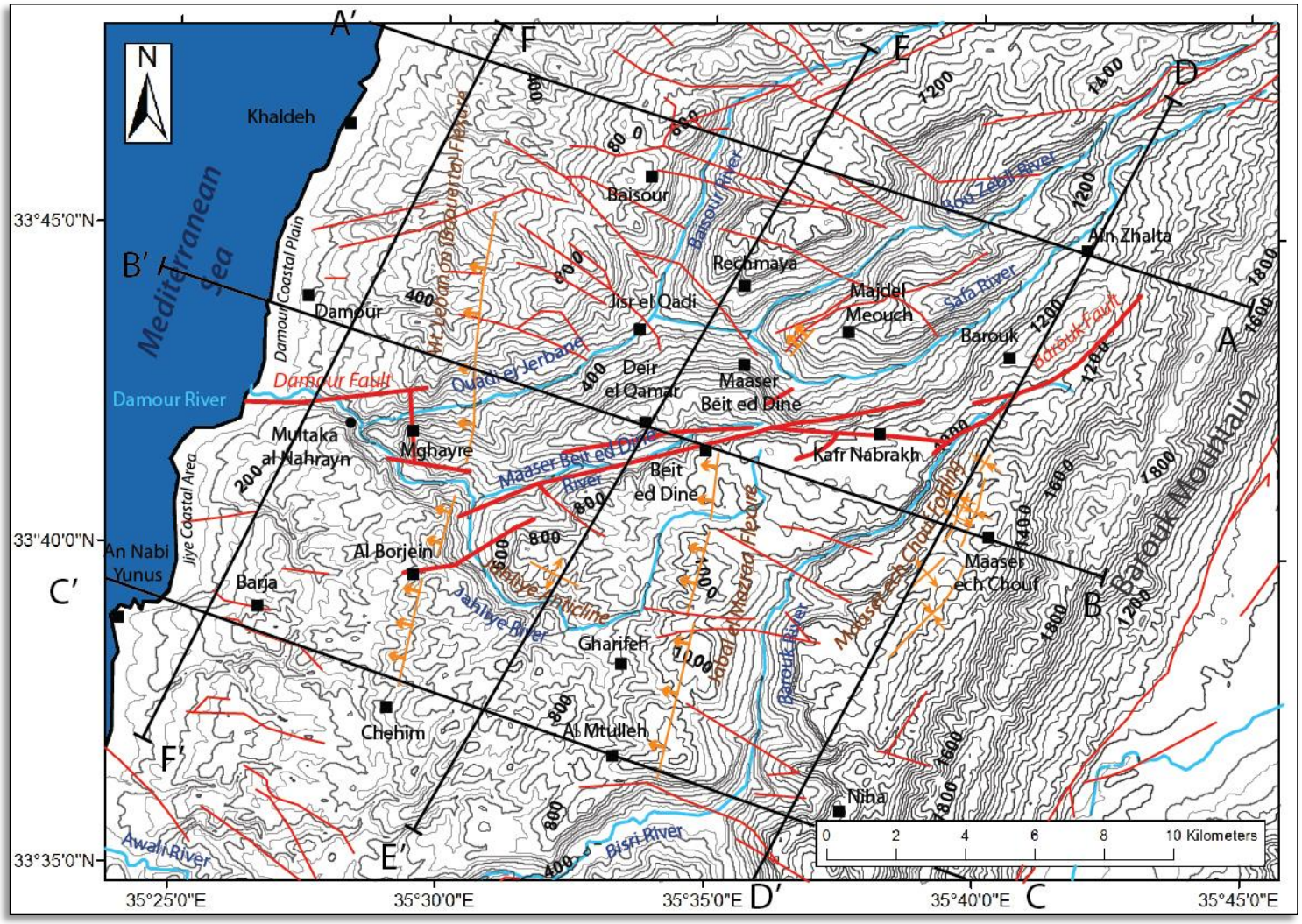

Figure 3.1: Topographic Map of the SCML, showing the location of the 6 topographic profiles (AA' → DD'). The elevation contours are extracted from NASA SRTM with a 50m interval. The faults are adopted from Dubertret (1955).

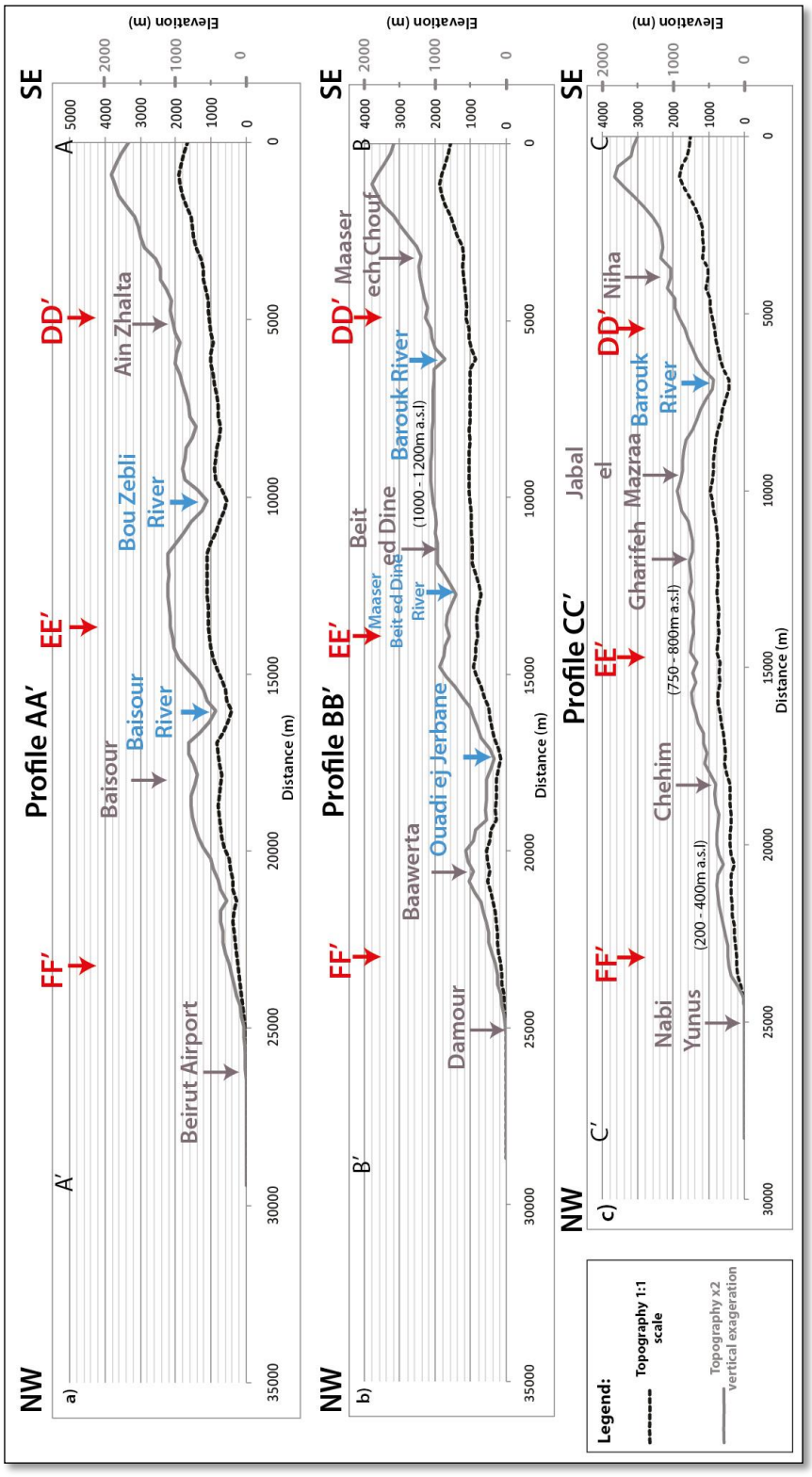

Figure 3.2: Topographic profiles AA' → CC' oriented NW–SE within the SCML.

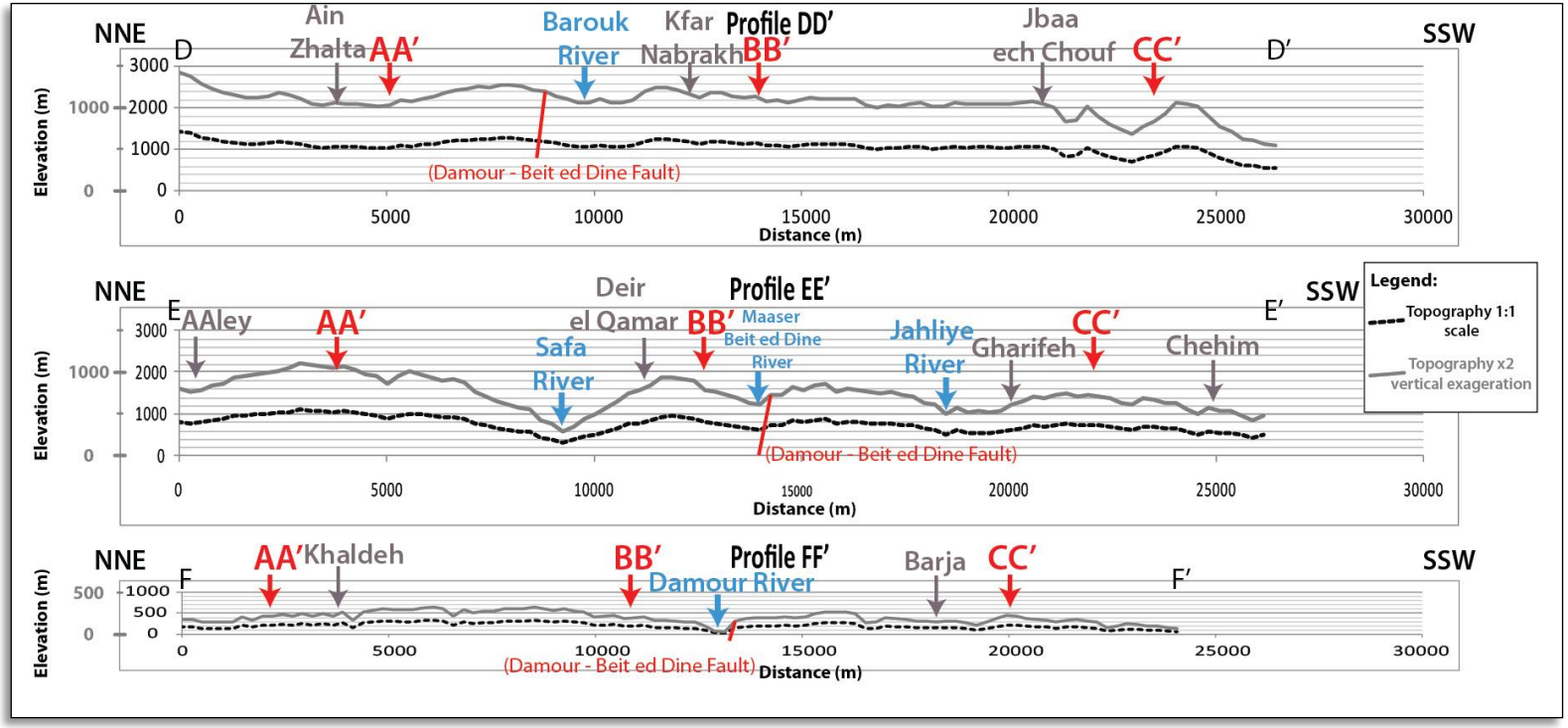

Figure 3.3: Topographic profiles DD' →FF' oriented NNE – SSW within the SCML.

Its eastern flank is narrow and steep: the elevation drops fast by almost 900m over only 1Km of distance towards the Bekaa as it is truncated by the Yammouneh Fault (Fig. 3.1). The differences in topography and drainage patterns on both sides reflect the control of the deep geological structures on the organization of incisions.

3.1.1. Drainage System of the Area

The Southern Central Mt. Lebanon is a topographic barrier associated with important rainfall and meteoric precipitation over its western slopes. An important drainage system is developed on these slopes between the Barouk Mountain and the Mediterranean Sea. Two main rivers, the Barouk (Awali) and Damour rivers, dissect the topography and drain the area through deeply incised river valleys where the headward erosion of associated tributaries have reached the upper slopes of the Barouk Mountain (Fig. 3.1). Over the eastern slopes, water runoff flows into the Bekaa through a set of short and steep gullies that leave little marks in the topography (Fig. 3.1).

3.1.1.1. The Damour River

The Damour River shows a dendritic pattern with tributaries converging downstream into deeply incised valleys (Fig. 3.1). It consists of two main branches with very different morphometric properties, flowing separately north and south of the DBF until they merge at Multaka al Nahrayn forming the lower short segment known as Damour River proper. The northern branch has a main upstream channel: the Safa River. It follows a NE-SW direction, veering almost 90° to the north at the level of Maaser Beit ed Dine to

meet with the Bou-Zebli tributary downstream from Rechmaya. At Jisr el Qadi it collects the water from Baisour channel and follows the straight, NE-SW direction again along Ouadi ej Jerbane towards Multaka al Nahrayn. Except for the 90° bend of the Safa River near Maaser Beit ed Dine, the overall path of this drainage is straight and NE-SW oriented. The river valleys channelizing these streams are wide, deep and well-marked in the topography (Fig. 3.2). Relatively flat floodplains form their bottom where alluvial terraces are cut and abandoned, indicating the presence of uplift in the area.

The southern branch has very different morphometric characteristics. Its main channel -the Jahliye River- has a tortuous and almost semi-circular path from its headwaters east of Beit ed Dine to where it merges with Maaser Beit ed Dine tributary downstream from Jahliye village and continues till the confluence with the northern branch at Multaka al Nahrayn (Fig. 3.1). It has a steep river profile, entrenched in a narrow path (profile EE', Fig 3.3) suggesting important vertical incision rate.

That the Damour River is actively incising the topography is evident not only from the geomorphology of the area but also from the sedimentary record of the lower Damour channel. A number of fluvial terraces can be seen in and around the active floodplain of the river downstream from Multaka al Nahrayn. Moreover on the main road from Damour to Deir el Qamar, abandoned alluvial terraces located ~50m.a.s.l, -or 30m above the active present riverbed- are observed on the northern flank of the Damour River valley (Fig. 3.4). The sequence observed is characterized by cyclic fining upward conglomeratic deposits, suggestive of their probable fluvial origin (Fig. 3.5) and denoting therefore possible important uplift rate of the region.

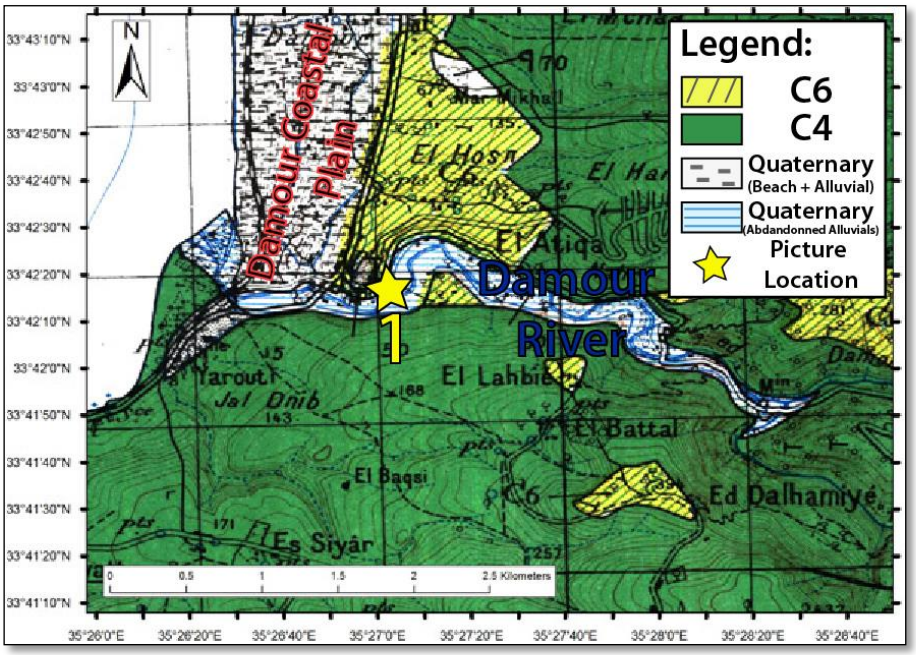

Figure 3.4: Abandoned alluvial deposits (Quaternary in age) flanking the Damour River.

Figure 3.5: Field view of the Quaternary deposits flanking the Damour River, 30m above the present-day channel bed. A cyclic fining upward conglomeratic sequence can be observed, indicating probable fluvial origin of these deposits (Location 1 on Fig. 3.4).

3.1.1.2. The Maaser Beit ed Dine Wind Gap

Wind gaps are valleys carved in the topography and no longer flown by the river that has created them (Ollier, 1985). These geomorphologic features are commonly associated to structurally controlled drainage deflection and thus are reflective of changes in the leandscape induced by active tectonism (Reicherter et *al.*, 2011; Perruca et *al.*, 2014).

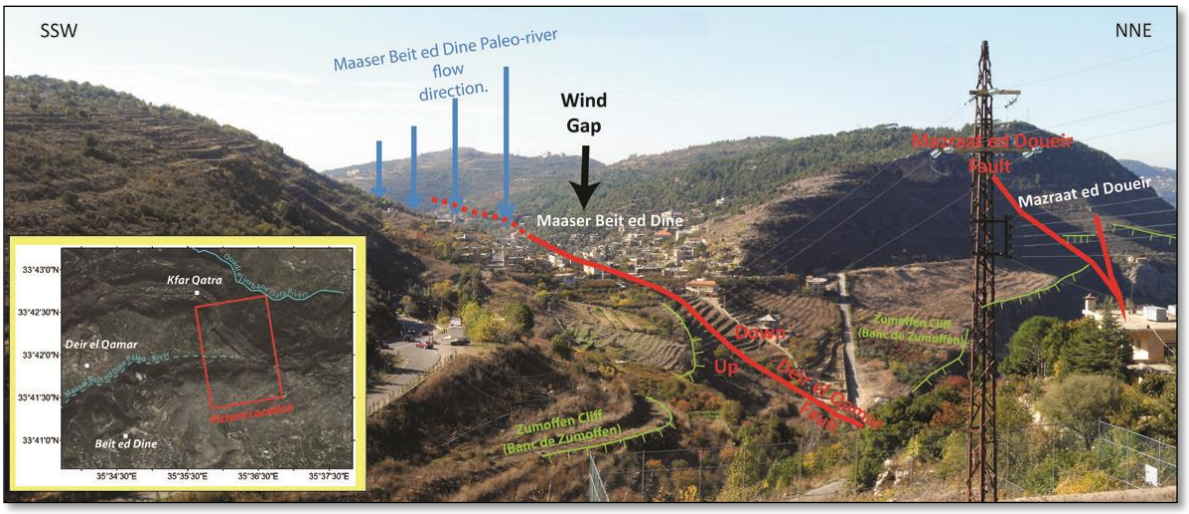

Figure 3.6: Panoramic view of the Maaser Beit ed Dine Wind, as it expresses itself in the topography. The inset map shows the location of this Wind Gap.

The Maaser Beit ed Dine tributary is a straight NE-SW segment with no important catchment area upstream (Fig. 3.1). Similar to the Jahliye River this is a seasonal river but unlike the later, it has no deep incision (profiles BB' Fig. 3.2 and EE' Fig. 3.3), and its riverbed lies on the bottom of a wide and shallow valley that opens to the east, as wind gap (Fig. 3.6), 460 m above the Safa River valley just north of Beit ed Dine. The Maaser Beit

ed Dine wind gap channel direction and position are well suitable to be considered as a paleo-channel of the upper Safa River that was captured by the headward erosion of a tributary of the lower Safa River near Maaser Beit ed Dine.

3.1.1.3. The Barouk River

The upper Barouk river system has a relatively simple N-S channel, oriented parallel to the Barouk Mountain and draining its western slope between the villages of Barouk north and Niha south (Fig. 3.1). The river flows in N to S direction, in contrast to most other rivers of the western flank of Mount Lebanon. It makes a sharp right angle turn to the west, downstream from Niha, as it enters the Bisri valley and keeps on this ~E-W flow direction until it reaches the Mediterranean Sea north of Saida. The river takes on different names -successively called Bisri and Awali Rivers- along its channel downstream (Fig. 3.1). The morphology of its drainage system is strongly related to the active tectonics and structures of the area as it intersects the major Roum Fault and Jezzine Anticline, but only the upper part (the Barouk channel) of this river system is included in our study area, and thus we will not discuss these features.

3.1.1.4. The Maaser ech Chouf Wind Gap

Another wind gap is also identified in the morphology of the studied area and associated with the drainage system of the Barouk River (Fig. 3.7). A flat bottom channel in the Dahr el Midane area trending parallel to the Barouk River west of Maaser ech Chouf, opens wide ~40m above the present day Ouadi Bou Jerios channel of the Barouk River at its NE end (Fig. 3.8). Its southern part seems to bend westward to connect with the Barouk

River downstream. The flat floor of the wind gap is covered with alluvial material remnant of old fluvial deposits, and is therefore suitable for agricultural activity that developed over this narrow and elongated parcel of land in sharp contrast with the landscape of the surrounding mountainous area. The position, shape and floor material of the wind gap leaves little doubt on its origin: the result of drainage deflection. The capture of the Ouadi Abou Qachqich channel headwaters flowing down the Ouadi Bou Jerios by the headward erosion of a tributary of the Barouk River implied the abandon of the Maaser ech Chouf palaeo-drainage (Figs. 3.7 and 3.8).

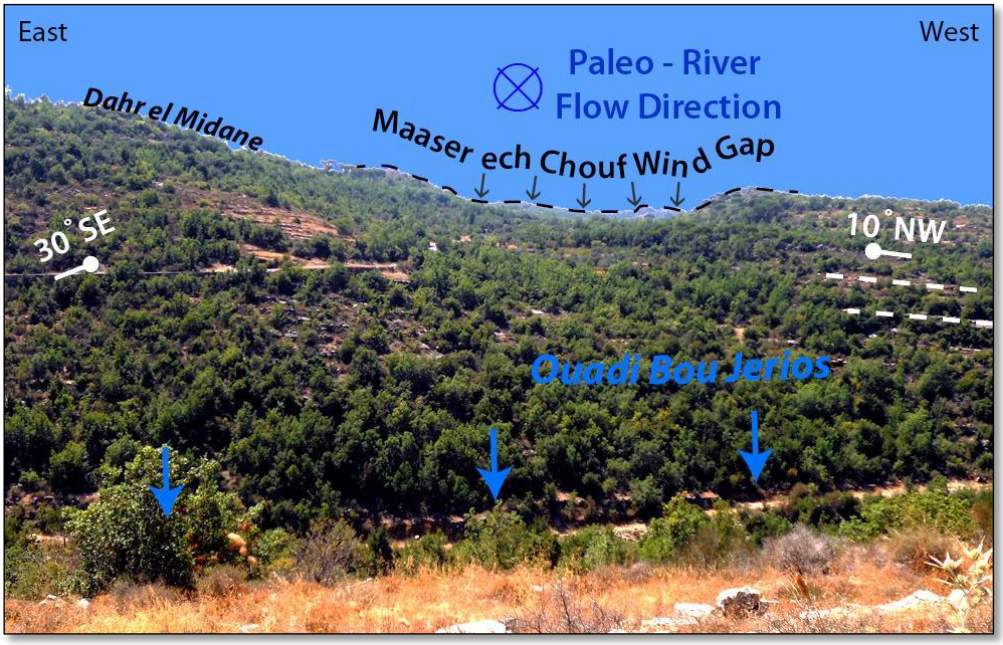

Figure 3.7: Panoramic View of the Maaser ech Chouf Wind Gap. Before the sufficient growth of the Maaser ech Chouf anticline to create river deflection the Maaser ech Chouf Paleo-river used to possibly flow southward as indicated by the blue symbol. The growth of the Maaser ech Chouf anticline (layering is not clear on this distant view due to vegetation) has possibly forced the Maaser ech Chouf river to leave its original channel and to capture the present day Ouadi Bou Jerios tributary, leaving a wind gap in the area (See location on Fig. 3.8).

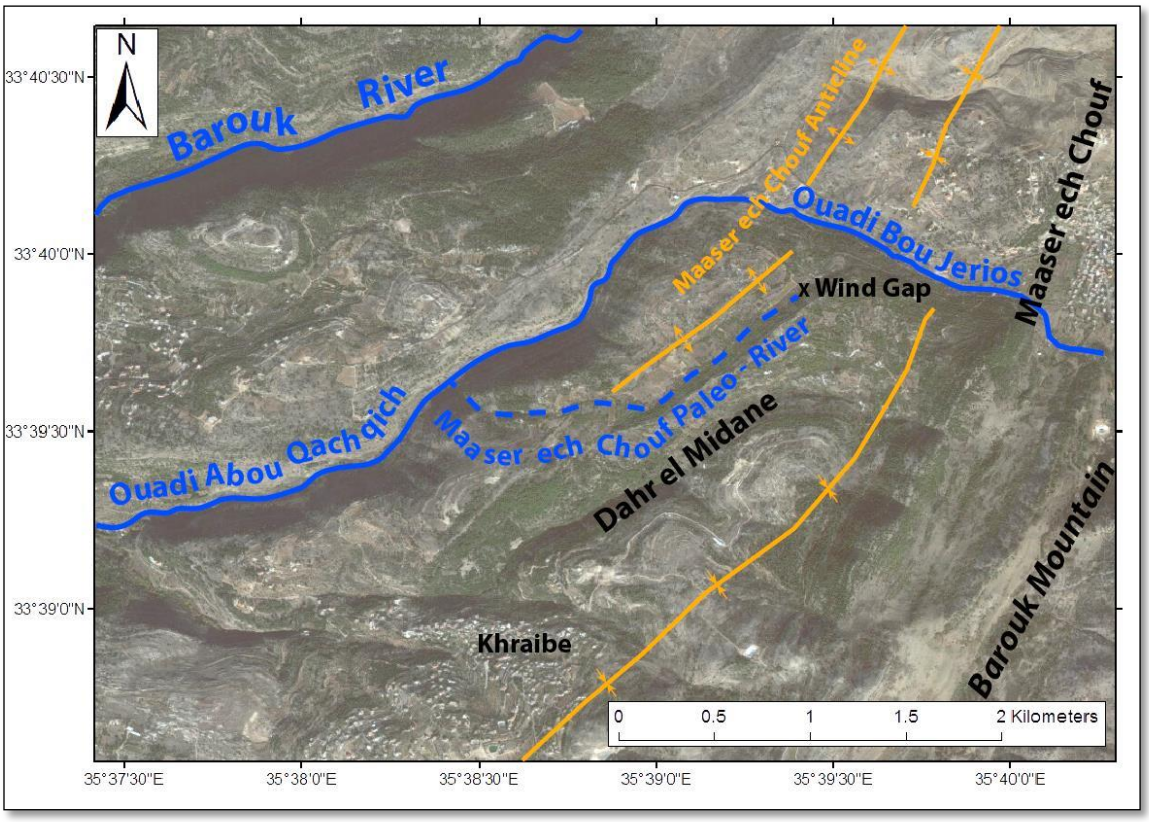

Figure 3.8: Map view of the Maaser ech Chouf Wind Gap, located at a great proximity to the hinge of the Maaser ech Chouf Anticline.

The position of the wind gap, located at the hinge of the Maaser ech Chouf anticline suggests a possible genetic relationship between the drainage geometry and the tectonics of the area (Figs. 3.7 and 3.8). First, the hinge extension may have played important role in localizing river incision and channeling of the runoff. The growth of the underlying anticline increased the vertical incision rate of the Barouk channel and its tributaries to the west at the same time when the uplift was putting the wind gap channel out-of reach of the headwaters. This ended in the capture of the Ouadi Bou Jerios waters

and the abandon of the Maaser ech Chouf channel. Thus it can be taken as a solid proof of the recent tectonic activity of the structures in the area.

3.1.2. Topography of the Area

The analysis of the topography of the area was done using available Digital Elevation Models (DEM) downloaded from SRTM service provided by the NASA website. The resolution of these grids is 30s, corresponding to about 90m for Lebanon. Two sets of topographic profiles (AA' to CC', and DD' to FF') oriented respectively perpendicular and parallel to the dominant structural (Yammouneh Fault) and topographic signal (coastline and Mount-Lebanon range) are executed for that purpose (Figs. 3.3 and 3.4).

At mid-elevation between the coastal area and the Barouk Mountain lies a terrain of complex morphology with different morphological characteristics north and south of the Beit ed Dine Fault (Fig. 3.1).

3.1.2.1. Topography South of Damour-Beit ed Dine Fault

To the south of Beit ed Dine, the eastward increase in elevation takes place through three distinct flat levels in a step-like geometry. The lowermost level is a slightly west-sloping terrain, connecting the coastal area with the rising mountainous relief to the east (Fig. 3.1). This level shows a gradual increase in elevation from 50m a.s.l at Jiye, but is best observed between 200 and 400m around Barja and Al-Borjein (Fig. 3.1 and Profile CC' of Fig. 3.2). It ends with an abrupt increase in the topographic gradient that coincides with an increase in structural westward dips of the geological layers over the Baawerta

Flexure. This marks the transition to the second higher, tabular plateau hanging at an elevation of ~ 750m-800m.a.s.l and extending eastward to Gharifeh (Fig. 3.1 and Profiles BB' and CC' of Fig. 3.2). The Jahliye River cuts through this surface just north of Gharifeh.

The topography starts building up again over the flexure of the Cretaceous layers of Jabal el Mazraa thus forming an eastward boundary for this second flat surface. A third higher flat surface hanging at an elevation of 1000-1200m.a.s.l (Fig. 3.1 and profile CC' of Fig 3.2) lies behind the flexure's top, stretching east to the feet of Barouk Mountain at Maaser ech Chouf (Fig. 3.1). This level is best described as a NNE-SSW elongated plateau. The area of Kafr Nabrakh and Ain Ouzain represents its northernmost extension. The Barouk River incises this surface along its length thus disrupting its flat morphology.

3.1.2.2. Topography North of the Damour-Beit ed Dine Fault

There is a clear difference in the topography and morphology of the coastal area North and South of the Damour River. The flat and tabular surface seen in the south disappears to the north where a gradually westward sloping surface connects the coastal plain with the inner-land up to elevations of around 500m.a.s.l. The decrease in the slope gradient becomes more evident as we move north into the Khaldeh coastal area (Fig. 3.1 and Profiles AA', BB' of Fig. 3.2).

An abrupt increase of the topographic slope, associated with Baawerta flexure demarks the passage to a higher geomorphologic domain that differs from its counterparts to the south of Beit ed Dine. Here the landscape consists of high relief area, with interfluves

dissected by the erosion of the Safa River's tributaries. A first set of hills culminates at ~800m.a.s.l.-900m.a.s.l. in the Deir el Qamar-Kfar Matta locality, traversed by "Ouadi ej Jerbane" which incises for ~700m in the topography. A second set is located more to the east at higher elevation (1050m.a.s.l.-1200m.a.s.l) carved by three upstream tributaries of the Safa River (Fig. 3.1). Each one of these sets seems to have a plateau like geometry which may be the equivalent of the flat surfaces seen on the southern side; however this is hard to confirm in such a highly faulted and eroded region (Fig. 3.1), especially in the absence of an abrupt topographic gradient change, which may suggest the transition from one level to the other.

Analysis of the topographic profiles DD' to FF' oriented NNE-SSW, and in particular profiles EE' and FF', shows a difference in elevation between the two topographic surfaces north and south of the Beit ed Dine fault. The northern side is consistently higher in elevation than its southern counterpart.

3.1.3. Landslides in the Southern Central Mt. Lebanon Area

Landslides are characterized by mass movement of rocks, debris and soil toward the lower part of a defined slope (Agliardi, 2012). These leave a clear geomorphologic signature in the topography materialized by an upslope detachement scar creating an anomaly in the topography associated with material depletion and downslope deposition of transported material (usually as debris cones or fans) characterized sometimes by transverse pressure ridges (Agliardi, 2012).

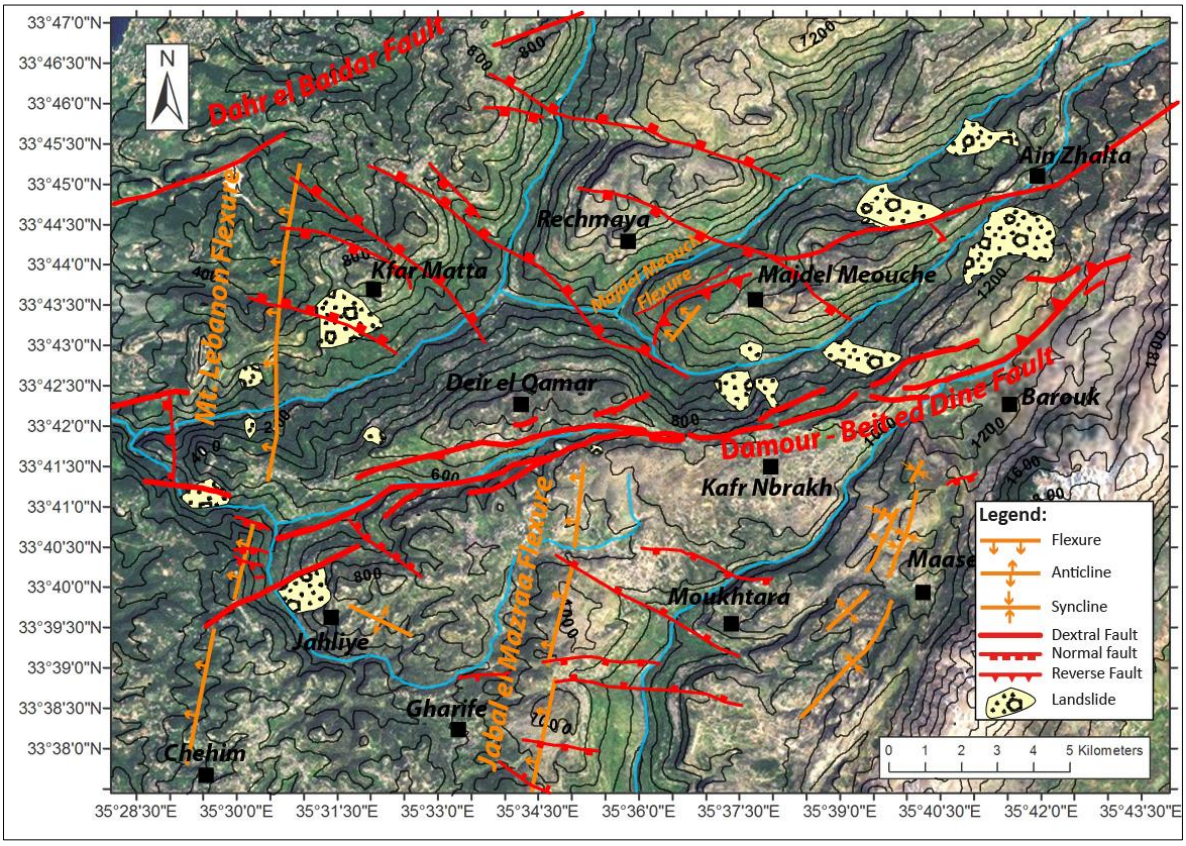

Figure 3.9: Satellite image of the southern central Mt. Lebanon, showing the mapped landslides of the area and their relation to the major geologic structures.

The morphologic signs of landslides make these easily discernable on aerial photos and satellite images. Based on these characteristics of landslides, a mapping of mass wasting in the southern central Mt. Lebanon conducted using aerial photography/satellite imagery, shows the geographical distribution of landslide features distributed in various parts of the study area, with some concentrated near the central region of the SCML, the limited by el Barouk to the east and Debbiye/Jahliye to the west (Fig. 3.9). In fact this area is traversed by the Damour-Beit ed Dine fault; thus landslides are located at a great

proximity to this structure, mostly to its north (Fig. 3.9), where the Safa River's incision exposes formations with weak lithologies, such as the C1 (Chouf Sandstone Formation). Many of these landslides show as Quaternary terrains on the geological map by Dubertret (1945). The most prominent example of mass movements in the SCML is the Kafr Nabrakh landslide (Fig. 3.10). This landslide shows obvious disturbance in the topography and geology of the area.

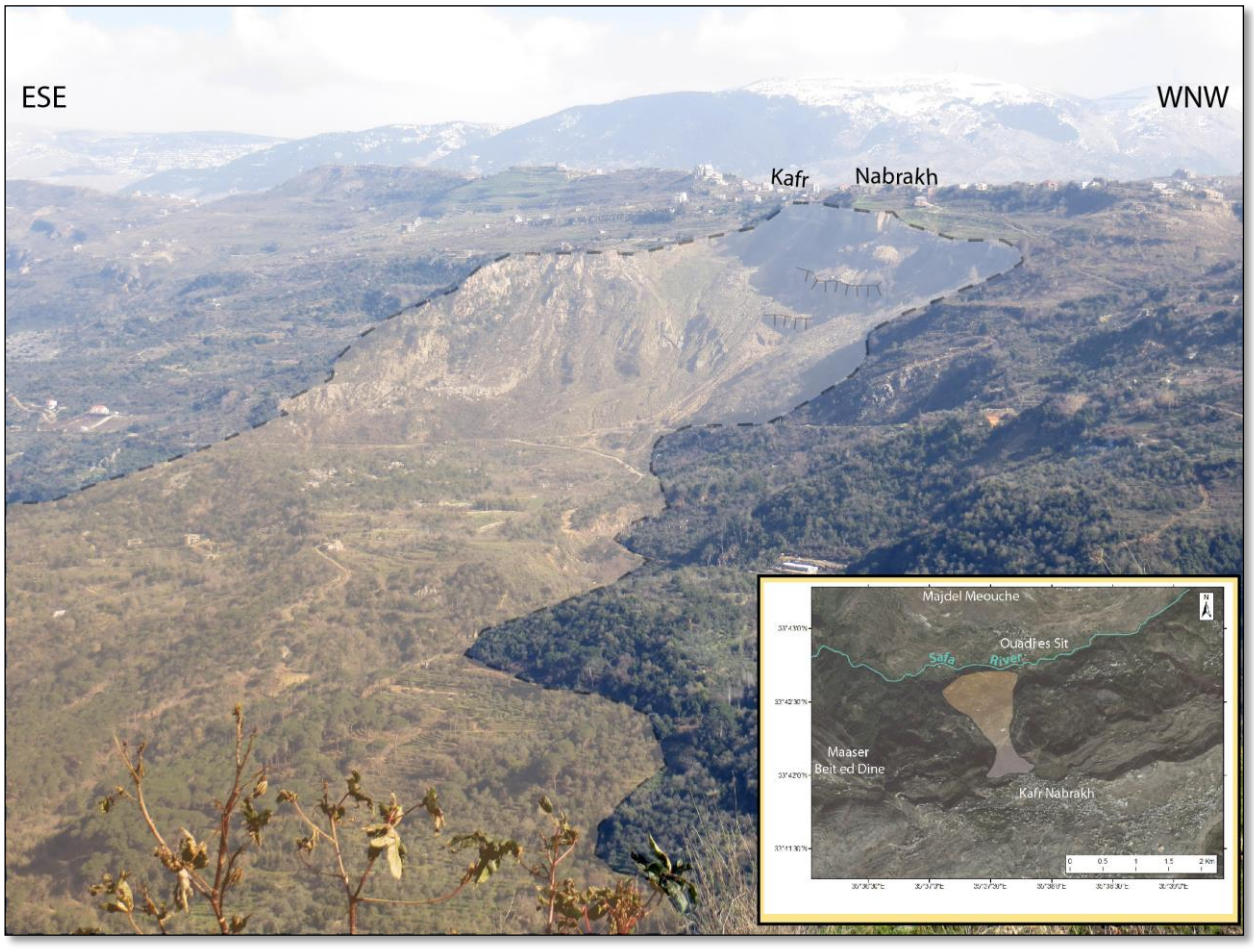

Figure 3.10: The Kafr Nabrakh landslide, an example of mass wasting in the SCML, mapped on the field and on satellite imagery.

3.1.4. Summary of Geomorphological Observations in the SCML Area

The eastward step-like increase in elevation and relief of the southern central Mt. Lebanon is correlated with monoclinal structures marking the transition between flat surfaces. This morphology is clearly exhibited in the area located south of the Damour-Beit ed Dine fault, characterized by localized drainages. The region north of the DBF is at higher elevation compared to the southern counterpart, denoting higher uplift rates to the north.

The drainage network of the southern central Mt. Lebanon is structurally controlled. Water flowing down the Barouk Mountain water divide, is transported toward the Mediterranean Sea via dendritic channel networks of several order drainages. The highest ranks tributaries are the major rivers of the study area. They flow along an overall ~WSW trend; however striking river deflections toward the N or the S are noticed whenever a major structural element is encountered. These structural elements are either monoclines/folds that act as barriers diverting the streams, or faults that act as planes of weaknesses along which these streams are channelized, forming localized bypasses for the surface waters through these barriers.

The Maaser Beit ed Dine Wind Gap is a consequence of the Safa River's tectonically controlled deflection around Maaser Beit ed Dine. Remarkably this wind gap is located at the intersection of the main branches of the Damour-Beit ed Dine fault system, which advocates a genetic relationship between this morphologic feature, the divergence of the Safa River and the activity of the Damour-Beit ed Dine Fault.

The Maaser ech Chouf wind gap is also a product of active tectonics, materialized by folding and uplift. This has influenced the flow scheme of Ouadi Bou Jerios and the Maaser Beit ed Dine drainage, secondary tributaries of the Barouk River.

Similarly the abandoned alluvial terraces flanking the Damour River are evidence of active folding and uplift of the southern central Mt. Lebanon, which has forced the Damour River to incise deeper in the topography to catch up with the base level. The landslides' geographic distribution along the Damour-Beit ed Dine fault may also reflect a direct causative relationship between these morphologic features and the Quaternary activity of the fault.

3.2. The Structural Map of the Southern Central Mt. Lebanon

The key structural elements of Southern Central Mt. Lebanon, previously identified are presented in chapter 2. Our field investigations combined with aerial photos/satellite images interpretation revealed the presence of a few previously unidentified folds and faults mapped on figure 2.11 that we present below.

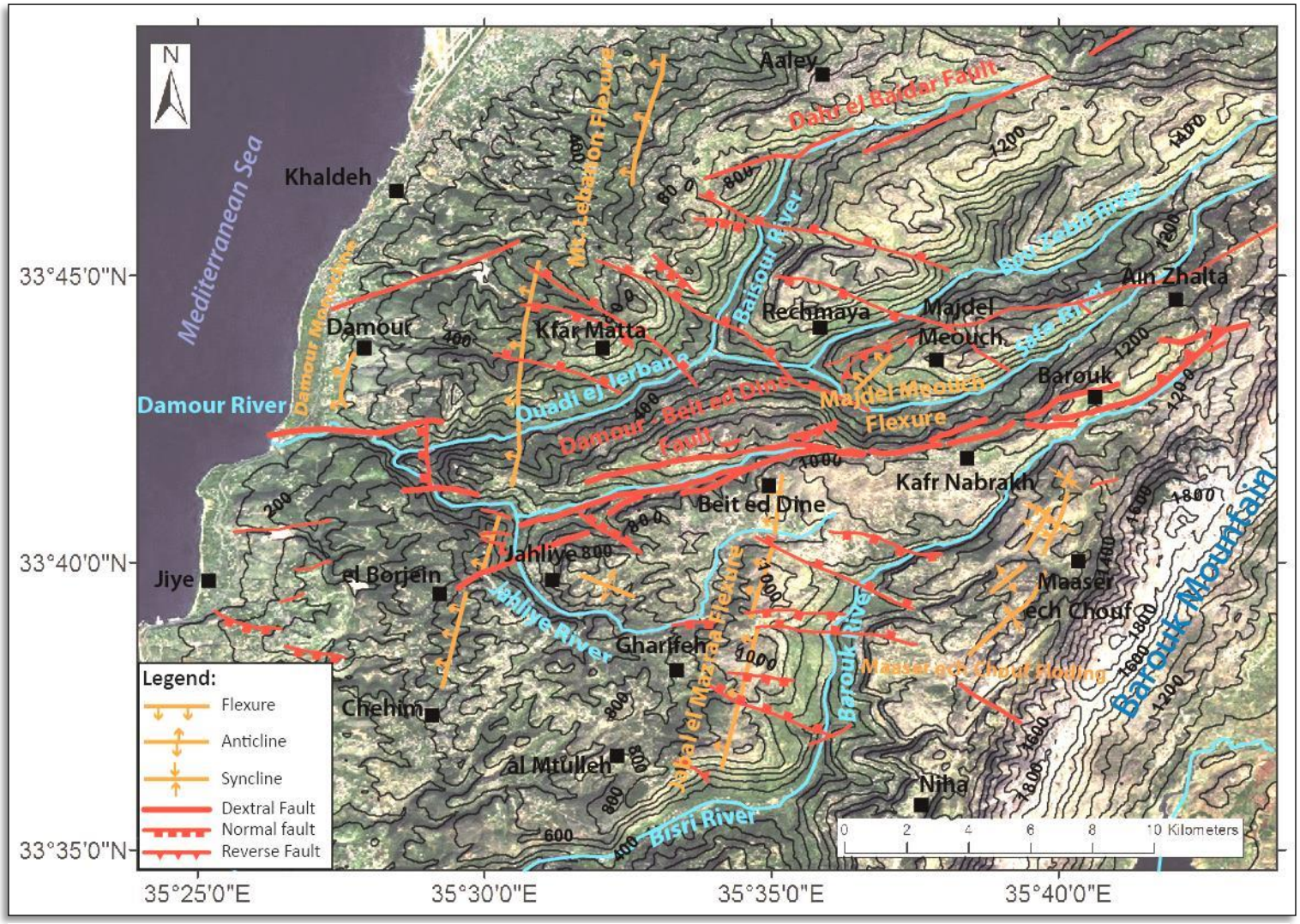

Figure 3.11: Structural Map of the southern central Mt. Lebanon, showing the mapped faults and folds, delineated on the field and satellite imagery/aerial photographs.

3.2.1. Folding of the Southern Central Mt. Lebanon

Additional folds indentified in this study are presented in this section and added to the structural map of the SCML (Fig. 3.11). These are:

3.2.1.1. The Damour Monocline

To start with, the Damour Monocline, a ~2Km structure is mapped in the Damour area, bounding the eastern side of the Damour Coastal Plain (Fig. 3.12). This monocline is seen as an abrupt change in the dip of the C6 strata. At an outcrop along the main Damour highway these layers have dip values of~73°W, unconformable capped by tabular quaternary alluvials (Fig. 3.13). Mapped on satellite images this monocline appears to follow a NE-SW trend and bends more to the east north of Damour (Figs. 3.11 and 3.12).

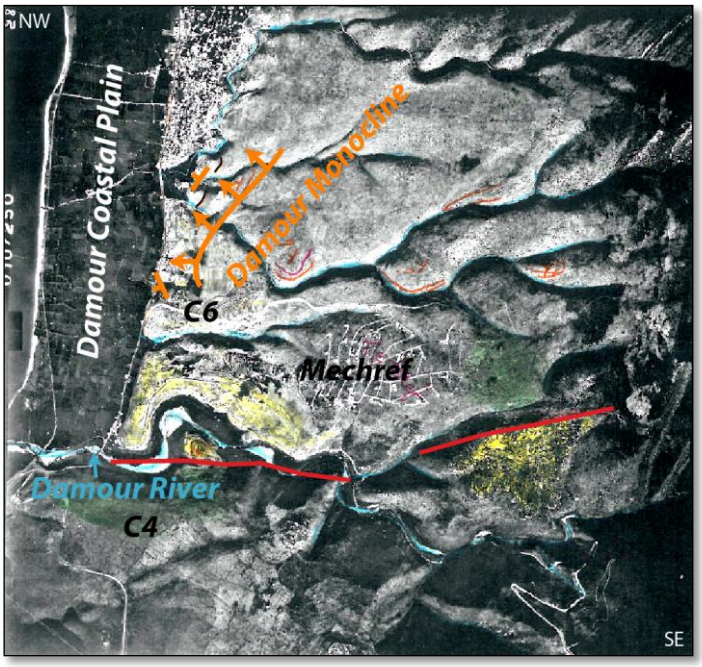

Figure 3.12: Aerial Photo showing the Damour Monocline (orange symbol) in the vicinity of the Damour coastal plain. The red line represents the Damour segment of the DBF.

Figure 3.13: The C6 (Chekka Formation) outcrop located at the side of the Damour Highway, showing the steeply dipping strata of the Damour Monocline. Notice the unconformable lying Quaternary alluvials, topping the C6 strata. (See Fig. 3.12)

3.2.1.2. The Jahliyeh Anticline

Located between Jahliye and Maaser Beit ed Dine rivers, the Jahliye anticline can be mapped in the Cenomanian strata where relatively gentle dips over its four closure directions can be seen (Fig. 3.14). The hinge line of this fold trends NE-SW and is thus different from all other known structures in the area (Figs. 3.11 and 3.14). The Jahliye River flows around this anticline in an almost semi-circular path before merging with the Maaser Beit ed Dine channel to the north (Fig. 3.14).

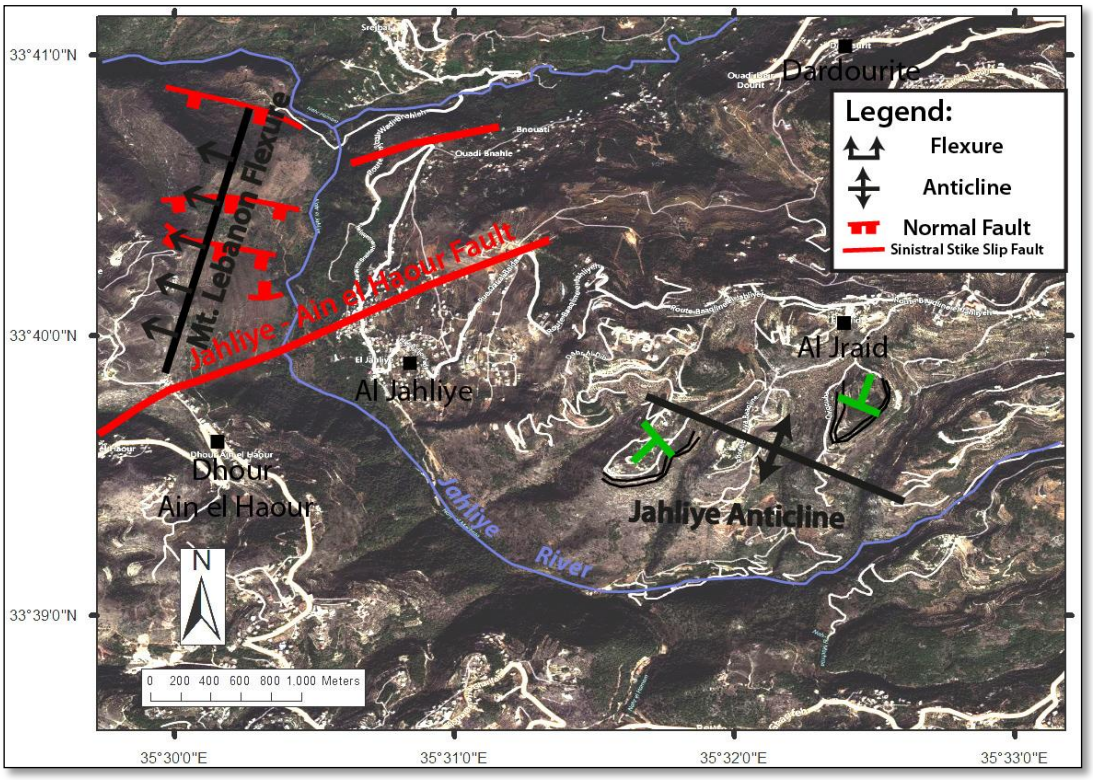

Figure 3.14: Satellite image showing the mapped Jahliye anticline and the semi-circular path of the Jahliye River around it.

3.2.1.3. The Gentle Warping Along the Ouadi es Sit/Safa River Valley

Gentle warping is also clear in Majdel Meouche-Ouadi es Sit area (Fig. 3.15). Taken as reference the massive cliff forming units of the Mdeirej Formation (C2b) show long wavelength, short amplitude undulations along Safa River. These gentle folds are also frequently offset by the different faults in the area making it difficult to estimate their exact orientation, and are considered to trend N-S to NNE-SSW.

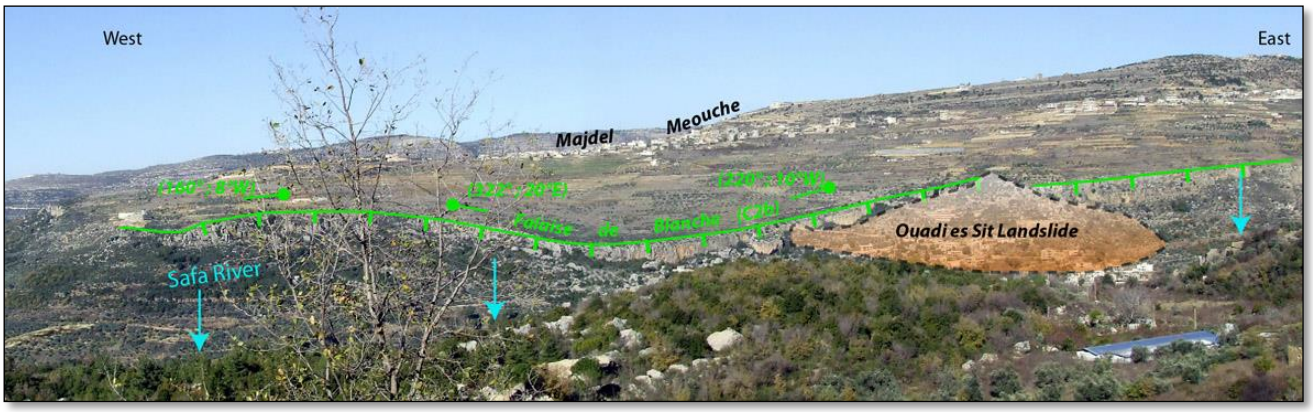

Figure 3.15: Panoramic view of Majdel Meouche (looking north), showing gentle warping in the mapped Falaise de Blanche marker cliff. (Width covered by the picture is 2Km).

3.2.1.4. The Jabal el Mazraa and Maaser ech Chouf Folds

A close inspection of the Maaser ech Chouf-Gharife area revealed the existence of a broad and asymmetric fold associated with the Jabal el Mazraa Flexure previously described (Chap 2). In fact the Flexure, first presented as a west dipping monocline, is the steeply west-dipping forelimb (dipping 35˚- 40˚W) of this asymmetric structure. The gently east dipping strata of the backlimb (dipping less than 10˚E) merge to the east with the tight Maaser ech Chouf Folds described in Chapter 2. Structural mapping suggest that the hinge line of the Maaser ech Chouf fold anticline has a NNE-SSW trend and is located east of the Barouk river channel (Fig. 3.11).

Further to the east in the area between Maaser ech Chouf north and Niha south, the eastward dip values of the layers increase as they go into a series of anticline and syncline with axes trending NNE-SSW between Jabal el Mazraa anticline to the west and the Barouk Monocline to the east (Fig. 3.11).

3.2.1.5. Interpretation

Most of the newly identified folds have a structural orientation along a ~NNE-SSW axial direction compatible with those previously described for other structures within the study area and also at the scale of Lebanon. For example, this is the strike of the Yammouneh Fault and the Lebanese Flexure as well. Therefore, these newly mapped structures are related to the main ~NE-SW compression that generated the large compressive structural elements of Lebanon as a result of the compressive component of the transpression on the Lebanese restraining bend and the consequent uplift of Mt. Lebanon.

The Jahliye anticline oriented WNW-ESE is an exception. It may be probably related to an older compressive tectonic phase, predating the Late Miocene-present one, during which the compressive stresses were oriented differently (NNE-SSW). No other similarly trending structure is identified within the study area.

The clear asymmetric geometry of the most prominent structures in the area (Jabal el Mazraa anticline, Damour and Jahliye/Ain el Haour Flexures) suggest the presence of speculative blind thrusts or reverse faults in the subsurface, responsible for these structures. Moreover, the mapping of the large number of anticlines and synclines leaves no doubt that the southern central Mt. Lebanon, previously believed to be a tabular terrain (Heybroek, 1942 and Dubertret, 1945), is in fact a dominantly folded zone where active shortening is taking place.

3.2.2. Faulting in the Southern Central Mt. Lebanon

Two fault systems are observed in the southern central Mt. Lebanon area and were described in chapter 2. The first is embodied by the ~E-W Damour-Beit ed Dine fault (DBF); the second is materialized by smaller scale NW-SE striking faults located on both sides of the DBF. In this section we provide our recent observations and remarks on these structures.

3.2.2.1. The Damour-Beit ed Dine Fault System (DBF)

The Damour-Beit ed Dine fault system consists of a splay of sub-latitudinal faults that extend between el Barouk and el Damour/Jiye (Fig. 3.11). Re-inspection of this structure revealed several related geologic observations provided here from west to east.

3.2.2.1.1. The Jahliye-Ain el Haour Fault

Available geological mapping (Heybroek, 1942; Dubertret, 1945) of the Jahliye-Borjein area suggests that the DBF in the area has two sub-latitudinal, left-stepping fault branches (Beit ed Dine Fault and Jahliye-Ain el Haour Fault) before disappearing in the Mt. Lebanon Flexure to the west at Ain el Haour (Figs. 3.11 and 3.16). Other Lower Cretaceous minor normal faults also associated with these two branches are developed in the lower Cretaceous units and possibly disappear in the Cenomanian Sannine Formation (see section 3.5 for the relation between normal and strike slip displacements on the DBF segments). Right-lateral offset of the geology associated with the two major E-W branches is visible in

the lower Ouadi Beit ed Dine (Dubertret, 1945). The C1/C2a boundary is offset by around 1km by the Beit ed Dine Fault (Fig. 3.17).

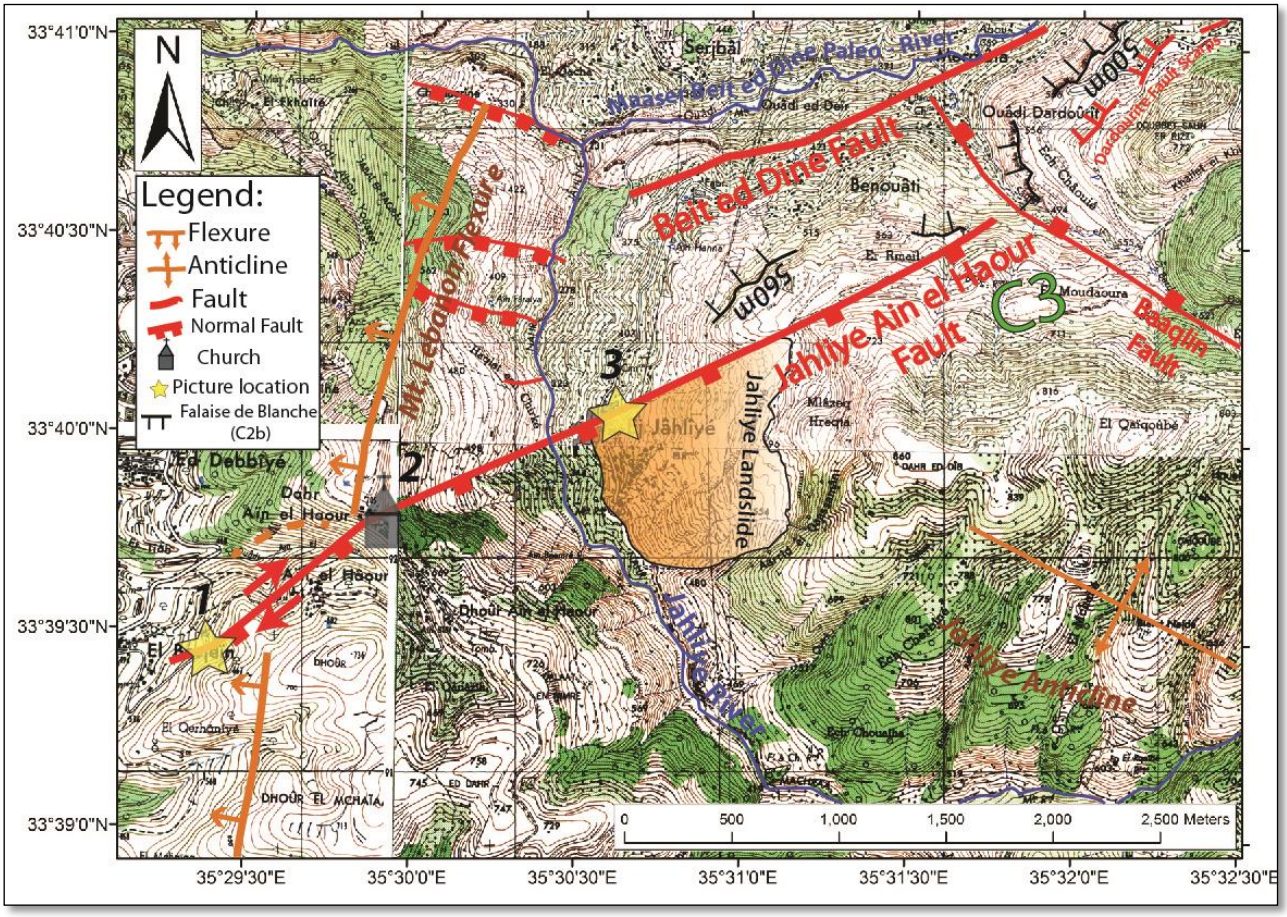

Figure 3.16: Topographic map showing the Jahliye-Ain el Haour Fault as it steps to the left from the Beit ed Dine Fault. Notice the right-lateral offset of the Mt. Lebanon Flexure by this structure.

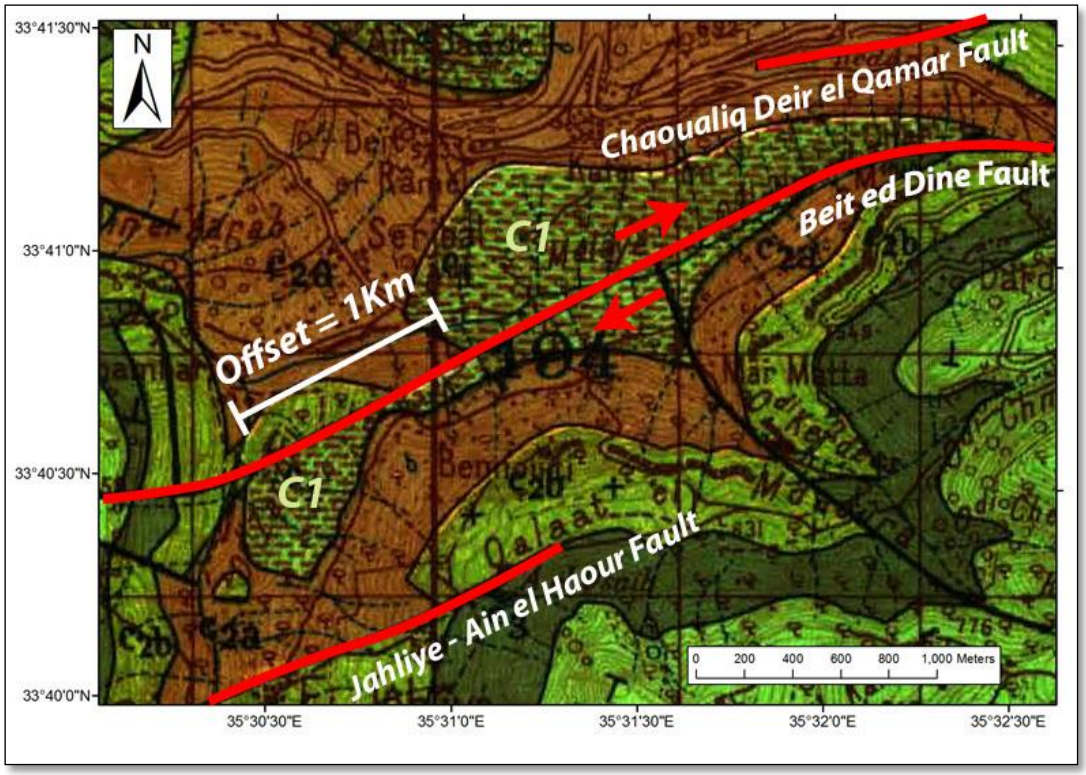

Figure 3.17: Geologic map showing the 1Km right-lateral offset of the C1/C2a boundary by the Beit ed Dine Fault as it passes through Ouadi Beit ed Dine.

Figure 3.18: Panoramic View of al Jahliye, showing the Jahliye-Ain el Haour Fault as it juxtaposes the C3 and C2b. This fault passes on the northern boundary of the Jahliye Landslide. (See location 3 of Fig. 3.16).

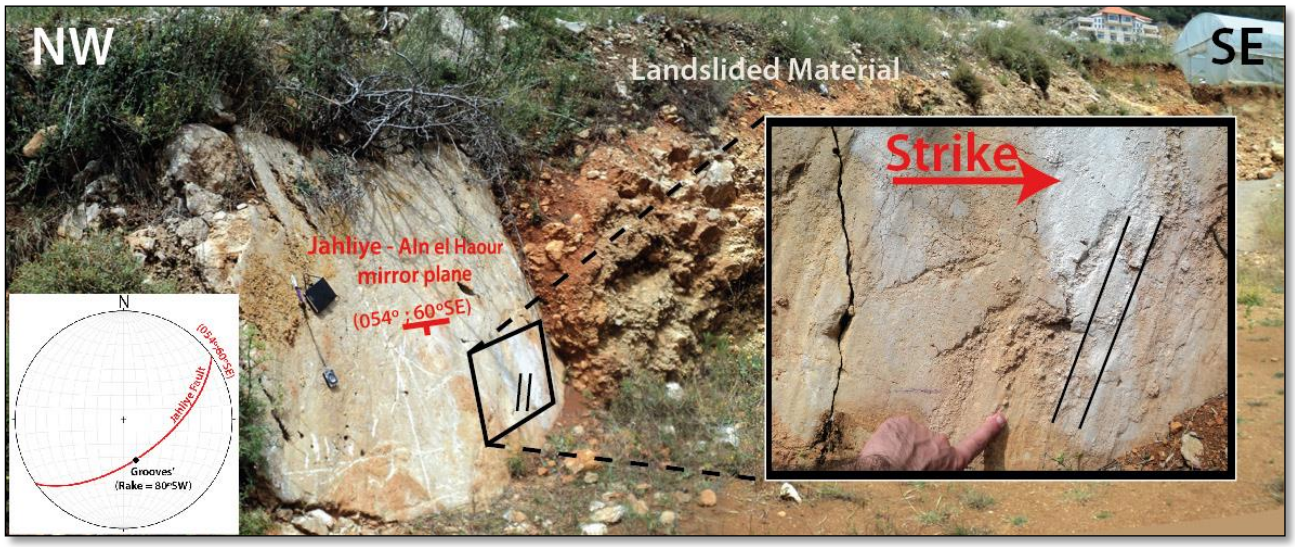

Figure 3.19: A close view of the Jahliye-Ain el Haour Fault as it passes near the Jahliye Town-Hall. Notice the oblique lineaments on the fault plane's surface, raking 80˚SW as indicated on the inset stereonet (See location 3 of Fig. 3.16).

The trace of the southernmost of these two branches (Jahliye-Ain el Haour Fault) cuts the topography and structure of the northwestern flank and pericline of the Jahliye anticline, northeast of Jahliye village. Detailed geological observations were possible at two different locations along this fault (Fig. 3.16). A first site located near the town hall of Jahliye village (Fig. 3.18), where recent site preparation work uncovered a fault plane, between hard limestone of the Mdeirej formation to the north and unconsolidated alluvium from a large landslide area to the south. The fault plane with a strike of 054° and a dip of 60°SE is smooth with grooves and lineations raking 80°W (Fig. 3.19).

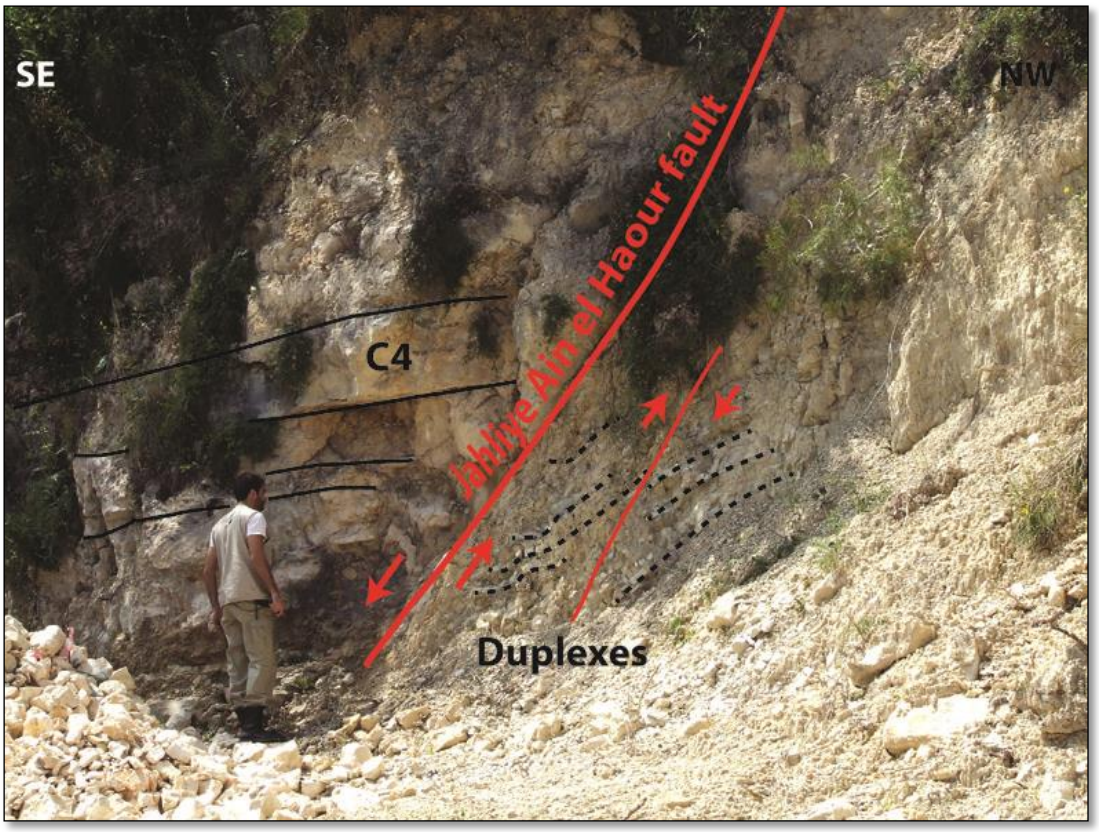

Figure 3.20: The Jahliye-Ain el Haour Fault as it passes in El Borjein creating a 15m wide fault zone. Small scale duplexes are seen within this fault zone. (See location 1 of Fig. 3.16).

At a second site located more to the west, on the roadside from El Borjein to Ain el Haour, a 15m wide fault zone in Cenomanian layers, with two mirror fault planes striking N60˚E and dipping around 70°SE is observed (Fig. 3.20). The limestone beds caught between these mirror planes are deformed by tight folding and fractures. Some of the faulting suggests a reverse component with small-scale duplexes (Figs. 3.20 and 3.21).

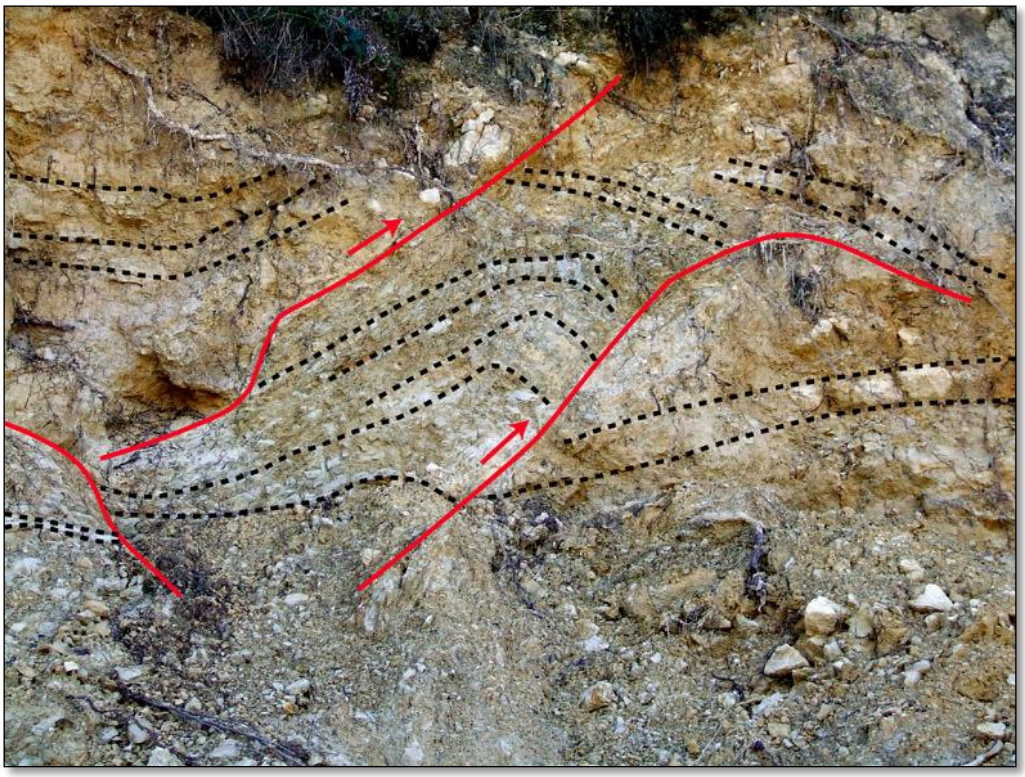

Figure 3.21: Close view of the thrust duplexes seen within the Jahliye-Ain el Haour fault zone at el Borjein. (See location 1 on Fig. 3.16).

Mid-way between the two sites, in the Dhour Ain el Haour area located over the Mt-Lebanon Flexure, a steep SE dipping piercement of the Jahliye-Ain el Haour fault, east side down is observed. The topography seems to be affected by the dip-slip component of this fault as the east side (the hanging-wall) appears to be slightly at lower elevation (Fig. 3.22) than the west side (the foot-wall). The Flexure is also dextrally offset by this fault by around 500m (Fig. 3.16).The faults observed in Jahliye (Fig. 3.18) and east of el Borjein (Fig. 3.20) have similar strikes. On map view they are also aligned with the trace of the Dhour Ain el Haour fault and thus are considered to be of the same fault trace: the Jahliye-Ain el Haour fault segment.

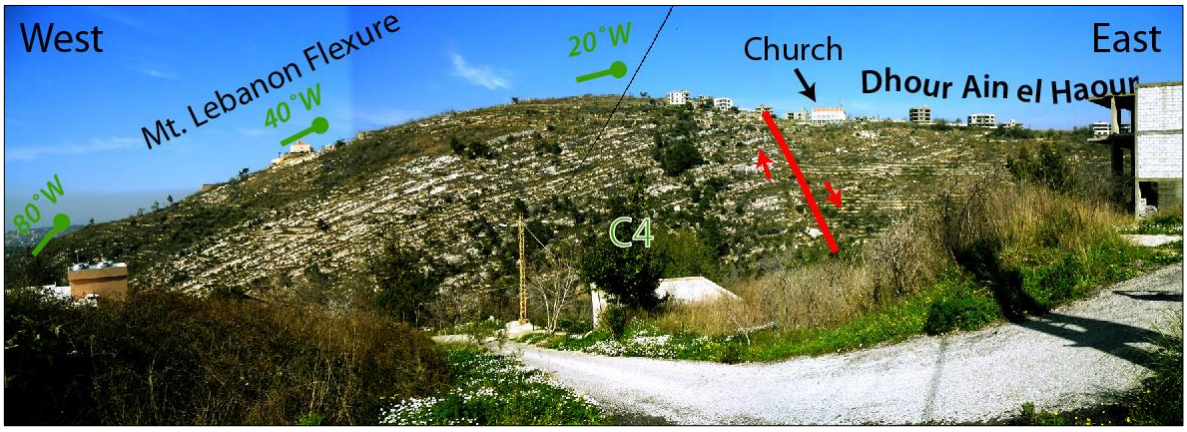

Figure 3.22: Panoramic view of Dhour Ain el Haour, showing the Jahliye-Ain el Haour Fault (Red) as it passes at a proximity to the Dhour Ain el Haour Church (See location 2 on Fig. 3.16).

3.2.2.1.2. The Dardourite Escarpments

Dardourite is located on the left side of the Maaser Beit ed Dine valley along the road leading from Baakline to Deir el Qamar (Fig. 3.23). The geologic succession of the layers from the Chouf Formation to the Sannine Formation can be clearly followed from base to top of this slope surface. At around mid-elevation along this face, is a clear break in the topography forming~15m high cliff, aligned in a NE direction over ~1.5Km (Fig. 3.23). This escarpment is made of four segments with the same orientation and elevation, covered by thick vegetation and with houses built on top of them preventing direct inspection. Stratigraphically, these escarpments are located above the cliff-forming Mdeirej formation and thus could not be mistaken with it (Fig. 3.24).The possible cliff-forming contender for such a stratigraphic position at the boundary between the C2b and the C3 formations is the Banc de Zumoffen. However, the latter is not as expressed in the local stratigraphy and topography. No other examples of cliff forming units in the C3 formation are known from

the area, however one cannot rule out the possibility that these escarpments are the result of a small local cliffy unit in the stratigraphy of the region. Another possibility, given the sharp and linear trace of these cliffs in the morphology, parallel to that of the DBF in the area and also aligned with the fault trace observed in Jahliye and Dhour Ain el Haour (Fig. 3.23). They can thus represent a possible cumulative escarpment of a previously unidentified fault branch of the DBF. More work is needed in order to assess which of the two interpretations is the correct one.

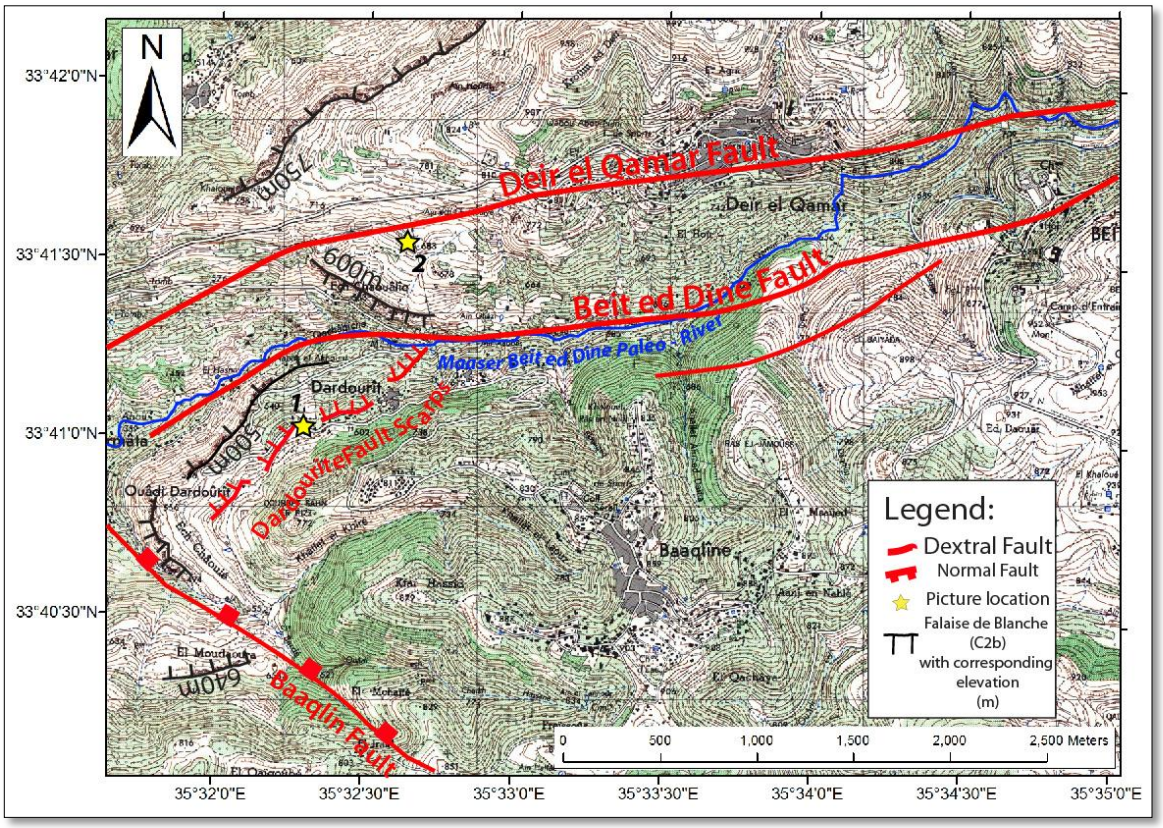

Figure 3.23: Topographic Map of the Dardourite-Chaoualiq Deir el Qamar area, showing the Deir el Qamar / Beit ed Dine faults, the major branches of the DBF, and the Dardourite fault scarps, a secondary branch of the DBF parallel to the main structures.

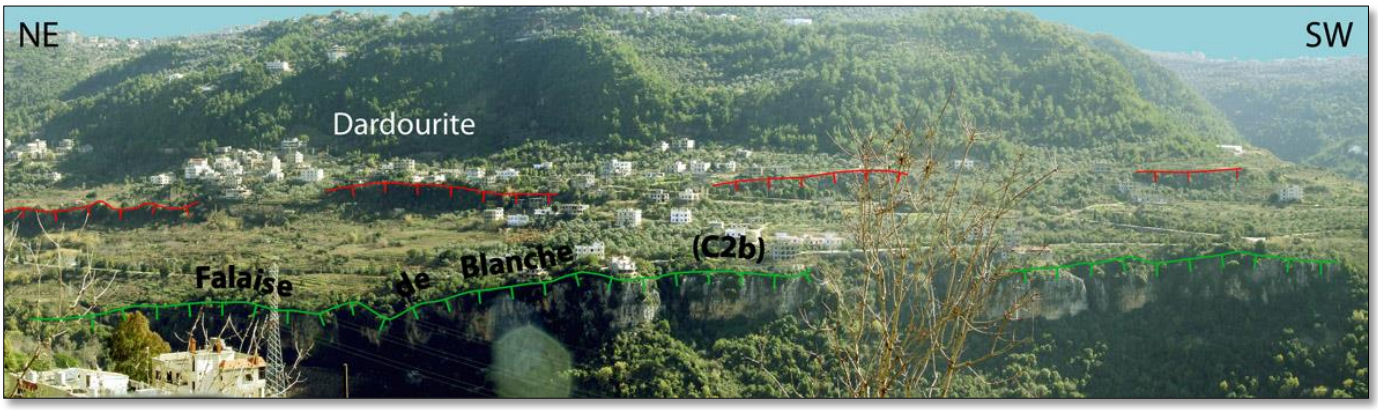

Figure 3.24: Panoramic view of Dardourite, showing the Dardourite fault scarps(Red) as they express themselves in the topography of the area (See location 1 on Fig. 3.23).

3.2.2.1.3. The Deir el Qamar Fault Scarp

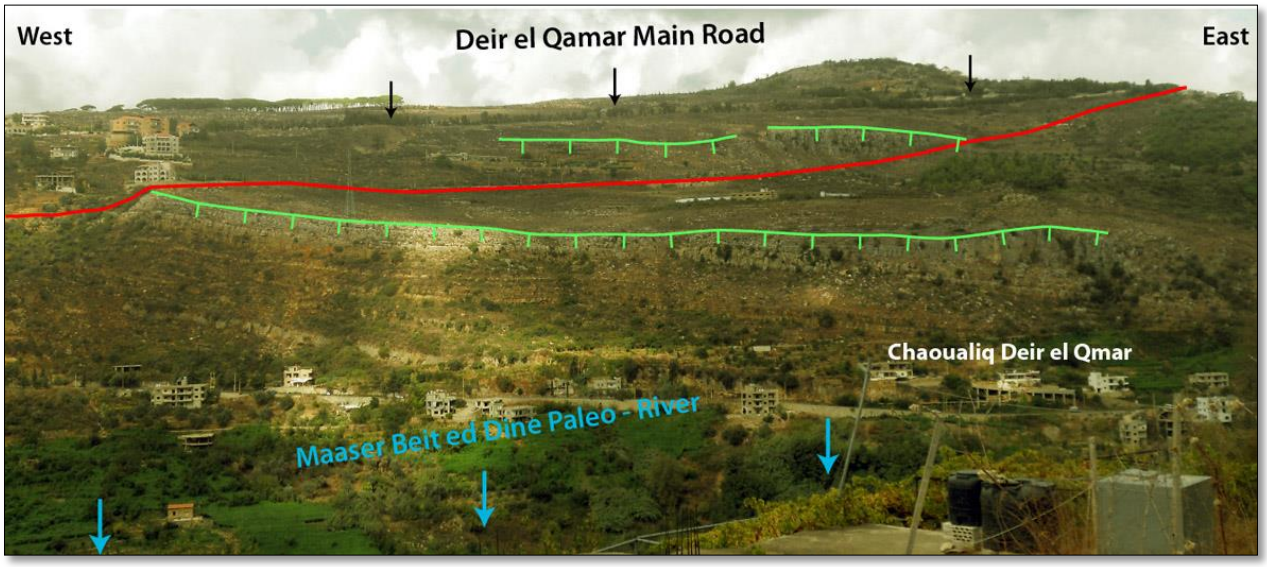

Figure 3.25: Panoramic view of Chaoualiq Deir el Qamar, showing the Deir el Qamar Fault (Red) as it offsets the Mdeirej Formation, resulting in a duplication of the Falaise de Blanche cliff (Green). The width covered by this picture is around 750m (See location 2 on Fig. 3.23).

On the northern side of the Maaser Beit ed Dine valley, west of Deir el Qamar, in the area called Choualiq Deir el Qamar, a duplication of the "Falaise de Blanche" layer of the Mdeirej Formation clearly signals the presence of the Deir el Qamar fault (Figs. 3.23 and 3.25). The characteristic cliff can be seen tabular towards the top with its offset, eastward tilted lower counterpart, 150m below close to the valley bottom (Fig. 3.23). Here the vegetation is not dense, and direct investigation of the upper cliff-face was possible. From a distance in the field and on satellite imagery one can see over ~500m, a linear light colored zone that starts at the base of the cliff to the east and cuts down slope, away from the "Falaise de Blanche" with a strike of ~080˚E (Fig. 3.26). It also corresponds to subdued and weathered cliffs with a break in the topography. Adjacent to this major linear rupture runs a minor rupture which nearly mimics the major structure, with slight bending toward the NW. This minor rupture leaves in the topography another small weathered cliff which dips around 65-72°S (Fig. 3.27). Close inspection of this linear structure revealed the presence of smoothed surface in a number of places at its base, with marks of striations raking 35-40°SW (Fig. 3.27). Thus we interpret this slope break and cliff to be the surface expression of the Deir el Qamar fault. Its light colored, smoothed and striated base can be the remnants of the free face of the last earthquake rupture that happened on this fault.

Right-lateral geological separation is also observed along the Deir el Qamar fault in the Choualiq Deir el Qamar area where the mapped C2a-C2b contact is offset right-laterally by ~1km (Fig. 3.28). The relative importance of the vertical to horizontal apparent displacements observed along this fault is compatible with the rake of the lineations

measured over the free face of the fault scarp mentioned earlier and with a normal oblique, right-lateral kinematics of this fault.

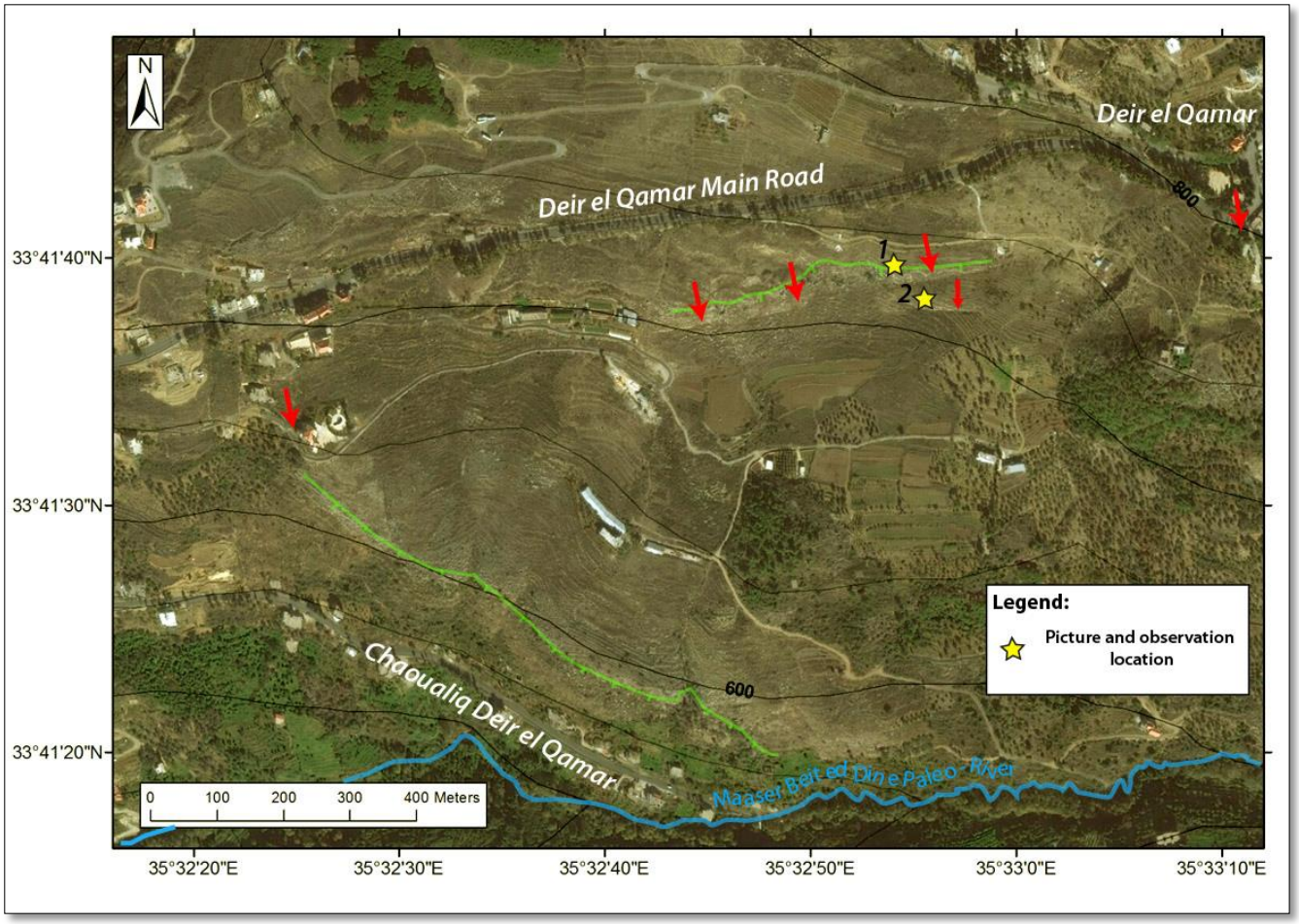

Figure 3.26: Satellite image of the Chaoualiq Deir el Qamar area, showing the Deir el Qamar Fault (Red arrows) as it offset the Falaise de Blanche (Green) and creates a fresh fault rupture in the topography. (See location 2 on Fig. 3.23).

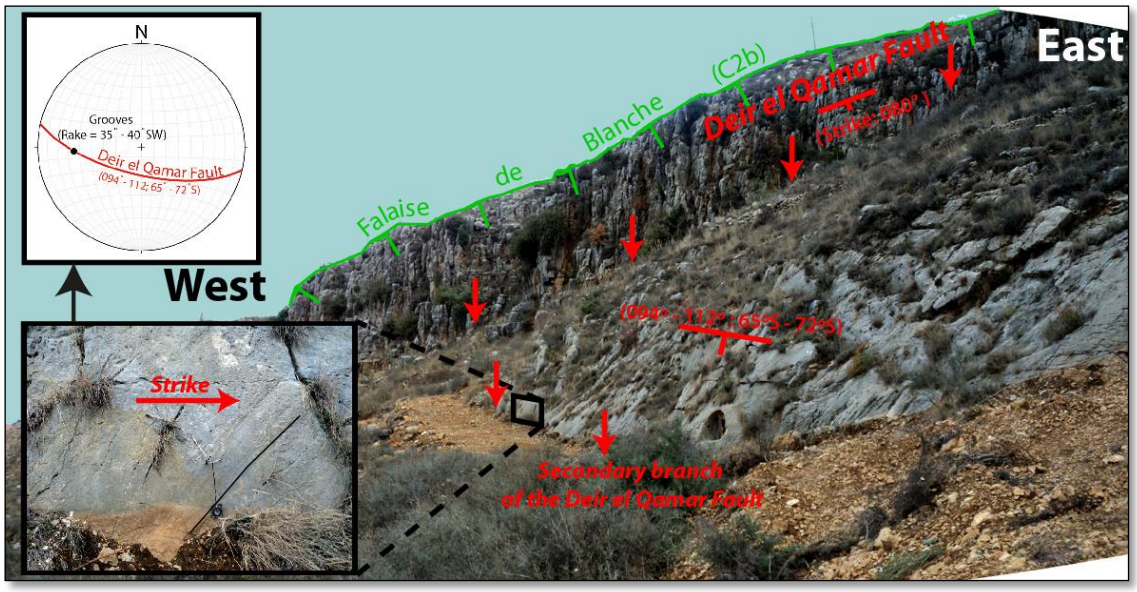

Figure 3.27: Close view of the Chaoualiq Deir el Qamar Fault scarp. The Deir el Qamar Fault clearly offsets the C2b Cliff (See Location 1 on Fig. 3.26). A secondary fault branch passes at a small angle few meters to the south of the major structure, creating an obvious fault plane (See Location 2 on Fig. 3.26). Notice the lineaments on this fault surface.

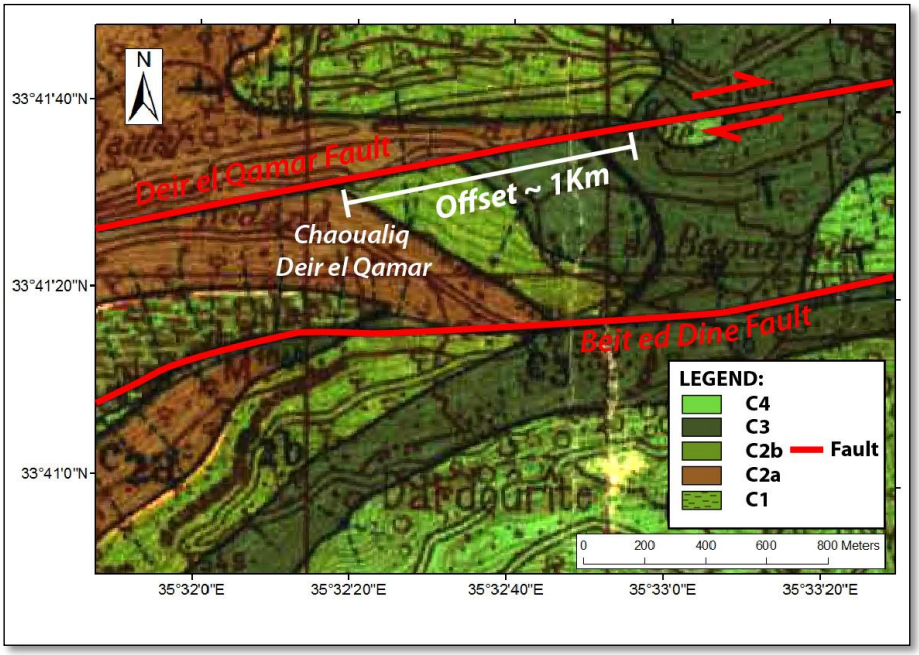

Figure 3.28: Geologic map of the Chaoualiq Deir el Qamar area, showing the right-lateral offset of the Deir el Qamar Fault (Dubertret, 1945).

Finally, in the Barouk-Ain Zhalta area, the Damour-Beit ed Dine fault bends toward the NE (Dubertret, 1945). This change in direction is accompanied by a change in the shape of the fault, where it becomes convex eastward (Fig. 3.11).

3.2.2.2. The NW-SE Faults of the Southern Central Mt. Lebanon

A set of NW-SE faults is observed on both sides of the Damour-Beit ed Dine fault. To the north of the study area, these are long, extensive and abundant. To the south, however these are shorter and confined to narrower areas on the geologic/structural map (Fig. 3.11).

In the absence of clear outcrops on the field that would enable direct measurements of their attitudes, we based our interpretation on the overall geometry of the mapped fault traces.

To the north of the Damour-Beit ed Dine fault, these NW-SE structures exhibit an oblique-slip mode of displacement. Their dip-slip component is normal as constrained by offset of geologic marker beds (Banc de Mreijat (C2a), Falaise de Blanche (C2b) and Banc de Zumoffen (C3)). Furthermore, this vertical displacement is associated with growth faulting indicated by noticeable thickening on the downthrown block, of the stratigraphic member located between the Falaise de Blanche and the Banc de Zumoffen. On the other hand, the horizontal slip component is depicted to be left-lateral as constrained by offset of the geologic boundaries on Dubertret (1945) geologic map and compared with our mapping.

Examples of NW-SE faults located to the north of the Damour-Beit ed Dine fault include:

3.2.2.2.1. The Bire Fault

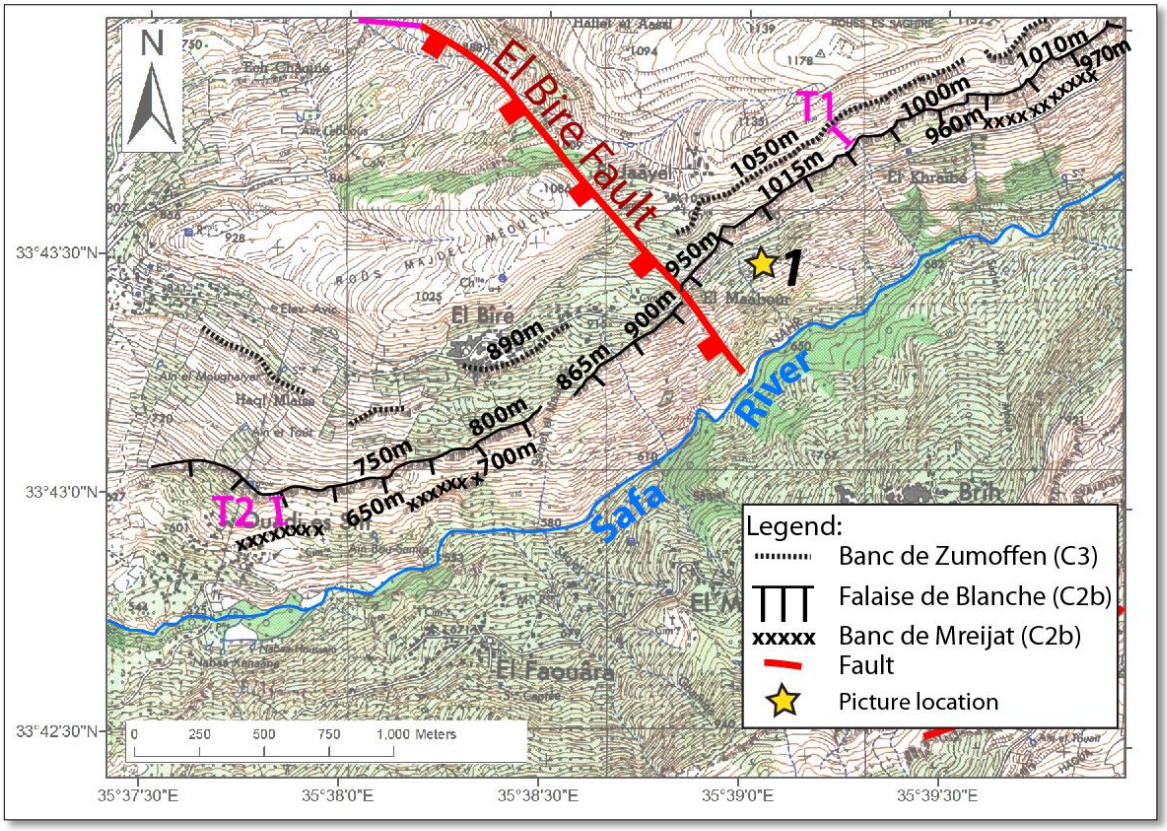

Figure 3.29: Topographic Map of the Bire area, showing the mapped Bire fault and its corresponding offset. The difference in displacement for the different marker cliffs suggests growth faulting.

It is a N140°E striking (Fig. 3.29), steeply dipping normal fault (Figs. 3.29 and 3.30). It vertically offsets the Falaise de Blanche for 50m (Fig. 3.29). Like most of the faults in this region, important change in the thickness of lower Cretaceous layers can be observed astride these faults thus indicating the Mesozoic age of the structures. We take the

Bire Fault as an example to highlight the importance of the change in thickness of these layers across the faults. From available geologic and topographic documents and satellite imagery we measure the thickness of the strata between the following characteristic markers:

- The Banc de Zumoffen and the Falaise de Blanche (T1),
- The Falaise de Blanche and the Banc de Mreijat (T2)
- The sum (T3) of the entire thickness between the Banc de Zumoffen and the Banc de Mreijat, for both blocks astride the Bire Fault (Fig. 3.29) are calculated and summarized in Table 3.1.

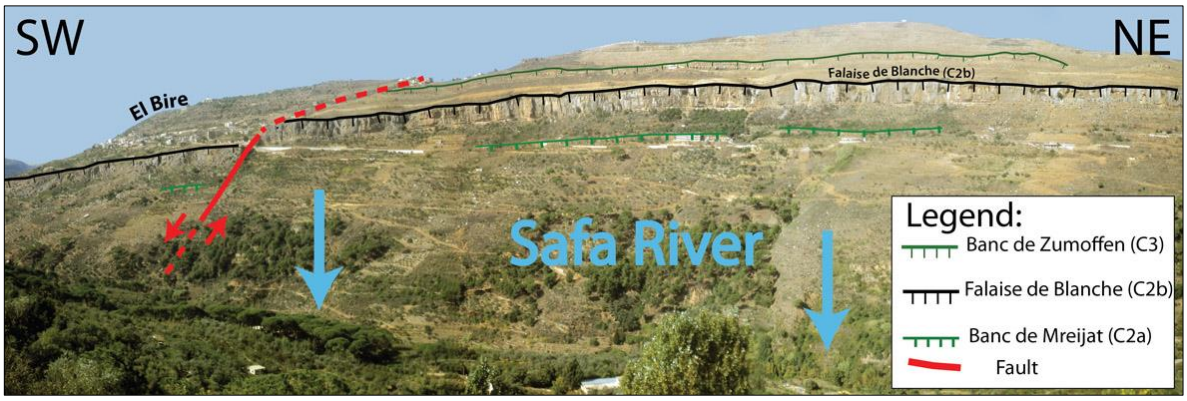

Figure 3.30: Panoramic view of the Bire area, showing the steeply dipping Bire fault and its effect on the geology. (See location on Fig. 3.29)

In the vicinity of the Bire fault the thickness variation of T1 is negligible (~35m) but becomes important to the west where T1 values become ~90m on the hanging wall block (Table 3.1).

As for T2, it shows a 10m increase in thickness on the hanging wall side compared with the footwall (Table 3.1).

In sum T3 = T1 + T2 shows an increase in thickness on the hanging wall, ranging between 10m and 65m in less than few tens of meters in distance (Table 3.1 and Fig. 3.29).

Table 3.1: Summary of thickness values of T1, T2 and T3 measured astride the Bire Fault.

T1, T2 or T3	**Hanging Wall Block**	**Foot Wall Block**
T1	35m – 90m	35m
T2	50m	40m
T3	85m – 140m	75m

In addition to this Mesozoic-old vertical normal separation, the Bire Fault depicts around 80-100m sinistral strike-slip separation of the C2a-C2b boundary on the geologic map of Dubertret, 1945 (Fig. 3.31).

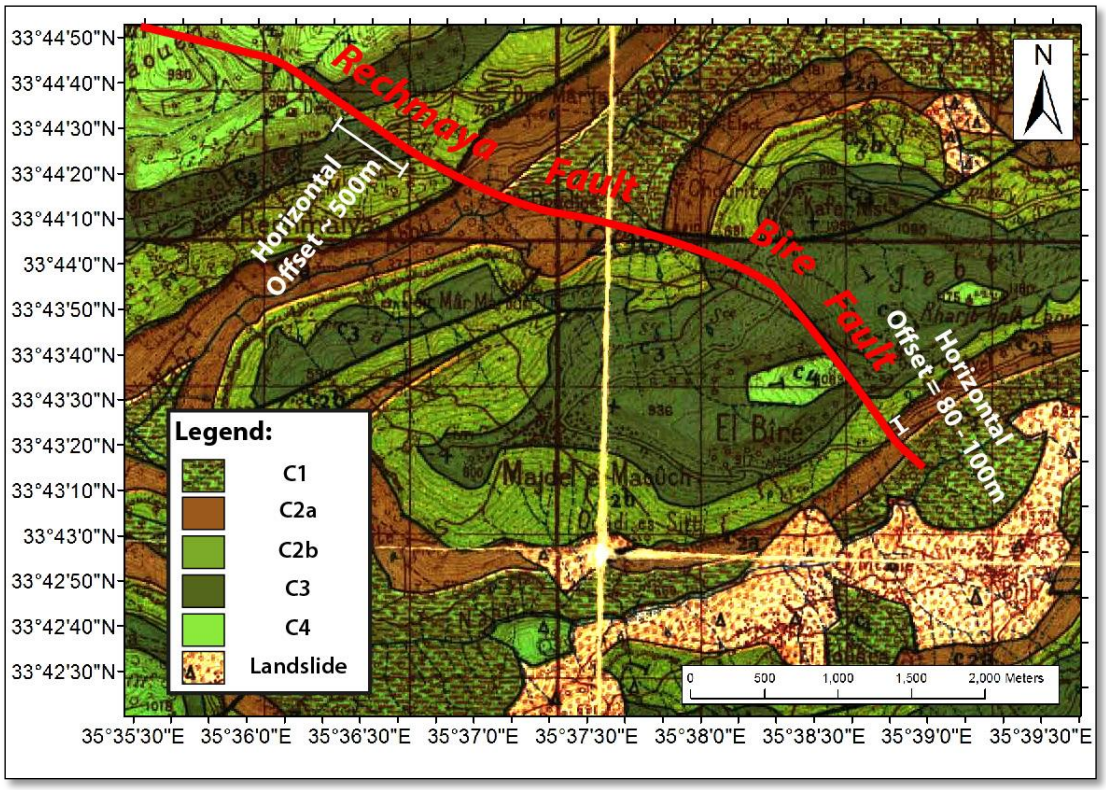

Figure 3.31: Geologic map of the Rechmaya-Bire area, showing the horizontal offsets of these structures, depicted from the displacements on the C2a/C2b and C2b/C3 boundaries (Dubertret, 1945).

3.2.2.2.2. The Rechmaya Fault

It connects with the Bire Fault west of KfarNiss (Fig. 3.32). It is a steeply SW dipping normal fault striking N293°E (Figs. 3.32 and 3.33).It offsets vertically the Falaise de Blanche by around 230m and has an associated ~500m left lateral horizontal offset of the C2b-C3 boundary (Figs. 3.31, 3.32 and 3.33). Thickening of the stratigraphic unit lying between the Banc de Mreijat and the Falaise de Blanche on the downthrown block by 60m (Fig. 3.32), are indicators of the normal, growth faulting origin of this Mesozoic age structure.

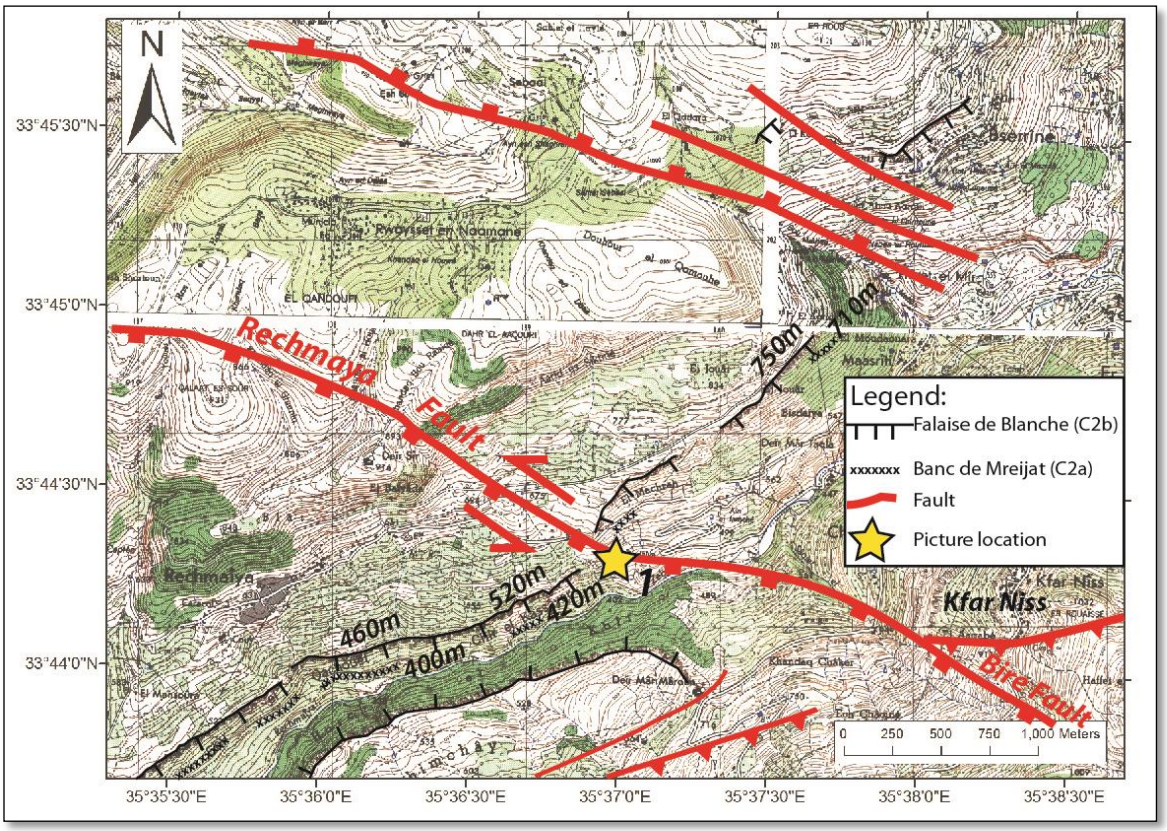

Figure 3.32: Map showing the Rechmaya fault and its effect on the geology.

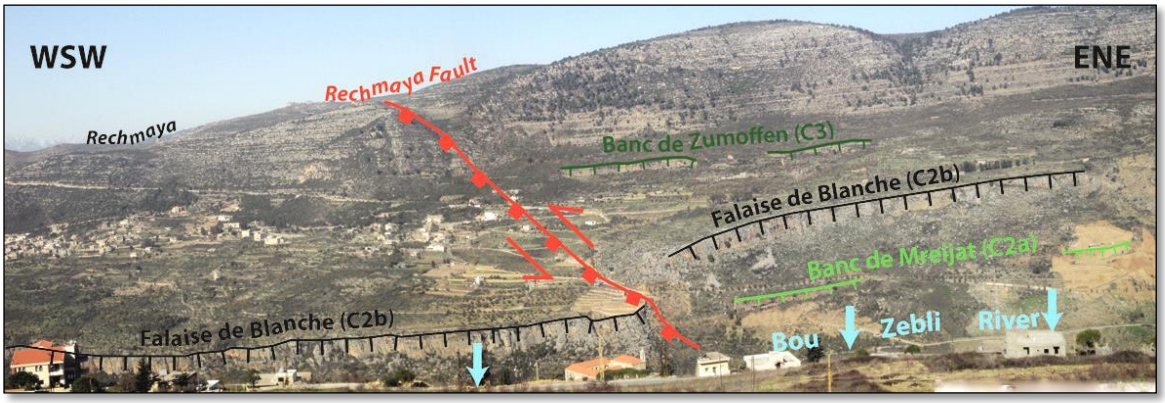

Figure 3.33: Panoramic view of Rechmaya, showing the Rechmaya fault. Notice the left-lateral displacement in the Falaise de Blanche, in addition to the normal vertical offset. (See location 1 on Fig. 3.32).

3.2.2.2.3. The Ain Trez Fault

This is another steeply dipping normal fault (Figs. 3.34 and 3.35), striking N132°E, which extends for more than 5Km between Ammiq and Dfoun, passing through Ain Trez (Fig. 3.34) where it juxtaposes the Barremian Chouf Sandstone (C1) formation on the footwall block to the upper Aptian Mdeirej (C2b) formation on the hanging wall block (Figs. 3.34 and 3.35).

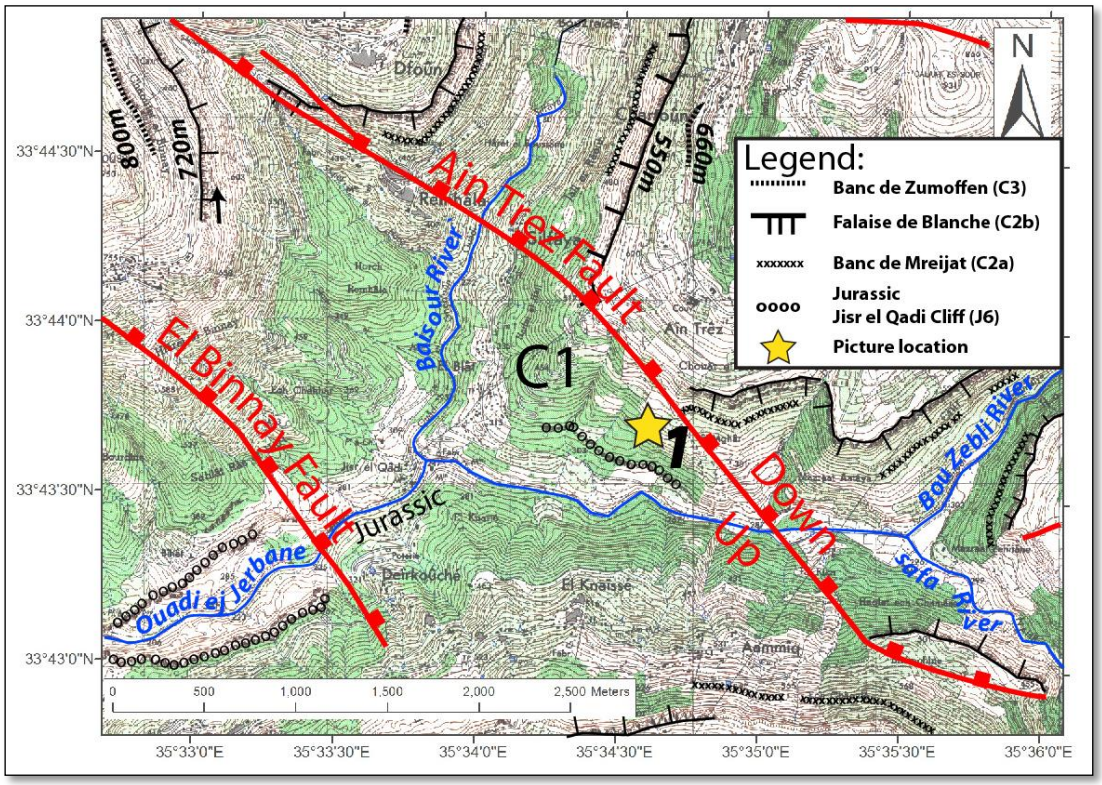

Figure 3.34: Map showing the Ain Trez fault and its effect on the Banc de Zumoffen, Falaise de Blanche and Banc de Mreijat marker beds.

In Dfoun, the Ain Trez Fault offsets vertically the Falaise de Blanche for 170m; the Banc de Zumoffen's vertical offset is however 140m (Fig. 3.34). This difference in vertical displacement for different stratigraphic markers astride the Ain Trez Fault is concordant with thickening of the stratigraphic unit between the Falaise de Blanche and the Banc de Zumoffen, from 80m on the footwall block to 110m on the hanging wall block (The banc de Mreijat is only located on the hanging wall block and thus cannot be used for measurement) suggesting growth faulting in Lower Cretaceous times (Fig. 3.34).

Figure 3.35: Panoramic view of Ain Trez, showing the steeply dipping Ain Trez Fault. (See location on Fig. 3.34).

3.2.2.2.4. The NW-SE Faults South of DBF

As seen on satellite and aerial imagery, the NW-SE faults south of the DBF exhibit only normal offset. The Moukhtara fault was visited on the field and presented here as an example. It is a N119°E striking, steeply dipping normal fault that extends for 6Km in the Moukhtara-Jdeidet ech Chouf area (Figs. 3.36 and 3.37).

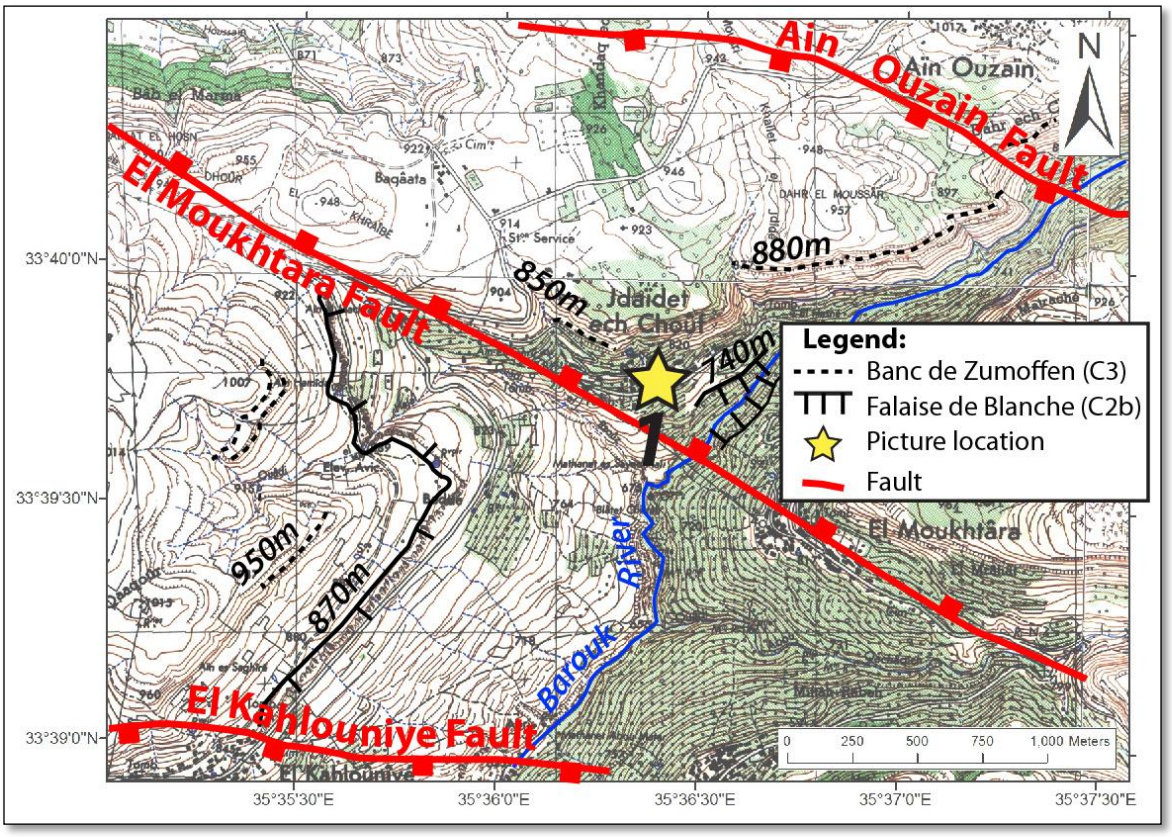

Figure 3.36: Map showing the Moukhtara Fault and its corresponding offset in the geology.

It exhibits a vertical, normal offset of ~100m accompanied by 30m-60m thickening of the sedimentary unit lying between the Falaise de Blanche and the Banc de Zumoffen on the downthrown fault block (Fig. 3.36), suggesting growth faulting.

Figure 3.37: Panoramic view of Jdaidet ech Chouf/Baddeh area, showing the Moukhtara fault and the associated vertical offset of the Falaise de Blanche. (See location 1 on Fig. 3.36).

3.3. Formations' Thickness Measurement and Distribution Maps of the Southern Central Mt. Lebanon Area

The thickness of geologic formations is an important element that provides insight not only on the sedimentation rates (or accommodation water depth) conditions of a certain area (i.e. sedimentary environment), but also serves as an indicator for the age of the deformation generating the observed structures within it.

For the purposes of understanding the structural evolution of the southern central Mt. Lebanon, and building more accurate geologic cross sections of the area, we have calculated the thicknesses of the fully exposed geologic formations over the entire SCML. Maps depicting these measured values -for each formation separately- are generated, in order to observe the variations in thickness astride the study area.

3.3.1. Methodology

Thicknesses of the geologic formation are measured based on the geologic and geo-referenced topographic maps of the southern central Mt. Lebanon area using Geographic Information Systems software. The overlay of both map types showed a good fit. Based on the overlay the elevations of boundaries of formations taken from the geologic maps are read on the topographic maps.

Using appropriate set of derived trigonometric formulas, integrating the surface exposure, the topography, the dip of the formation and other factors, the thickness at each of the selected measurement points is calculated.

Given the topography of the area and its relatively tabular structures, most of the measurement points are concentrated along valley flanks where river incisions enabled measurements of the formation thicknesses.

3.3.2. The C1 Formation

The C1 is the oldest formation totally exposed within the study area. Its entire thickness surface exposure is confined to both flanks of Ouadi el Jerbane (Fig. 3.38); thus thickness measurements of the C1 formation are limited to this locality and range between 214m and 290m, with slight increase toward the west .

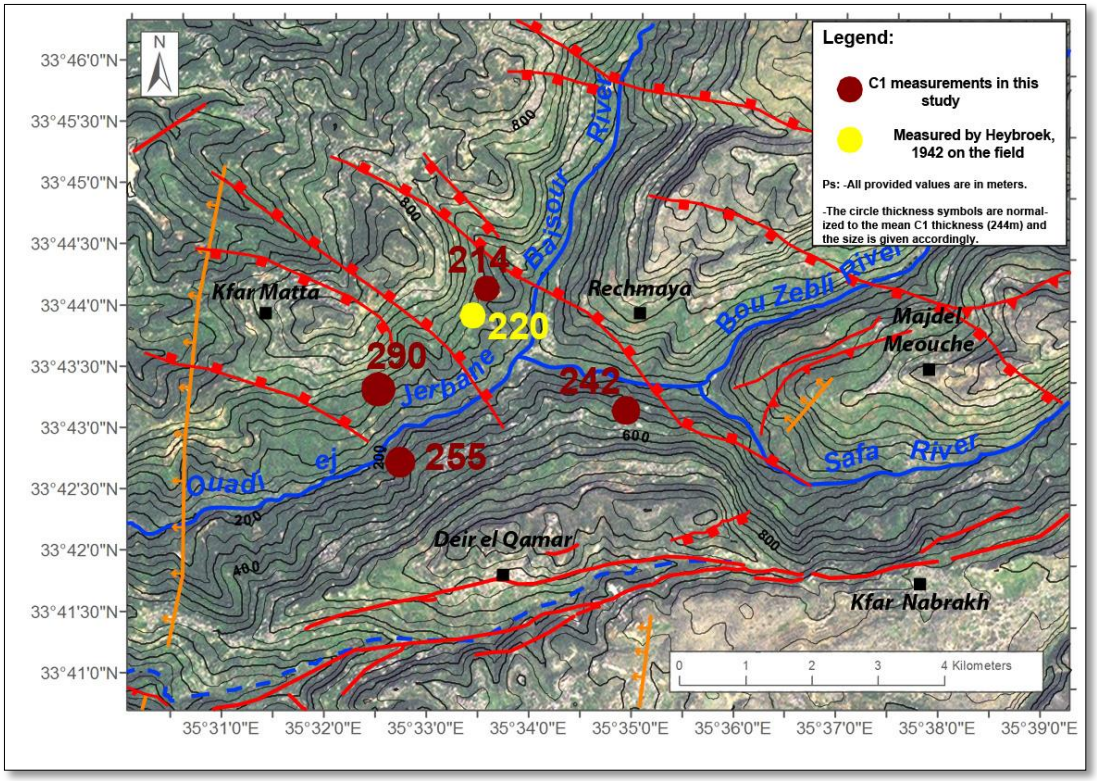

Figure 3.38: The C1 (Chouf Sandstone) thickness measurement map, within the SCML.

3.3.3. The C2a Formation

The Abeih formation (C2a) is the second oldest rock formation entirely exposed within the study area. Most of its complete surface exposures are located to the north of the Damour-Beit ed Dine fault. To the south of this fault, its exposure is confined to the area near Mtulleh (Fig. 3.39). The calculated thickness measurements are concentrated on the northern side of the fault. The values range between 65m and 184m. The thickness distribution north of the DBF shows minimum values in the area between Rechmaya and the DBF, flanking the Safa River and Ouadi ej Jerbane; in these localities the C2a thickness varies between 90m and 120m. Thicknesses of the C2a formation increase north and NW of this zone; a maximum of 184m is reached in the vicinity of Kfar Matta to the NW, and a

close value of 180m is measured to the north west of Ain Trez calculated on the western embankment of the Baisour River (Fig. 3.39). A detailed look at these values north of the DBF suggests that a range of thicknesses is associated with some of the NW-SE striking faults with thickening in the C2b on the hanging wall side. For example the Ain Trez Fault shows an increase from 99m-110m in the footwall (west) to 144-151m on the hanging wall (east).

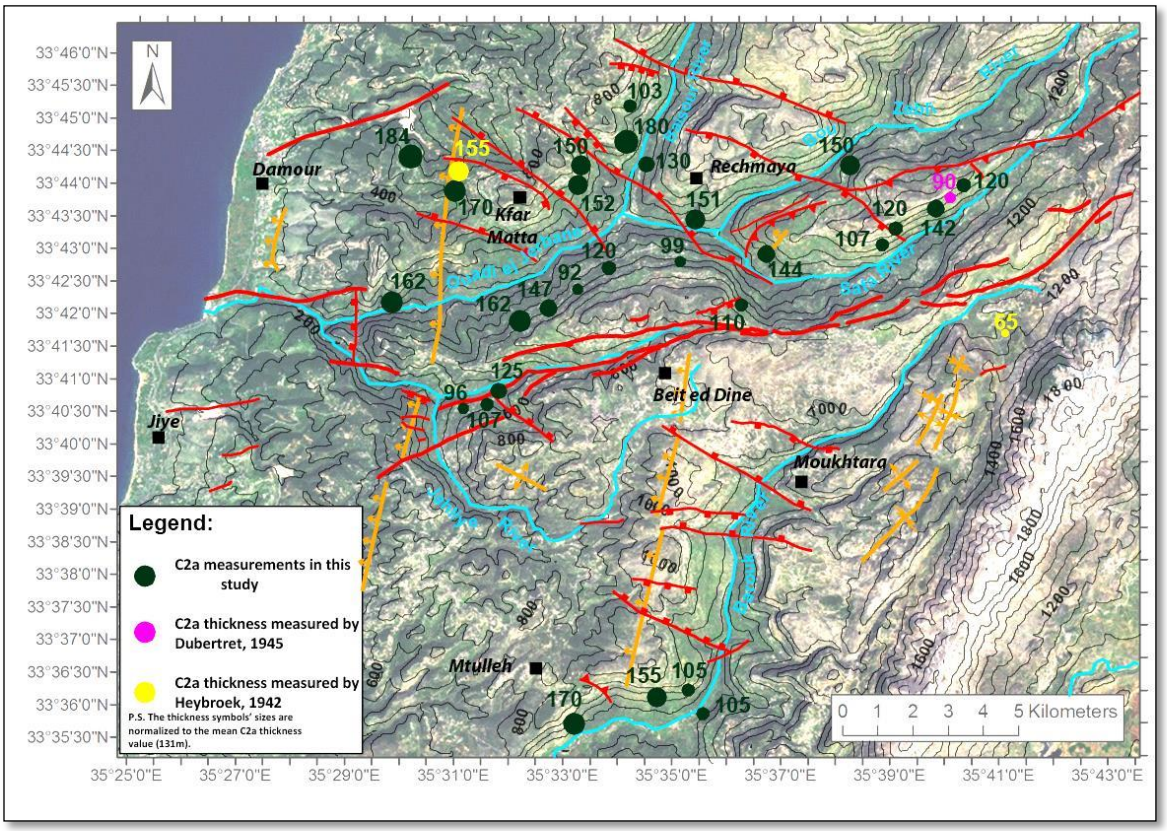

Figure 3.39: Map, showing the variation in thickness of the C2a formation within the SCML.

To the south of the Damour-Beit ed Dine fault, the C2a thickness is measured only near al Mtulleh, where a rapid westward increase from 105m to 170m takes place over a distance less than 5Km (Fig. 3.39).

3.3.4. The C2b Formation

The distribution map of the thickness measurements for the C2b formation is similar to that of the C2a. No net organization of the thickness values can be observed. These are at their minimum (40m) also in the vicinity of the Safa River and increase towards the W and NW to decrease again in the vicinity of the Baisour River. The maximum thickness value reached is 140m observed over the southern flank of the Bou Zebli valley (Fig. 3.40). Again NW-SE faults are associated with important increase in C2b thicknesses on their hanging wall side. For example the Ain Trez and Rechmaya faults have 20-40m thickening on their hanging wall.

To the south of the Damour-Beit ed Dine fault, the exposure of the full C2b thickness is restricted to the east. At the foot of the Barouk Mountain, values of 66m and 143m are calculated. At the flanks of the Barouk River on the other hand, thickness values range between 45m and 180m (Fig. 3.40).

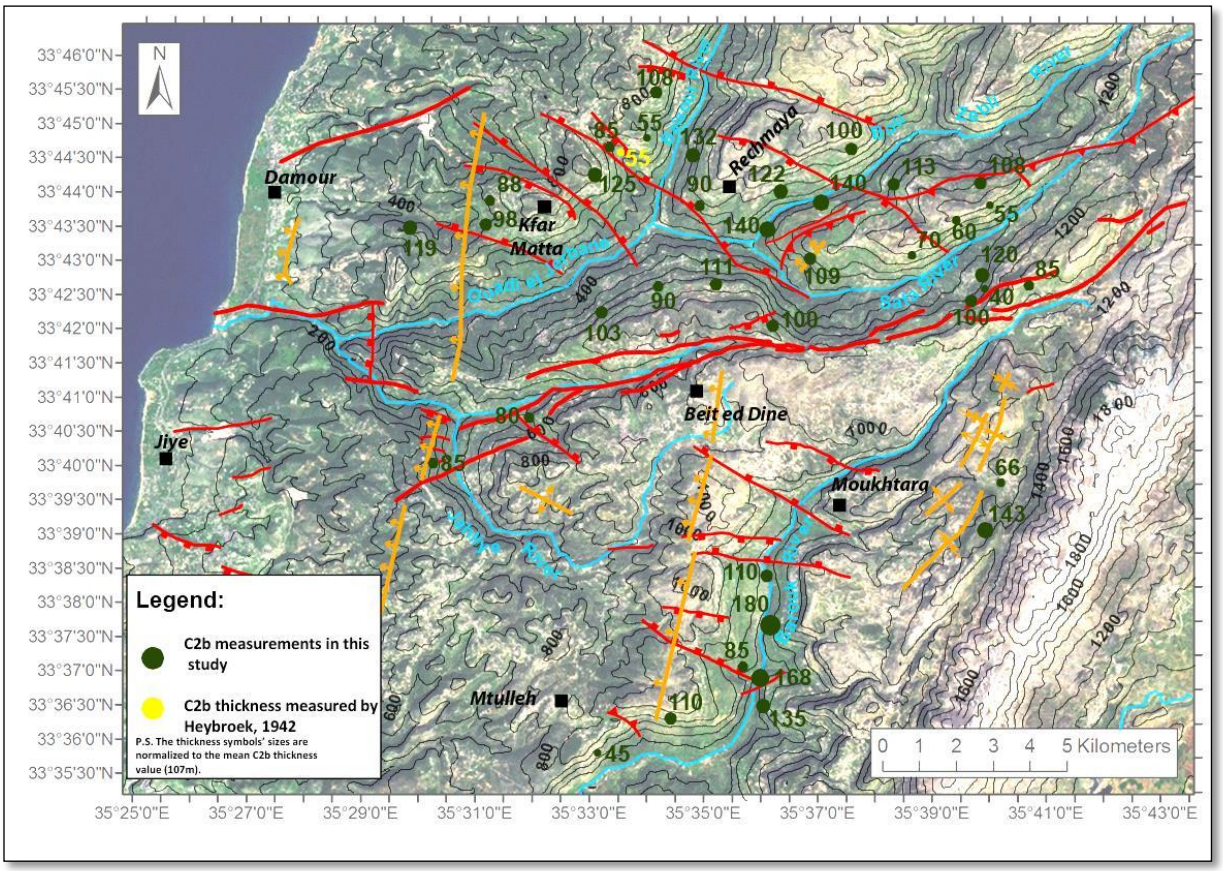

Figure 3.40: Map showing the distribution of the measured C2b thicknesses within the SCML.

3.3.5. The C3 Formation

The C3 thickness measurements are shown on figure 3.41. They are geographically more spread around the Damour-Beit ed Dine fault. In this region the minimum values are located around Ouadi ej Jerbane (62m-104m). The NW-SE striking faults show thickening of the C3 on their hanging wall side. In Kfar Matta area for example, the thickness of C3 layers is significantly larger in the area between the north and south bounding Mesozoic normal faults. The same situation is also observed in the Rechmaya-Ain Trez area.

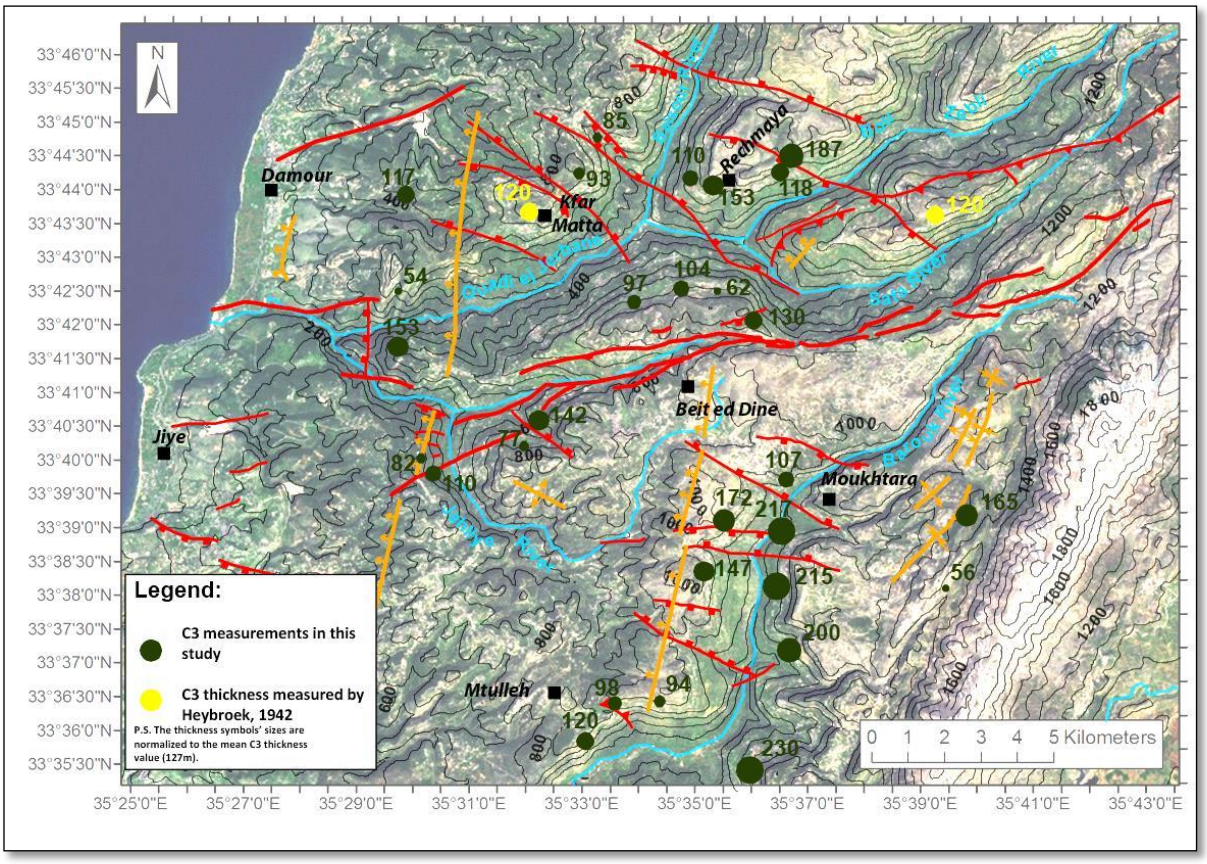

Figure 3.41: Map showing the distribution of the measured C3 thicknesses, within the study area.

To the South of the Damour-Beit ed Dine Fault, the measurement points are concentrated over the flanks of the Barouk River. In this area the thicknesses vary between ~100m and 230m (Fig. 3.41).

A comparison of the thickness values on both sides of the DBF, suggests that larger values are to the south of this structure, probably related to a southward thickening of the C3 astride the Damour-Beit ed Dine fault. Yet, the confirmation of this idea necessitates a denser number of measured points.

3.3.6. Interpretation and Discussion

Common traits in the distribution of the thickness values for the C2a-C3 sediments can be used to analyze the paleogeography and geological evolution of the area during the Mesozoic Era. The constant increase in formation thicknesses over the hanging wall of the NW-SE faults located north of the DBF ranges between 20m and 120m and is related to the growth activity of these Mesozoic faults. It is likely that a grabben-like depocenter was active during the C2a-C3 stages in the area of Kfar Matta. Similarly, the Rechmaya and Ain Trez normal faults bound a depocenter of the same structural origin in that same time. These patterns can be considered as a clear evidence of the existence of old paleo-relief in the sedimentary Mesozoic basin of the area.

Moreover, the bulk thickness values over the entire area constantly show relatively higher values south of the DBF suggesting the existence of a difference in the paleo-bathymetry of the area, probably controlled by the existence of a Mesozoic DBF structure. More measurement points spread over the area south of DBF are essential to verify this observation.

3.4. Geologic Cross Sections of the Southern Central Mt. Lebanon

Five interpretive cross sections are provided in this study. These are based on the geologic mapping of Dubertret (1945), integrating our own field observations, structural measurements and modifications as well as the measured thickness values presented in previous section, and available well log data taken from Beydoun (1977). The topography along each profile is extracted from the NASA SRTM files.

The locations of the cross sections are shown on figure 3.42. Cross sections AB and CD are latitudinal profiles parallel to, and located on both sides of the DBF. Cross sections EF and GH are oriented N-S almost at right angle to the DBF. Cross section IJ is oriented in a NE-SW direction cutting almost perpendicular to the NW-SE striking faults located to the south of the DBF.

Cross sections AB and CD show the western limbMt. Lebanon structure, to the north and the south of the Damour-Beit ed Dine fault respectively. To the north (Fig. 3.43), the Damour Monocline and the Mt. Lebanon Flexure mark the start of the structural and relief build-up of Mt. Lebanon. This uplift is distributed over three accentuated folds noticeable on this section: the Mt. Lebanon Flexure, the Majdel Meouche Flexure and the Barouk Monocline. Between these structures, relatively flat terrains consisting of broad gentle folds and horizontal strata are dominant.

The steep NW-SE faults (70˚-80˚ dip) dissect this section; the majority consists of apparent normal faults -in Cenozoic these reactivated to the north of the DBF in an oblique-slip mode- having vertical offset as great as 300m. However, two faults with reverse slip component were mapped: the Barouk Fault, and the Majdel Meouche fault responsible for the Majdel Meouche Flexure. Furthermore, this cross section shows a westward thickening of the C1 and C2a formation, in a direction opposite to the increase in topographic elevation, in conformation with the thickness measurements provided in section 3.3.

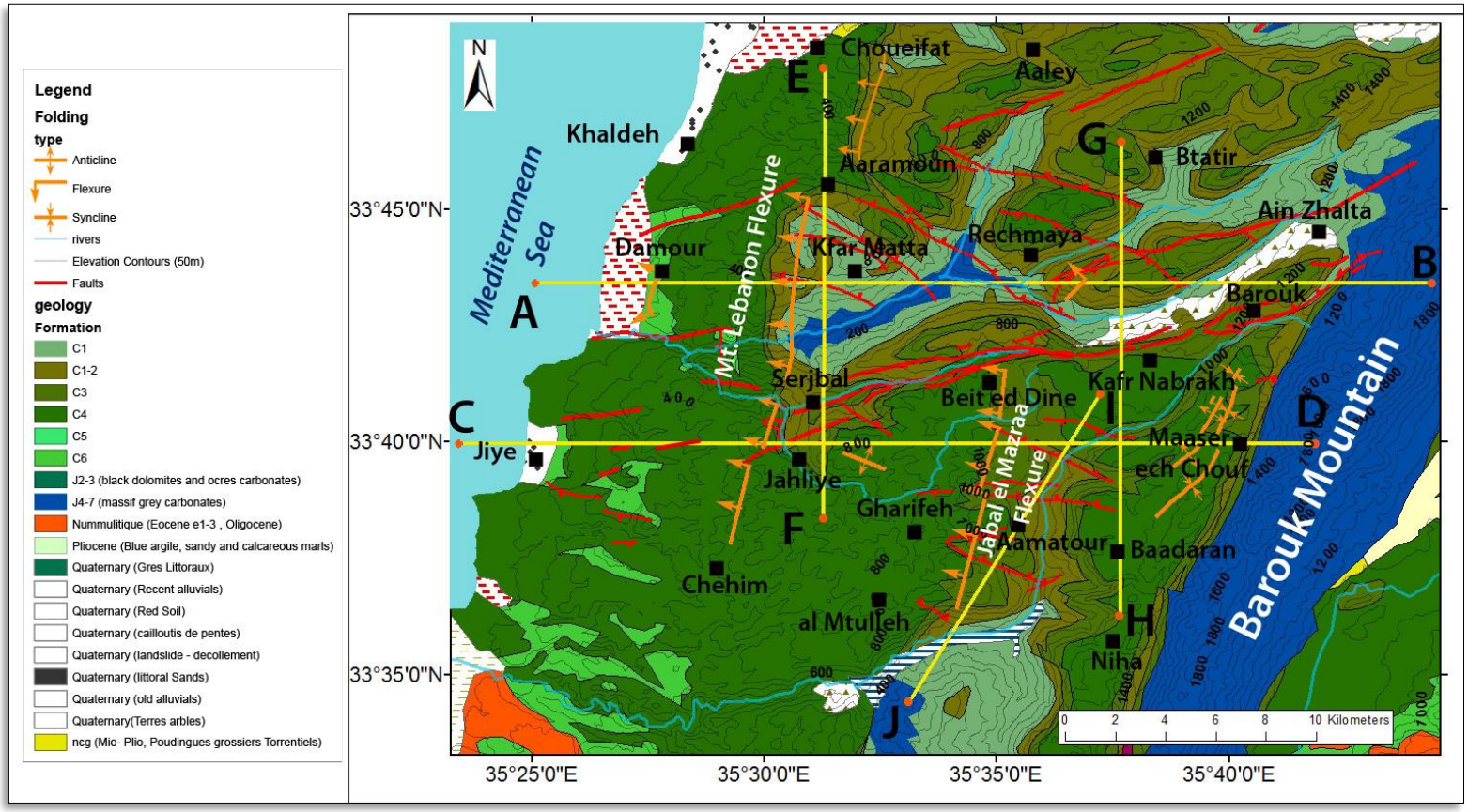

Figure 3.42: Geologic map of the SCML (modified from Dubertret, 1955), showing the location of the five geological cross sections.

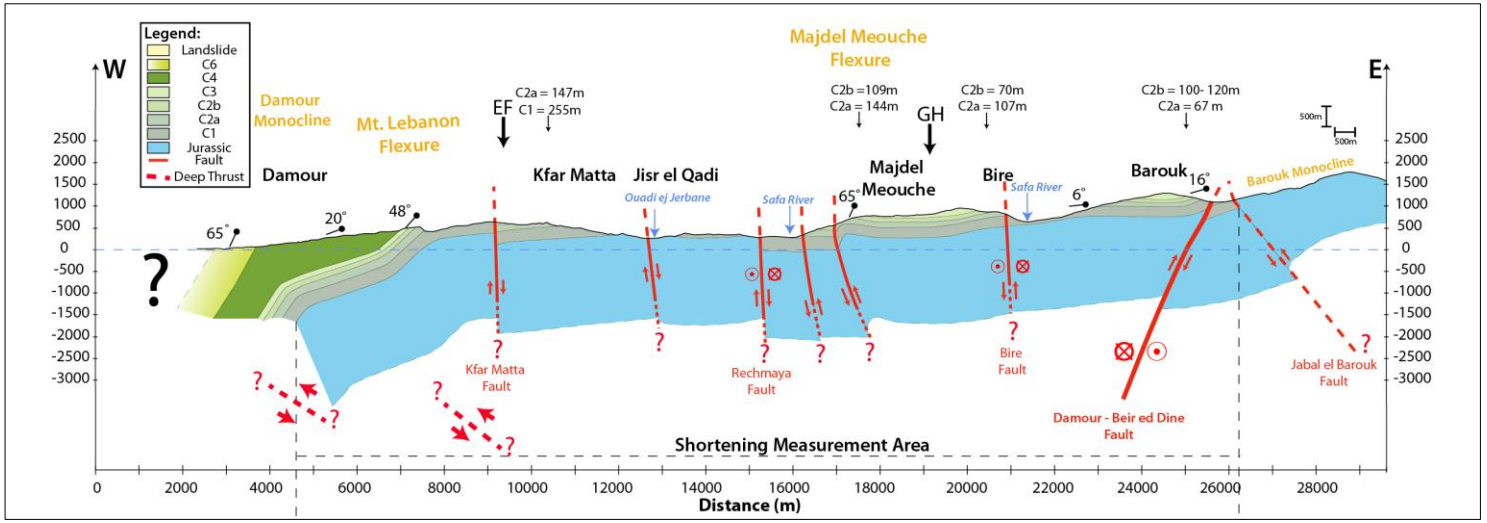

Figure 3.43: Cross Section AB, showing the E-W structure of the SCML, north of the DBF.

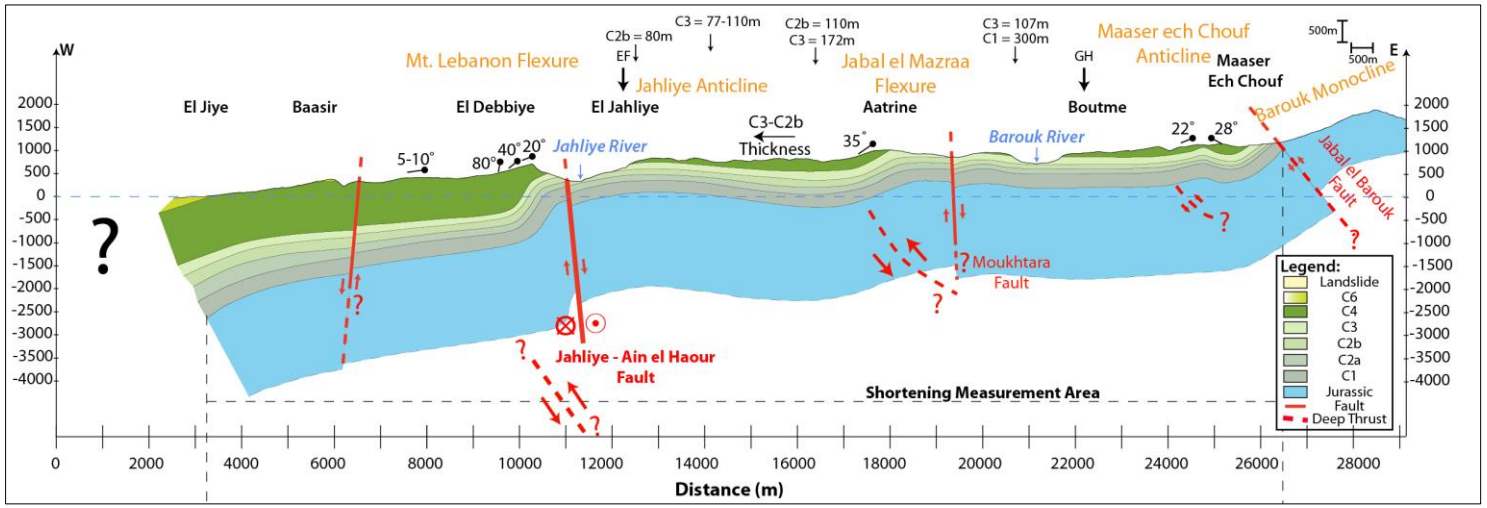

Figure 3.44: Cross section CD, showing the structure of the SCML, south of the DBF.

The shortening estimation of this section is 3.48%; this value is a minimum since it doesn't account for the restoration of the extension on the normal faults.

To the south (Fig. 3.44), the remarkable build-up of Mt. Lebanon starts also at the Mt. Lebanon Flexure. Smaller number of faults dissects the terran in this area making the overall structure more clear. The most noticeable folds seen on this profile are the Mt. Lebanon Flexure, the Jabal el Mazraa Flexure and the Barouk Monocline. Between these major structures, lies relatively flatter geology consisting of broad gentle folds giving the illusion of tabular geology. This is concordant with the topography, which shows a step like plateau geometry, in which the transition from one level to the other takes place through the major flexures and monoclines. It should be noted that the flat terrains correspond to the gently folded geology. Furthermore, steep normal faults offset the geology. The most important is the Jahliye-Ain el Haour fault a branch of the Damour-Beit ed Dine fault, which shows vertical normal offsets as well as right lateral strike slip displacement.

This section also exhibits an eastward increase in topographic elevation, which is opposed by a westward increase in the thickness of the C1, C2a, C2b and C3 strata. A shortening by a minimum of 3.3% was estimated for this cross section.

The vertical offsets seen on this section are also partially due to the strike-slip component along most of these structures bringing units of different structural domains next to each other.

Beside the faults mapped and checked in the surface geology, some others were interpreted from the overall structures of the area and show as dashed red lines on the sections. Therefore, we infer the existence of blind thrusts at depth below the surface under

each of the asymmetrical folds seen on the surface, in compliance with the general rules and common well known examples in similar structural settings (Suppe, 1983; Mitra, 1990). In particular major ramp/flat geometry should exist under the Mt. Lebanon Flexure, transferring shortening towards the offshore Mt. Lebanon Thrust System (Elias et *al.*, 2007). To the east, the extreme low thickness of the Chouf Sandstone (C1) Formation at the foot of the Barouk Monocline east of Barouk and Maaser ech Chouf associated with the large scale box fold of the Barouk structure are taken as indicators for the presence of west-vergent reverse faulting. This type of kinematics is more compatible with the geological setting than the normal offset as previously associated with this structure by Heybroek (1942).

Cross-sections AB and CD clearly show the difference in structural elevation of the two areas. The northern side of the DBF is constantly at higher elevation than the southern counterpart. The amounts of shortening on both sections being similar, the difference of structural elevation is therefore related to the overall kinematics of the deep DBF separating both sections: uplifting the northern side relatively to the south.

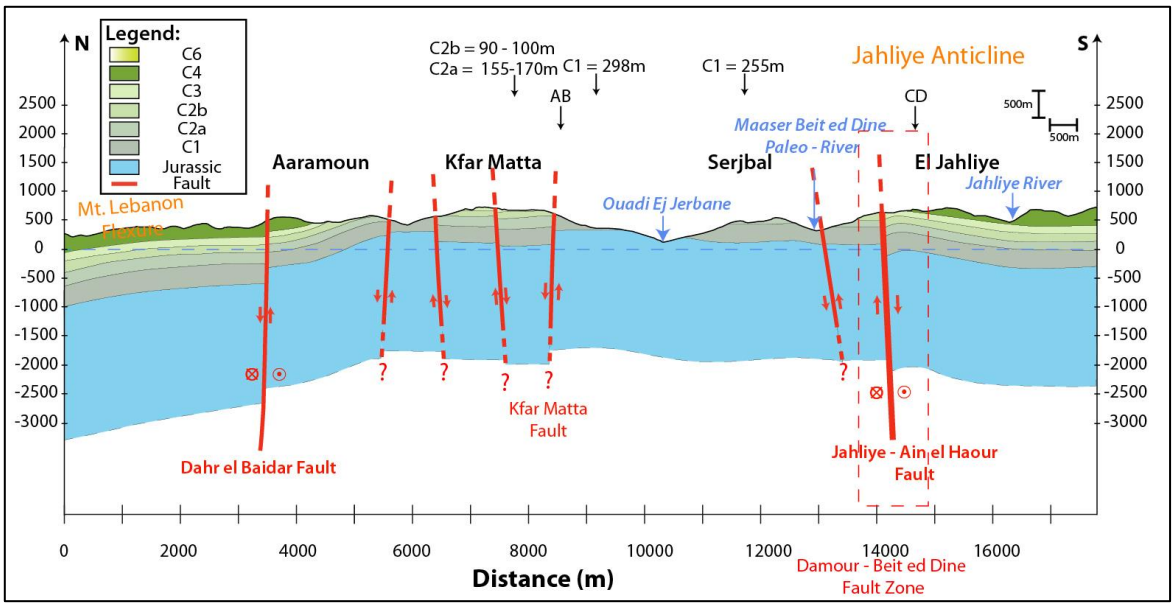

Figure 3.45: Cross section EF, showing the N-S structure of the west SCML.

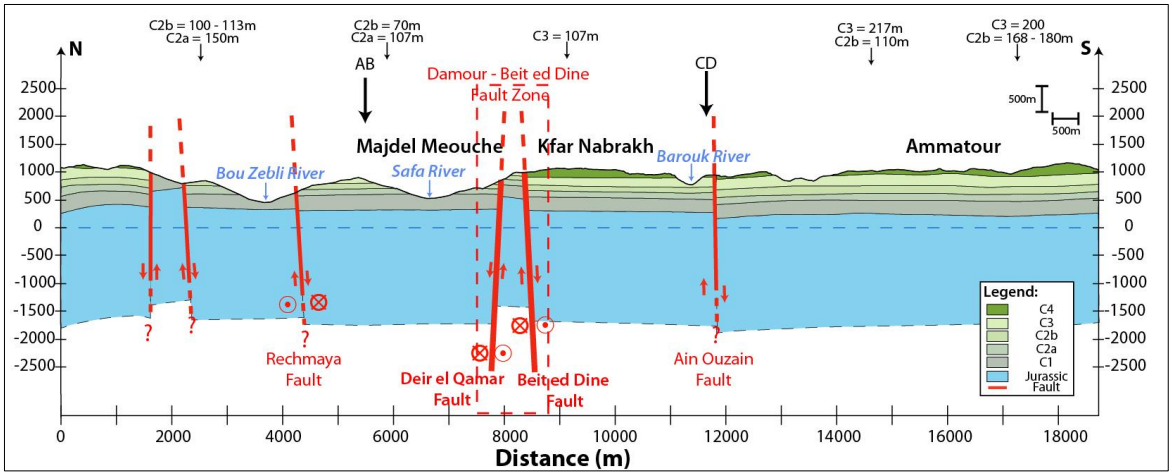

Figure 3.46: Cross section GH, showing the N-S structure of the east SCML.

Cross sections EF and GH are longitudinal interpretative cross sections that cut astride the DBF, to the west and the east of the study area respectively. To the west (Fig. 3.45), the most obvious vertical offsets are seen on the Jahliye-Ain el Haour Fault and the

Dahr el Baidar Fault (at Aaramoun). The offset along the Jahliye-Ain el Haour fault is more or less representative of the real displacement along this branch of the Damour-Beit ed Dine fault, because of the presence of gently dipping strata at the contact of this structure. The important vertical throw seen on the Dahr el Baidar fault at Aaramoun is in fact the result of the right-lateral offset of the Flexure by this fault, bringing the deeper and gentler sloping beds of the foreland to the west, next to the shallower and steeper beds of the hinterland to the east.

To the east on the other hand (Fig. 3.46), profile GH, shows that the elevation variation of the geologic formations along this direction is very small. In fact the only remarkable changes seen are local and confined to the Deir el Qamar and the Beit ed Dine faults. It should be noted however that these profiles do not cut exactly parallel to the strike of the structures of the southern central Mt. Lebanon area, which may result in miss-interpretation of the dip-slip effect of the Damour-Beit ed Dine fault on the geology. In other terms, the northern area of the southern central Mt. Lebanon may be higher geologically compared to the south, since profile GH shows that geological areas in a more foreland position in the north are at the same level as areas of more inland positions in the south.

Finally, cross section IJ (Fig. 3.47) cuts perpendicular to the NW-SE faults in the Ain Ouzein-Beiqoun area. With the exception of the Mtulleh reverse fault, all other faults display normal vertical offset.

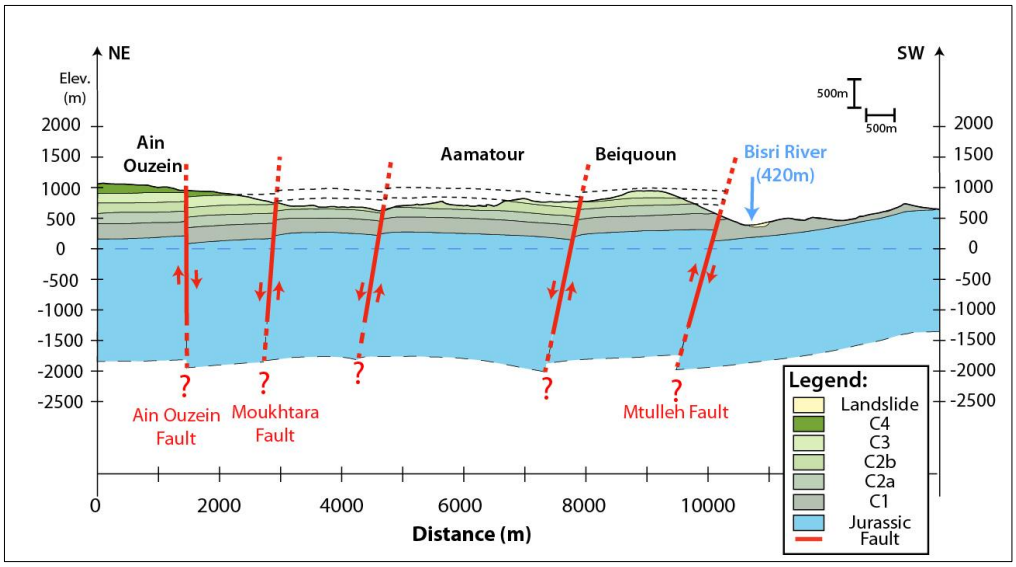

Figure 3.47: Cross section IJ, showing the structure astride the NW-SE faults located south of the DBF.

3.5. Discussion and Conclusion

3.5.1. The Structural Geology of the SCML

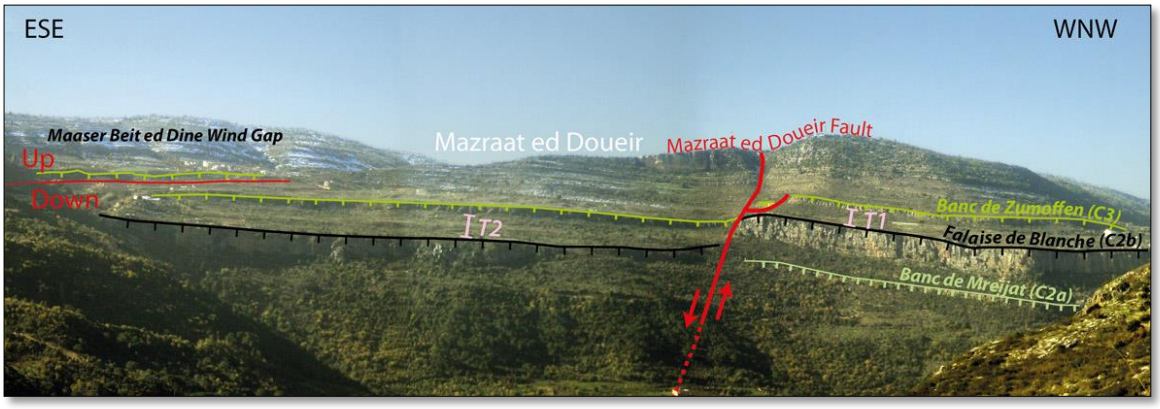

Figure 3.48: Panoramic view of Mazraat ed Doueir, showing the Mazraat ed Doueir Fault (See location 1 on Fig. 3.49). Notice the increase in thickness of the sedimentary unit located between the Falaise de Blanche and the Banc de Zumoffen (Modified from Homberg et *al.*, 2010).

The DBF is a series of ENE-WSW striking faults stretching over 20-25km between Barouk to the east and Damour to the west. The fault trace is clear in Lower Cretaceous layers and less well developed and continuous in the Upper Cretaceous units.

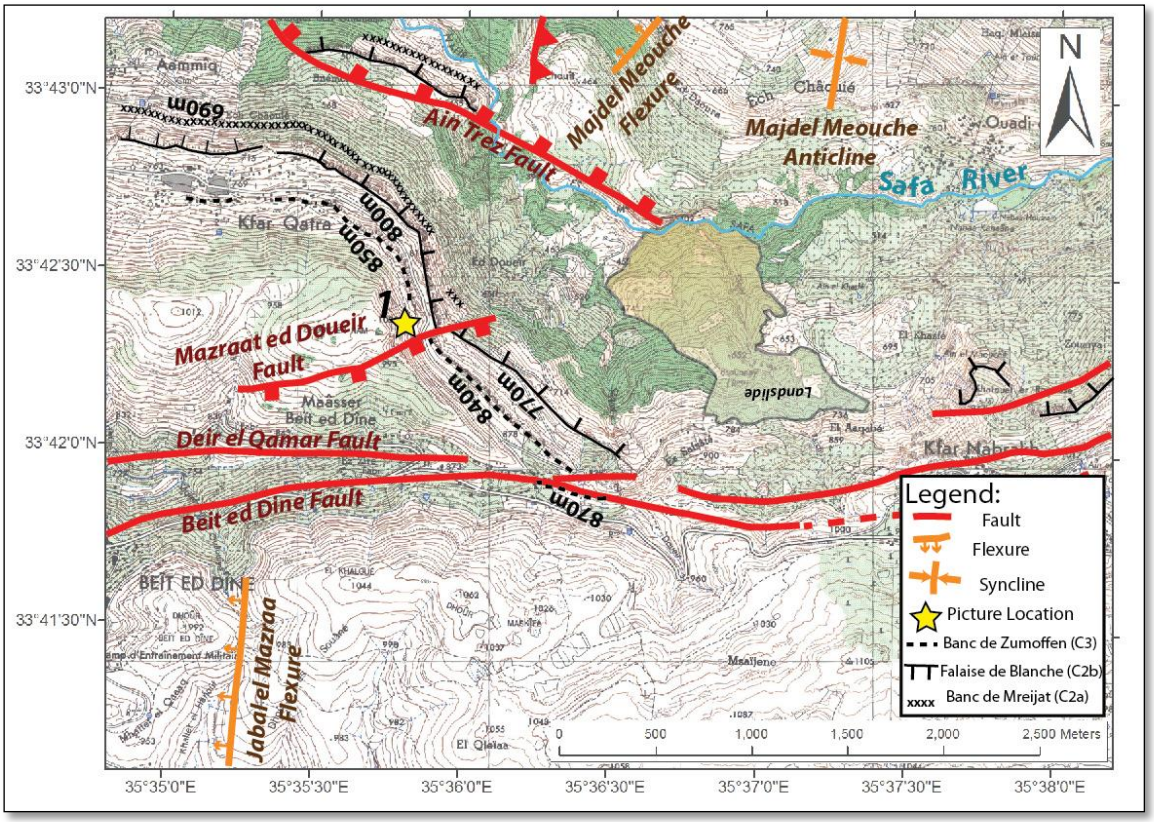

Figure 3.49: Map of Maaser Beit ed Dine, showing the Mazraat ed Doueir fault, a secondary branch of the DBF. Notice the increase in thickness of the sedimentary unit located between the Falaise de Blanche and the Banc de Zumoffen, on the hanging wall side of this fault.

Evidence for growth faulting in the Lower Cretaceous found on number of its branches (i.e. The Mazraat ed Doueir Fault (Figs. 3.48 and 3.49) and the Jahliye-Ain el

Haour Fault (Fig. 3.41)) constrain the inception age of the fault system most probably along with the similar ENE-WSW faults of Mt. Lebanon located to its north, in the Aptian-Albian times, during an early extensional phase (Walley, 1988; Homberg et *al.*, 2010).

Up to 2 Kilometers of offset geological markers mapped along this structure indicate right-lateral shear. This dextral shear is also supported by the similar offset of the saw-like shoreline in the area as well as by the right-lateral offset of the Mt. Lebanon Flexure. The latter demonstrates that the present DBF is a tectonically active right-lateral fault. The right-lateral shear along this fault justifies the important compressive component on the NE-SW trending Majdel Meouche Fault and the extension observed over the N-S Mghaire Fault. Oblique-slip, however, may be taking place on this structure as suggested by the rake of lineations measured over two different fault mirrors found in two localities along this fault. The fresh fault scarps visited in Chaoualiq Deir el Qamar and polished by this shear are evidence for the recent ongoing tectonic activity of the DBF.

Other morphotectonic observations also support that the DBF is an active structure. In fact, the morphometric properties of the two areas north and south of the DBF are very different. The northern side is systematically at higher elevation astride this fault zone, and the drainage shows readjustments of river flow and profiles reflecting tectonic influence. The frequency and distribution of the landslides in the area can also be associated to the tectonic activity in the area.

No direct indicators of the timing of this change in kinematics from normal to strike-slip (oblique) were found in the geology mostly due to the almost total absence of Cenozoic layers in the area of investigation. As suggested by other authors **(**Carton et *al.*,

2009; Homberg et *al.*, 2010**)**, a Mid-Miocene tectonic phase dominated by transpression on the Lebanese Restraining Bend, associated with the initiation of left-lateral shear on the Yammouneh Fault, may have reactivated the ~E-W faults of Mt. Lebanon in a bookshelf deformation style, with a counter-clockwise rotation of the blocks bound by these faults (Mandl, 1986; Ron, 1987; Tapponier et *al.*, 2004; Jaafar, 2008). This could be the case of the DBF.

Significant differences in the attitude of the NW-SE faults found north and south of the DBF also support the bookshelf and block rotation model. These faults seem to belong to the same group of extensional structures initiated in Lower Cretaceous times. Remarkably though, the group of faults north of the DBF shows a left-lateral component of displacement that is not expressed on the faults of the southern group. Moreover, rose diagram analysis of the orientation of the two sets suggest that those to the north have rotated 10°-18°CW relatively to the southern group of faults (Fig. 3.50).

These differences are interpreted as resultants of the reactivation of the NW-SE fault to the north of the DBF only, in a secondary clockwise bookshelf faulting of blocks bound by the sinistral NW-SE faults. This secondary block rotation is induced by the right-lateral shear on the DBF and the Dahr el Baidar fault bounding these NW-SE structures to their south and north respectively (Fig 3.51). Its absence in the south is due to the lack of two bounding structures, the DBF being the southernmost of the right-lateral E-W faults.

This secondary block rotation is a consequence and proof of the right-lateral strike slip bookshelf reactivation of the ~E-W faults in general and the Damour-Beit ed Dine fault

in particular. A similar example of block rotation and associated secondary block rotation is also known elsewhere in similar tectonic settings (i.e. Kanaori et *al.*, 1990).

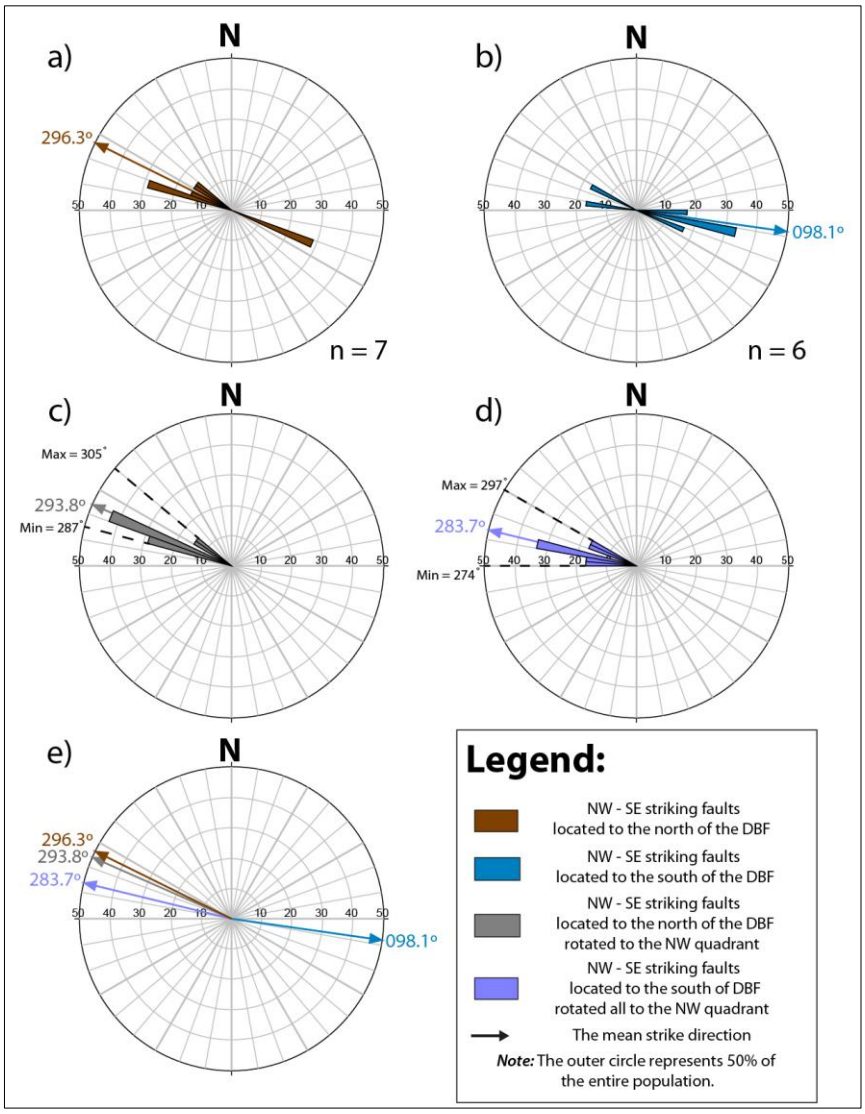

Figure 3.50: Rose diagrams of the strikes of the NW-SE faults within the SCML: a) North of the DBF, considering the dip direction. b) South of the DBF, considering the dip direction. c) North of the DBF, after adding 180˚ to the strike of faults located in the SE quadrant. d) South of the DBF, after adding 180˚ to the strike of faults located in the SE quadrant. e) Rose diagram showing the mean orientation vectors for previous four plots.

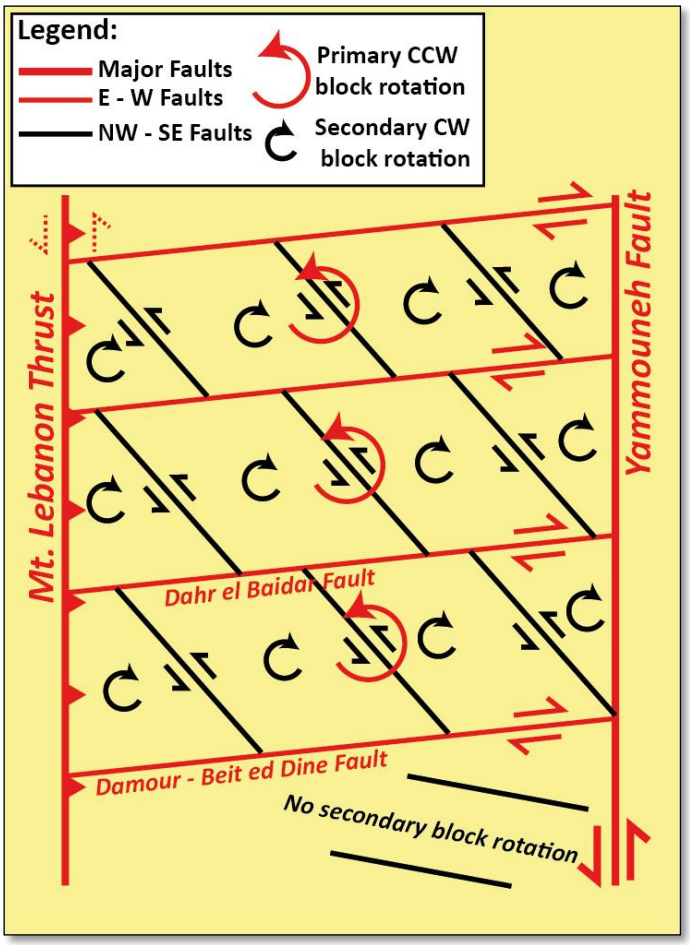

Figure 3.51: Schematic diagram showing a plannar view of the primary CCW bookshelf faulting in Red (Tapponier et *al.*, 2004) and secondary CW bookshelf faulting in Black within the Mt. Lebanon and the SCML included (modified from Kanaori et *al.*, 1990).

Our study showed the existence of compressive structures, like folds (symmetric and asymmetric) and flexures. These structures accommodate the compressive component of the Mid-Miocene to present transpression tectonic phase. The majority of the folds in this area are oriented NE-SW, conformable with the general fold trending of Lebanon. These have shortened the southern central Mt. Lebanon area for at least 3.3%-3.48% in a SSE-NNW direction. A suspected deep ramp-flat geometry of inferred west-vergent blind

thrusts (or reverse faults) under the mapped asymmetric folds and flexures, may therefore be a possible structure responsible for the major flexures and monocline as well as the uplift of Mt. Lebanon in this area. The surface expression of these deep structures is depicted in a step-like topographic buildup of the southern central Mt. Lebanon area, clearly observed to the south of the Damour-Beit ed Dine Fault.

The old normal faults still display the imprint of their original normal offset generated in Mesozoic time. A reverse component may be present on these reactivated old normal faults and structures. In this case this offset has probably not been totally inverted and results in under-estimation of the importance and amounts of shortening.

3.5.2. A primary and secondary block rotation model from Central Japan: An Analogous example to the SCML bookshelf deformation

The Central Japan area is traversed by two major NW-SE striking, left-lateral structures, the Neodani and the Atera faults.

The Neodani Fault (NOF) is a 60Km long structure that passes through the village of Mizota (Fig. 3.52). Detailed mapping of the fault showed that it consists of small en-échelon segments showing some overlap (Kanaori et *al.*, 1990). Investigations conducted by Matsuda (1974) allowed the estimation of ~3Km displacement on this NW-SE striking, Paleozoic-Mesozoic aged, active structure, constrained from offsets in geomorphologic features. Yet most importantly, the Neodani fault ruptured in 1891 generating the magnitude 8.0 Nobi Earthquake, one of the strongest events known in Japan (Kanaori et *al.*, 1990).

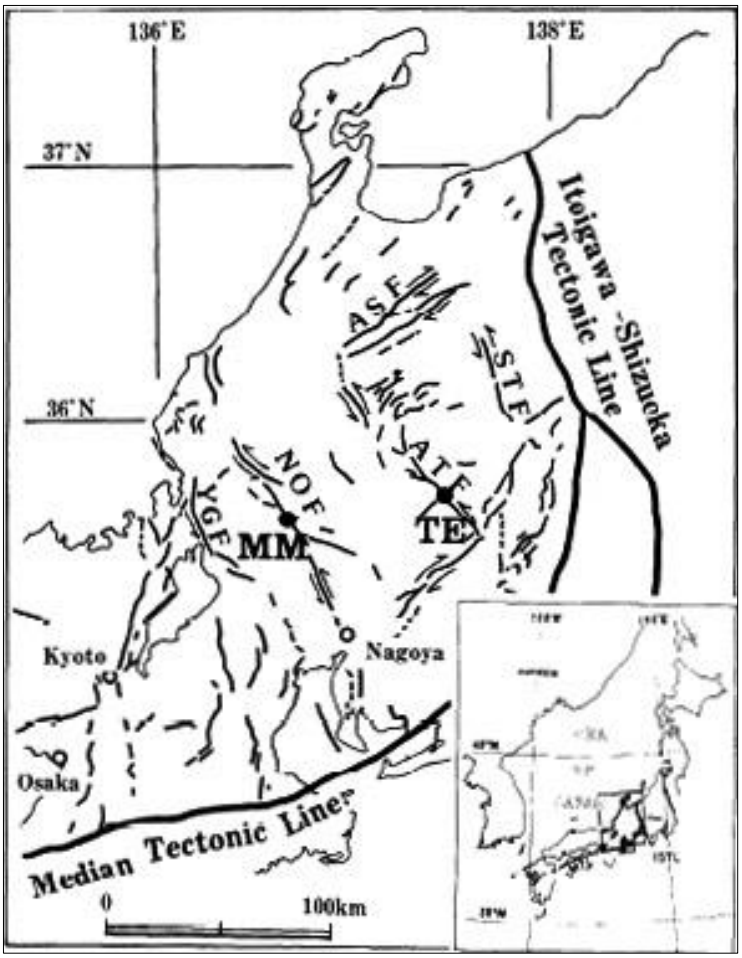

Figure 3.52: A structural Map of Central Japan showing the Neodani Fault (NOF) as it passes through the Village of Mizota (MM) and the Atera Fault (ATF) as it passed through the village of Tsukechi (TE). Both structures are left-lateral faults (the map is after Kanaori et *al.*, 1990).

The Atera Fault (ATF) is another ~60Km long structure that passes through the village of Tsukechi, to the NE of the Neodani fault (Fig. 3.52). Detailed mapping of this fault showed that it consists of smaller en-échelon segments showing some overlap (Kanaori et *al.*, 1990). Investigations conducted by Yamada (1978) allowed this latter to

estimate ~7Km of sinistral displacement on this NW-SE striking, Paleozoic-Mesozoic aged active structure, constrained from offset dacite intrusions by the activity of this fault.

Outcrops in overlap areas along both structures were investigated and revealed the presence of first order NE-SW right lateral faults dividing this area of overlap into large blocks. In turn second order NW-SE left-lateral faults subdivide each block into smaller blocks.

According to Kanaori et *al.*, (1990) these fault systems form together an active system were the left-lateral shear on the overlapping major NW-SE faults rotated in a counter clockwise style the blocks bound by the primary NE-SW ones, which induced the right-lateral displacement on the latter. In turn the right-lateral shear of the NE-SW faults resulted in a clockwise rotation of smaller blocks bound by the secondary NW-SE one, which in turn induced left-lateral displacement of these second order structures (Kanaori et *al.*, 1990).

The Cenozoic reactivation of the DBF (and the other E-W faults of Mt. Lebanon) as dextral CCW bookshelf faults and the smaller NW-SE faults north of the DBF as secondary CW and sinistral bookshelf structures, shows similarity with primary and secondary block rotation suggested for the central Japan area by Kanaori et *al.* (1990).

CHAPTER 4

SEISMICITY OF THE SOUTHERN CENTRAL MT. LEBANON

In this chapter we present a review of the historical and recent seismic activity of the southern central Mt. Lebanon. The long-term seismicity of the southern Mt. Lebanon area is retrieved from historical catalogs/documents. The recent seismicity is compiled from instrumental seismic data provided by the seismic network of Lebanon for the years of 2006-2010 and is used to study the seismic hazard of the area.

The aim is to explore a possible correlation between the seismicity of the SCML and the active structures of the area reviewed in chapter 3.

This chapter starts by providing a theoretical review and discussion of the techniques and concepts in earthquake seismicity analysis. It then presents and discusses the historical and instrumental seismicity of the SCML area separately and finalizes by concluding on the potential seismic hazard of the SCML and the contribution of the DBF to this hazard.

4.1. Review of Earthquake Seismicity Analysis

Seismology is the study of elastic waves propagation in the ground, in the aim of acquiring insight on the structure of the earth's interior. The seismic sources generating these waves are either artificial (buried explosives, airguns…) or natural. Natural seismic sources are mainly active faults; slip on these produces earthquakes and releases elastic energy and heat (Stein & Wysession, 2004).

Since our study focuses on fault source seismicity, we will elaborate more on the part of seismology that deals with the study of fault related earthquakes.

The "Elastic Rebound" theory is widely adopted to explain the mechanism of fault source earthquakes. According to this theory the distant ground on opposite sides of an active fault is continuously moving, while in contrast, friction along the fault plane locks its movement and results in strain accumulation with time. The increasing strain reaches a failure threshold that triggers the rupture along the locked fault and the release of elastic waves (Yeats et *al.*, 1997; Stein & Wysession, 2004; Lowrie, 2007).

Usually ruptures initiate along an asperity under the surface, which lead to the definition of a point source for the nucleation of earthquakes also termed the hypocenter. The projection of the hypocenter on the surface is known as the epicenter (Yeats et *al.*, 1997; Stein & Wysession, 2004; Lowrie, 2007).

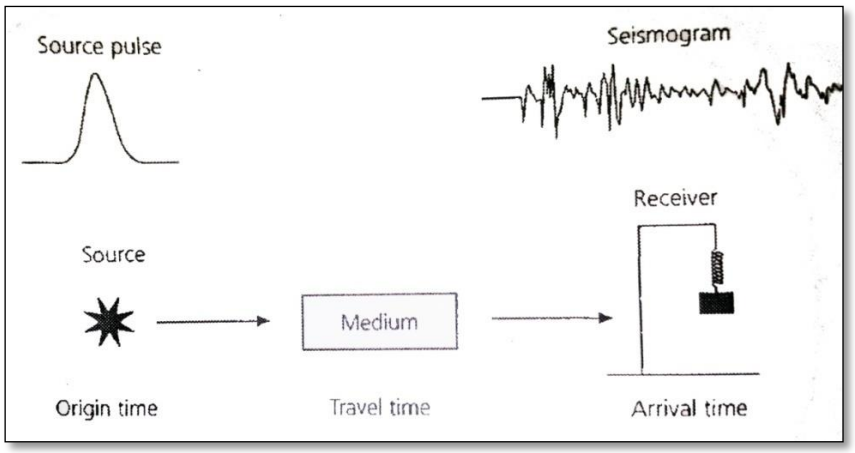

Figure 4.1: A seismic source generates seismic waves that travel and interact with the seismic medium. Receivers record seismograms of these waves (after Stein & Wysession, 2004).

The released waves spread away from their focus (hypocenter) and propagate in the heterogeneously structured earth's interior. They are reflected, refracted and diffracted as they travel from one medium to another according to difference in specific velocity of each medium (Stein & Wysession, 2004). At the surface, seismometers record seismograms of the ground motion (Fig. 4.1) resulting from the emergence of these waves (Stein & Wysession, 2004).

These seismograms are tools used by seismologists to determine the magnitudes, the locations and the focal mechanisms of their corresponding earthquakes.

Subsequently, these recorded earthquakes and their corresponding attributes are gathered in earthquake catalogs, essential in seismic hazard assessments.

4.1.1. Locating an Earthquake

Several methods for locating earthquakes are developed. Among those we will discuss (1) the manual method and (2) the fundamentals of computerized methods.

The manual method is the simplest way to estimate the location of an earthquake. It relies on the difference in first arrival times of P and S waves recorded by at least three stations (Havskov & Ottemöller, 2010). In fact the difference in the velocity between the faster P-waves and the slower S-waves leads to an increasing difference in travel time between these first arrival phases (Fig. 4.2a) as the distance between the earthquake's epicenter and the recording seismic station increases (Yeats et *al.*, 1997).

Once the first arrival P and S waves difference in travel time is determined on the corresponding seismogram, one can refer to standardized travel time charts (ex:

IASPEI, ak135 tables) to estimate the epicentral distance (Fig. 4.2a), which is the distance between the station and the epicenter (Yeats et *al.*, 1997).

This estimated distance defines the radius of a circle centered on the recording station (Fig. 4.2b). This procedure is repeated for at least two other stations. The epicenter is located at the intersection (Fig. 4.2b) of the three circles (Yeats et *al.*, 1997).

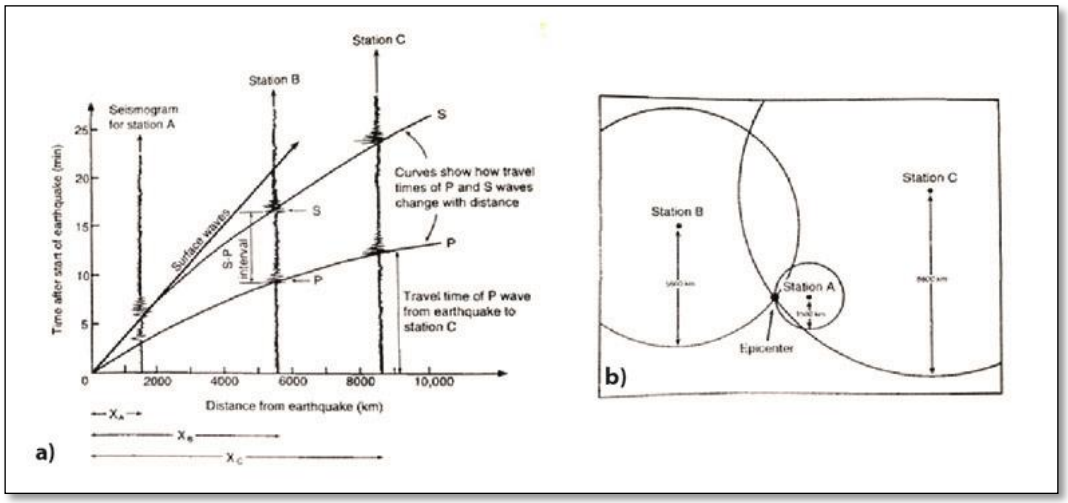

Figure 4.2: a) seismograms of an earthquake recorded by three stations A, B and C. The travel time difference between P and S waves increases with increasing distance (Yeats et *al.*, 1997).b) a minimum of three stations is required to locate the epicenter of an earthquake using this method (after Yeats et *al.*, 1997).

This method is simple and easy to apply, however it only provides an approximation for the epicenter of an earthquake and cannot account for the depth. Variations of the method make use of different types of seismic waves (body and also surface waves) to better constrain the different parameters of the source.

Computerized methods are more complicated yet more reliable/efficient approaches to locate earthquakes. These necessitate complex calculations which require the processing power of computers. Several algorithms and softwares are developed to meet this need.

These modern methods necessitate recorded data from at least 3 seismic stations and a velocity model (Havskov & Ottemöller, 2010). In brief the logic behind these approaches is:

First an initial hypocenter (x_0, y_0 and z_0) is assumed and the arrival time of the seismic wave at a seismic station (x_i, y_i and z_i) is computed using:

$t_i^{arr} = t_i^{tra}(x_i, y_i, z_i, x_0, y_0, z_0) + t_0 = t_i^{tra} + t_0$

Where t_i^{tra} is the calculated travel time using an assumed hypocenter and t_0 is the time at the origin hypocenter.

Then the seismic wave travel time is calculated several times using:

$$t_i^{tra} = \frac{\sqrt{(x - xi)2 + (y - yi)2}}{v}$$

Where v is the velocity.

Finally the modeled arrival time (t_i^{arr}) is compared to the recorded arrival time (t_i^{obs}) using:

$r_i = t_i^{obs} - t_i^{arr}$

The residual difference (r_i), relies greatly on the calculated travel time (t_i^{tra}); therefore several iterations are computed in order to obtain the minimum residual possible (Havskov & Ottemöller, 2010). This procedure is repeated for each recording station.

4.1.2. Accuracy of Earthquake Location

The earthquakes' location procedures show always a degree of uncertainty. Inaccuracies arise mainly from picking errors, modeling errors (Billings et *al.*, 1994) and from the seismic network geometry/density (Kim et *al.*, 2005).

Picking errors rely greatly on the quality of data, which is imposed by the accuracy and sensitivity of the recording seismic instruments, the signal to noise ratio, the accuracy of the arrival time and the available phase for picking (Kim et *al.*, 2005).

Modeling errors arise from the departure of the real earth velocity structure from the selected velocity models (Billings et *al.*, 1994; Kim et *al.*, 2005). Finally the geometrical distribution of the seismic stations within the seismic network and the number of stations recording the event, contribute greatly to the accuracy of location.

The errors introduced to the earthquake location by each of these classes are inseparable (Billings et *al.*, 1994). These are reflected in the resultant Root Mean Square (RMS) error, computed through the earthquake location modeling.

4.1.2.1. Velocity Models and their Contribution to the Accuracy of the Localization Process

Elastic waves velocity models are simulations of the velocity structure of the earth's interior. The main, direct method for seismologists to develop and calibrate these models is through experiments, in which explosives are detonated at well-known time and geographic coordinates and recorded by several seismic stations or networks hundreds to thousands of Kilometers away. Each model possesses one or several specific seismic phases (e.g. P-waves, S-waves…). Examples of such calibrations are found in Lienert (1997) and Murphy et *al.* (2010).

Velocity models available are of different scales and types. These vary from global scales (e.g. EMC-ak135, EMC-IASP91 and IASPEI) to more local scales (e.g. the Murphy et *al.* (2010) velocity model for California) and from one dimensional (1-D) -taking in consideration depth variation in the velocity- to three dimensional (3-D), which consider the lateral variation in the seismic velocity (Storchack et *al.*, 2007).

The accuracy of earthquake's location depends greatly on the selected velocity model (Linert, 1997; Havskov & Ottemöller, 2010). An experiment assessing the accuracy of earthquake location procedure using the 1-D regional IASP-91 velocity model, shows that the minimal error value reached is ±10Km horizontally (longitude and latitude) and 20Km in depth (Lienert, 1997). This example shows that the usage of 1-D velocity models may lead to great inaccuracies where the location of the hypocenters becomes magnitude dependent (Bilings et *al.*, 1994). Storchack et *al.* (2007) believe that such large uncertainties may be importantly reduced by using local (3-D) velocity models.

4.1.2.2. Seismic Network Geometry and Density and its Contribution to the Precision of Earthquake Location

The errors in the earthquake location resulting from the selected velocity model vary with seismic network geometry (Billings et *al.*, 1994).

The seismic network geometry surrounding an earthquake is defined through the azimuthal gap and the epicentral distance, which act as indicators for the accuracy of the hypocentral solution (Havskov & Ottemöller, 2010).

The azimuthal gap is the largest azimuthal angle between two stations recording a certain event. It mostly influences the accuracy of the epicenter's location (Bondár et *al.*, 2004; Schönholzer, 2009) and is usually desired to be reduced by having a seismic network surrounding the recorded earthquake (Bai et *al.*, 2006). Bondár et *al.* (2004) suggest that better epicentral locations may be obtained if the azimuthal gap is kept below 110˚. A gap greater than 180° indicates that all the recording stations are at one side of the event (Bai et *al.*, 2006; Havskov & Ottemöller, 2010). In this case small picking errors will lead to hundreds of kilometers deviations in the earthquakes' locations (Billings et *al.*, 1994).

The accuracy of the focal depth solution depends greatly on the epicentral distance, the distance between the epicenter and the closest recording station -in combination with the velocity model- (Bondár et *al.*, 2004; Schönholzer, 2009). Reducing the epicentral distance usually favors more precise focal depth estimates (Schönholzer, 2009).

In addition to the geometry of the seismic network, its density -the number of stations recording an event- plays an important role in the accuracy of the hypocentral solution. Usually, denser seismic networks advocate more reliable earthquake solutions (Bai et *al.*, 2006). Some seismologists suggest the usage of 10-15 stations may yield more accurate earthquakes' locations (Bondár et *al.*, 2004; Bai et *al.*, 2006).

4.1.3. RMS of Earthquake Locations and Implications on the Accuracy

The Root Mean Square (RMS) residual is a statistical value calculated from the least squares solution (e) for the (r_i) travel time residuals (see section 4.1.1.) of the (n) stations recording an earthquake using (Havskov & Ottemöller, 2010):

$$RMS = \sqrt{e/n}$$

$$e = \sum_{i=1}^{n} (r_i^2)$$

The RMS indicates the fit of the observed wave arrival time at the recording stations with the modeled/predicted arrival times (Havskov & Ottemöller, 2010).

This parameter-reported in seconds- reflects the errors arising from the accuracy of the velocity model and from observational errors. Therefore the RMS is often used as reference for the earthquake's location precision. Yet this value alone doesn't guarantee reliable solutions; seismologists must always check its conformity with their knowledge of the geology of the area (Havskov & Ottemöller, 2010).

For a small local seismic network, it is desirable to keep the RMS smaller than 0.5s in order to have reliable earthquake locations (Havskov & Ottemöller, 2010).

4.1.4. Earthquake's Magnitude

The earthquake's magnitude characterizes quantitatively the relative size of an earthquake at its source and thus the amount of energy released (Bolt, 1999; Stein & Wysession, 2004). This parameter is calculated from the maximum amplitude of the

designated seismic phase recorded on the seismogram, after correcting for the decrease in this amplitude associated with geometric spreading and attenuation of the elastic waves with distance (Stein & Wysession, 2004). Several magnitude scales are defined; the most adopted are the local magnitude (M_L), the body waves' magnitude (mb), the surface waves' magnitude (M_S) and the moment magnitude (M_W).

The local magnitude/Richter scale is a logarithmic base 10 scale developed by Charles Richter, in 1935, specifically for earthquakes occurring in California and recorded on "Wood-Anderson" seismograms with a natural oscillation of 0.8s (Richter, 1935). It utilizes the maximum amplitudes of P and S waves to estimate the local magnitude (Richter, 1935).

More recently, seismologists developed the body waves/surface waves magnitude scales in order to account for global seismicity.

The body wave magnitude, mb, is determined from early arrival of P and S waves using the following relation:

$mb = \log (A/T) + Q(ħ,\Delta)$

A is the amplitude of ground motion (micron)

T is the wave period (sec).

Q is and empirical term depending on (ħ) distance and (Δ) focal depth (Stein & Wysession, 2004).

On the other hand, the Surface waves' magnitude is measured from the Rayleigh and Love waves' amplitudes using the following relation:

$M_S = \log (A/T) + 1.66 \log \Delta + 3.3$ or

A is the ground motion amplitude (microns).

T is the wave period (sec).

Δ is the distance in degrees (Stein & Wysession, 2004).

The body and surface waves' magnitudes are easy to calculate from seismograms with no need to signal processing. However their corresponding magnitude scales saturate for mb = 6.2 and M_S = 7.3, underestimating thus events with larger magnitudes (Yeats et *al.*, 1997; Bolt, 1999; Stein & Wysession, 2004).

The invention of a seismic moment magnitude scale resolved the magnitude saturation issue. This scale utilizes the seismic moment (M_0) in the computation of the moment magnitude (M_W) using the following relation (Yeats et *al.*, 1997; Stein & Wysession, 2004):

$M_W = \frac{\log M_0}{1.5}$ - 10.73

M_W is in dyn-cm.

$M_0 = \mu \bar{D} S$

Where M_0 is the static seismic moment that describes the faulting process (Stein & Wysession, 2004).

4.2. Earthquake Catalogs and the Gutenberg-Richter Function

4.2.1. Determination of the Gutenberg-Richter Equation from Earthquake Catalogs

Earthquake catalogs are lists of earthquakes and their properties, gathered for a certain region and for a specific time span. The Gutenberg-Richter empirical relation utilizes earthquake catalogs' data for seismic hazard estimation. This function applies to a wide range of tectonic settings, depth/magnitude range, earthquakes populations and

to earthquake catalogs covering time ranges between few months to thousands of years (Marzocchi & Sandri, 2003). Therefore many seismic hazard studies use this function in their assessments.

This relation is given as:

Log N = a – bM

Where:

M = magnitude,

N = cumulative number of earthquakes with magnitudes ≥M,

a = positive real constant depends on the volume and time span considered,

b = positive real constant that is usually close to 1.

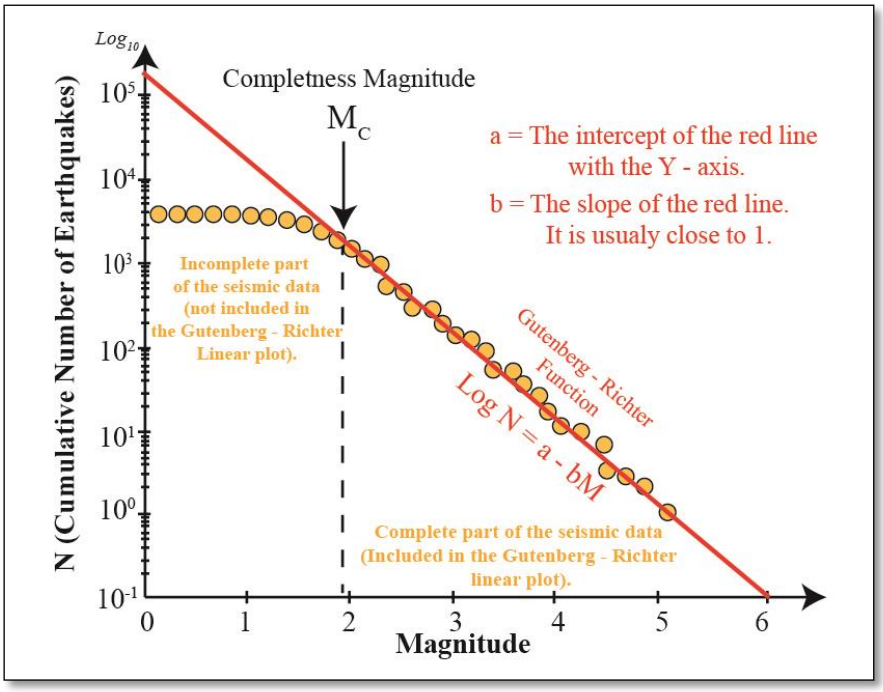

Figure 4.3: Frequency-Magnitude function plots as a straight line on a semi-log graph.

The Gutenberg-Richter relation power law gives an idea on the frequency of occurrence of an earthquake with a magnitude (M). It plots as a linear function on semi-log graphs; (b) is thus the slope of the best fit line and (a) is its intercept with the N axis (vertical axis) for M = 0 (Fig. 4.3).

4.2.2. Reliability of b-value Estimations

The reliability of the b-value estimation requires several criteria expressed and detailed in the literature (i.e. Kulhaneck, 2005; Amorèse & *al.*, 2010; Felzer, 2006). Those are:

1- Uniform Magnitude scale must be applied. Usually it is preferred to work with the Moment Magnitude M_W that doesn't saturate above $M \geq 7$.

2- The time span of the used catalog must be larger or comparable to the recurrence of the largest earthquake predicted.

3- The incomplete part of the seismic data should not be included in the computation of the b-value.

4- Declustering of catalogs by deletion of all foreshocks and aftershocks attributed to a main event must be conducted.

5- It is desirable that the catalog used, covers more than 3 units of magnitude.

6- The b-value should be solved with a sufficient number of events. Generally it is desirable to use at least 2000 earthquakes that are above the completeness magnitude of the catalog in the b-value estimation.

4.2.3. Significance of b and a Values

The most important aspect of the Gutenberg-Richter equation is that it allows the derivation of the (a) and (b) values.

The b-value, also known as the "Frequency-Magnitude Distribution" is a dimensionless constant that characterizes the relative proportion of large to small earthquakes for a specific region, in a certain time span (Kulhanek, 2005).

The b-value is deduced from the slope of the best linear fit for the Gutenberg-Richter plot, constrained from the complete part (to be discussed later) of the used earthquake catalog (Fig. 4.3).

Normally b-values are close to 1 (Enescu & Ito, 2003). For example Chan et *al.* (2012) estimated b-values between 0.88 and 0.93 for Taiwan. To the north west of Sumatra, frequency-magnitude distribution estimates yielded b-values between 0.7 and 1.6 for each of the 3 years preceding the 2004 Sumatra earthquake (Nuannin et *al.*, 2005).

Significant deviations of the b-value from its normal value (1) are frequently observed. Seismologists attempted to understand the reasons for b-values divergence from the normal, through several laboratory experiments. These show the presence of three main natural factors for these departures (Enescu & Ito, 2003). Mogi (1962) demonstrates that an increase in material heterogeneity induces an increase in the b-value. Scholz (1968) notes that an increase in the shear/effective stress results in a remarkable decrease in the b-value. Finally, Warren & Latham (1970) demonstrate that an increase in the geothermal gradient leads to an increase in the b-value.

Furthermore, case applications show that the b-value may vary with depth and time span and is greatly related to the type of tectonism of the studied area. In fact, studies on earthquake swarms, which are clusters of small to moderate earthquakes with no distinct main shock, yielded b-values of ~ 2.5. These swarms are usually associated with volcanic activity that last for short time periods (Stein & Wysession, 2004; Kulhanek, 2005). Another study conducted by Yang & Hauksson (2011), on the East Los Angeles Basin, shows a depth decrease in the b-value from 1.3 at 2Km to 0.4 at 17Km; a blind thrust at around 17 Km is held responsible for this decrease.

Areas with low b-values are usually predisposed to high differential stresses (Schorlemmer et *al.*, 2005), therefore they may host the initial ruptures for large earthquakes (Wyss & Stefansson, 2006). Subsequently, the b-value and its variation were used in several studies to predict earthquakes. A case example, provided by Chan et *al.* (2012), shows that the b-value of a certain area may decrease by 5% from its earlier values, one year before the occurrence of a large earthquake. Nevertheless the usage of the b-value as a precursor to forecast earthquakes remains under question.

The a-value represents the intercept of the Gutenberg-Richter linear plot with the vertical axis of the semi log graph at M = 0. This constant is an indicator for the seismicity rate (Wyss et *al.*, 2000). If data used to plot the Gutenberg-Richter function covers one year, then (a**)** tells us that on average once per year, an earthquake of magnitude (a/b**)** or bigger may happen (a if b = 1).

4.2.4. Declustering Earthquake Catalogs

Earthquake clusters consists of a concentration of earthquakes along a certain tectonic structure, in space and time. Common examples of earthquake clustering are observed in aftershocks series occurring after a main shock (Zaliapin & Ben-Zion, 2013). Therefore earthquake clusters are usually composed of events (foreshocks and aftershocks) that are spatially and temporally dependent on the main shock.

The seismic hazard estimation of a certain area necessitates knowing the best possible rate of main shocks occurring within it, which are most of the time independent events (Stark, 2011). Therefore seismologists decluster earthquake catalogs to obtain a set of independent events (Boyd, 2012) by removing foreshocks and aftershocks from the seismicity data (Stark, 2011).

Yet not all main shocks are independent events. Clusters are sometimes used in earthquake predictions (Gardner & Knopoff, 1974). In fact earthquakes clusters can cause adjacent quakes or trigger other main shocks located on distant faults with respect to the major fault source. This is what happened in Turkey during the 1999 earthquake sequence. The $M_W = 7.6$ Izmit earthquake that happened on August 17, 1999, triggered three months later (on November 12, 1999) the $M_W = 7.2$ Dücze earthquake (Durand et *al.*, 2010). Declustering of catalogs will take this relationship into consideration.

The Gardner & Knopoff (1974) and the Reasenberg (1985) methods are probably the most commonly applied approaches for declustering earthquake catalogs. The former method identifies events (mostly aftershocks) dependent on a main shock, based on a specific space and time window, and deletes these events (Gardner & Knopoff, 1974). The Reasenberg (1985) is a method which defines cluster by linking earthquake

events with their main trigger event. For example if A is the main shock triggering B, and B is the main shock triggering C, then A, B and C define a cluster. Only the biggest trigger event (A in this case) is kept during declustering (van Stiphout et *al.*, 2012).

4.2.5. Completeness of Earthquake Catalogs

The Gutenberg-Richter semi-log plots for earthquake catalogs show deviations below a certain magnitude termed Completeness Magnitude (MC), from the expected linear trend of the Gutenberg-Richter function (Fig. 4.3). Therefore the completeness Magnitude (MC) is the lowest magnitude above which we can assume that 100% of the events are recorded by the seismic network.

This suggests an under sampling for the events with magnitudes smaller than (MC), where the number of recorded events is less than what is expected (Woessner & Wiemer, 2005). These deviations occur for many causes:

1- Earthquakes are small to be recorded by enough seismic stations, because they fall below the detection sensitivity of the seismometers within the network.

2- Sometimes network operators disregard certain events below a certain threshold because they are of no interest to them.

3- Aftershocks sometimes pass undetected by the masking coda of larger events.

It is a common practice to remove the events with magnitudes smaller than (MC) from the seismic data used for the computation of the Gutenberg-Richter functions (Fig. 4.3).

4.3. Historical Seismicity of Southern Central Mt. Lebanon

Historical documents constitute an important source of information for historical earthquakes. These are used in building historical earthquake catalogs for several areas in the world (Guidoboni, 1994; Berberian, 1995; Tan, 2008; Ambraseys, 2009). In other cases archeological records and paleoseismic studies help constrain the ages of old historical quakes (e.g. Daëron et *al.*, 2005; Nemer et *al.*, 2008). In this section we review the historical seismicity of the SCML based on historical earthquake catalogs, in order to have better understanding for its long-term seismicity.

4.3.1. A Review of the Historical Earthquakes Felt in the Southern Central Mt. Lebanon

The historical seismicity of the area was built from reviewing available historical texts related to the area as well as published catalogs.

A reference catalog for the historical seismicity of Lebanon, entitled the "Seismicité Du Liban" (Plassard & Kogoj, 1981) summarizes most of these events. It includes major tremors that took place between -1365 B.C and 1978 A.D. The events felt -but not necessarily located- in the southern central Mt. Lebanon are summarized in tables 4.1, 4.2 and 4.3, in which the time subdivisions of the original catalog by Plassard & Kogoj (1981) are adopted.

Table 4.1: Summary of historical earthquakes felt in the southern central Mt. Lebanon. These are extracted from the historical earthquakes that struck Lebanon and the Levant region between -1365 B.C. and 1900 A.D. (Plassard & Kogoj, 1981).

Number	Date	Intensity	Remarks
1	-525 B.C.	10	• Total destruction of Tyr • Saida 2/3 destroyed • Epicenter might be located near Bisri.
2	19 A.D.	6	• Strongly felt in Saida.
3	349 A.D.	10	• Felt with intensity of 9 or 10 in Beirut. • Destruction of the Majority of Beirut.
4	July 6, 551 A.D.	11	• Destruction in Beirut. • Tsunami.
5	June & July, 1201	10	• Destruction of all major cities: Beirut, Tyr, Baalbek, Damascus
6	October 30, 1759 A.D. at 4 am	8	• Chouf habitants abandon their houses and move to the cultivated lands to live in tents.
7	November 25, 1759 A.D. at 19h : 30min	10	• Huge destruction in the Chouf area (Deir el Mukhalles, Kfar Hatta, Moukhtara). • More than 100 dead in the Chouf.
8	January 1, 1837 A.D.	9	• Destruction in Chouf, Chehim village.
9	October 12, 1856 A.D.	6	• Felt on the coast between Haifa and Damour. • Tsunami.
10	February 26, 1877 A.D.	3	• Felt in Saida.
11	January 23, 1881 A.D.	3	• Felt in Saida.

	at 17h 45min		
12	June 29, 1896 A.D. at 20h 43min	6	• Felt in Lebanon and in Syria. • Strongly felt in Bisri (Chouf area) according to a witness.

Table 4.2: Summary of earthquakes felt in the southern central Mt. Lebanon, extracted from all tremor that shook Lebanon and the Levant region between 1900 and June 14, 1921. (Plassard & Kogoj, 1981).

Number	Date	Magnitude	Remarks
13	March 1 - March 17 - October 7,1906	3.5	• 33°8-35°4 Offshore Khaldeh.
14	June 10, 1907 at 12h 15min	4.8	• 33°7-35°4 Offshore Khaldeh.
15	June 22, 1907	4.9	• Felt in Damour. • Panic among citizens. • Felt less in Beirut and Saida.

Table 4.3: Summary of felt earthquakes in the southern central Mt. Lebanon, extracted from all the events that shook the Levant region and recorded by the Ksara seismic station between June 14, 1921 and December 31, 1978. (Plassard & Kogoj, 1981).

Number	Date	Depth	Magnitude	Remarks
16	March 16, 1956 at 19h 43min 27sec	9Km	5.8	• 33°6-35°5 near Aazour (Chouf). • Felt in Chehim, Jezzine, Deir el Mukhalles, Saida, Damour, Deir el Qamar, Beirut and Beit ed Dine. • Great destruction in Chehim.

17	February 18, 1961 at 00h 15min 10sec	-	3	• 33° 3-35° 1 in the Beirut-Damour area.
18	February 18, 1965 at 23h 16min 09 sec	-	2.6	• 33°6-35°2 in the greater Saida region.
19	June 6, 1966 at 00h 46min 05sec	-	2.0	• 33°7-35°3 in the greater Damour-Saida region.
20	August 7, 1967 at 19h 54min 29sec	-	3.2	• 33°8-35°2 in the greater Beirut-Damour region.
21	April 16, 1971 at 21h 27min 43sec	7Km	4.7	• 33°6-35°5 near Bisri. • Felt in Aazour where a Landslide occurred. • Felt in Deir el Mukhalles, Jiyeh and Damour.
22	October 17, 1972 at 01h 07min 36sec	-	2.5	• 33°8-35°4 in the greater Khaldeh area. • Felt in Beirut and the Coastal area.

The Plassard & Kogoj (1981) is the latest catalog of earthquakes in Lebanon. However it holds a number of inaccuracies and missing information on some events. More recent results from paleo-seismology or other related fields have greatly refined

and completed the list (Guidoboni, 1994; Ambrasesys, 2009) and should be referred to for more specific studies on seismic hazard of the region.

An important historical reference, the book “The History of Prince Haidar Ach-Chahabi, volume 2” (Moghabghab, 2000) presents important events that happened in Mt. Lebanon and the Chouf area in particular in the 17th to 19thcentury. Among these events, the book presents first author reference to a massive landslide accompanied by a ground shaking in the Kafr Nabrakh area of the SCML. Below we present first the original text as written in Arabic, and then our translation to the English language.

"و في سنة ١١٨١هـ =١٧٦٧م خسفت الأرض جانب نهر الصفا تحت قرية كفرنبرخ وتزلزلت تلك اللأرض وانتقل الجبل الذي تحت قرية كفرنبرخ المذكورة الى عبر قرية مجدل المعوش و تلفت أرزاق لا تحصى تحت الردم وبيوت بما فيها من الناس و المواشي وعطل الردم جميع تلك الأراض حتى احتبس نهر الصفا عن جريه أياما" و ظل ماؤه معتكرا" جملة سنين. و كان يسمع صياح الديوك من تحت الردم وقيل أن رجلا" كان حاملا" قفيرا" من النحل على ذلك الجبل فما درى الا والجبل يمشي به حتى وجد نفسه في الجانب الاخر فاندهش وذهب عقله وعاش بعد ذلك مجنونا" حتى مات. وكان ذلك في اليوم الثاني عشر من شهر كانون الأول (ديسمبر) والى الان يقال لذلك المكان زحلة كفرنبرخ." (Moghabghab, 2000)

“In year 1181 Hijri = 1767 A.D. the lands below Kafr Nabrakh, facing the Safa River, subsided and the earth was shaken. The mountain below the previously mentioned Kafr Nabrakh village, moved toward the Majdel Meouche village. Infinite fortunes and properties were lost under the rubble, with all its contents and occupants of man and cattle. The rock debris covered all this land and blocked the flow of the Safa

River for days, and its waters were troubled for a number of years. Crowing roosters could be heard from below the dump. It was told that a man carrying a hive of bees found himself moving with the slump from one side to the other. After this surprising experience the man lost his sanity and lived insane for the rest of his life. This happened on the 12 of December 1767 A.D., and since, this place is called "Zahlet Kafr Nabrakh"."

The text above is an example highlighting how throughout history inhabitants of the Damour-Beit ed Dine area felt number of earthquakes, among which some should have been located inside the SCML area and resulted in devastating losses in lives and properties. That the date of the related event (12 December 1767AD) does not show on Plassard & Kogoj (1981) list suggests that it was a local event not felt, or little felt, elsewhere in the country which made it go unnoticed. It is very likely than that the tremors felt were due to a local earthquake, within the Chouf area.

For the purpose of historical earthquakes review the SCML as defined in chapter 3 is slightly extended northward to reach Beirut and southward to reach Saida.

4.3.2. Summary and Discussion

Plassard & Kogoj (1981) documented 22 historical earthquakes that have affected the southern central Mt. Lebanon between -525 B.C and 1972 A.D. The most destructive among those (e.g. events 4, 5, 6, 7, 8 and 16 summarized in the above tables) are located on the major faults of the LRB (Daëron et *al.*, 2005; Nemer & Meghraoui, 2006; Elias et *al.*, 2007). Among the remaining events, no particular quake is attributed to the DBF. Yet the uncertainty on the exact location of events 1, 12 and 15

as provided by Plassard & Kogoj (1981) and their proximity to the study area suggests that these may be located anywhere in the SCML and therefore may probably relate to ruptures of the DBF. Further investigation beyond the scope of this work is nevertheless needed to understand the exact origin of these quakes.

The text by Prince Haidar el Chehabi describes a sudden mass wasting event in Kafr Nabrakh in the year 1767 A.D. The effect of this landslide on the geology/topography of the area is clearly seen on the field (Fig. 3.10). It corresponds with the slid area of Kafr Nabrakh where slope processes over the time resulted in high topographic escarpments bounding the intensely disturbed geology of the southern flank of the Safa River valley. The event reported by Prince Haidar although it is one of the biggest, it is surely not the only one responsible for the present day topography of the area. In fact, mass-wasting slope processes in the area are still happening today. Moreover, as reported, the text strongly suggests that the earthflow event was accompanied by a tremor, likely of earthquake origin. In that case, this can be taken as a direct evidence of earthquake-triggered slope processes in the area, especially that the location of the causative escarpment is over the DBF zone.

The historical seismicity of the southern central Mt. Lebanon advocates that this area is prone to infrequent, but destructive earthquakes. This urges a further investigation of the seismic hazard of the area using recent seismic data provided by the newly deployed seismic network of Lebanon.

4.4. Instrumental Seismicity of the Southern Central Mt. Lebanon

4.4.1. The Seismic Network of Lebanon

The National Center for Geophysical Research (NCGR) of Lebanon is a governmental agency responsible for seismic monitoring in this country, since its establishment in 1975 by the National Council for Scientific Research (CNRS).

In the beginning of 2006, NCGR launched GRAL (Geophysical Research Arrays of Lebanon) starting with five broadband seismic stations located in Bhannes, Hawqa, Matarih/Saida, Fakeheh and Rachaya. Later, three additional seismic stations were installed in Beirut (July 2006), Naqoura (July 2008) and Deir el Qamar (March 2010) and connected to the GRAL seismic network (Table 4.4).

Table 4.4: The eight broadband seismic stations of GRAL and their respective geographic location (NCGR, 2010).

Station	Latitude	Longitude	Elevation(m)	Name	Date of Deployment
BHL	33° 54.25'N	35° 39.25'E	1000	Bhannes	May 1980
HWQ	34° 16.68'N	35° 56.78'E	1161	Hawqa	January 2001
MATL	33° 29.32'N	35° 19.78'E	5	Matarih	November 2000
FKH	34° 14.13'N	36° 24.11'E	1170	Fakeheh	December 2004
RCY	33° 29.08'N	35° 49.13'E	1360	Rachaya	June 2006
BEYL	33° 52.30'N	35° 29.59'E	49	Beirut	July 2006
NAQL	33°07.02'N	35°08.46'E	83	Naqoura	July 2008
DQRL	33°42.34'N	35°34.21'E	963	Deir Qamar	March 2010

The NCGR collects the earthquake data/seismograms recorded by GRAL in order to locate the events in space/time and to determine their magnitudes.

Subsequently the information on these events is gathered in monthly catalogs that are available to download in (PDF) format on the website of the CNRS/NCGR. This data is also shared with EMSC (Euro-Mediterranean Seismologic Center) database, who in turn contributes some unrecorded regional events, to the NCGR catalogs. A copy of the data is also available on the ISC bulletin. The current online available NCGR catalogs are for the years 2006-2011.

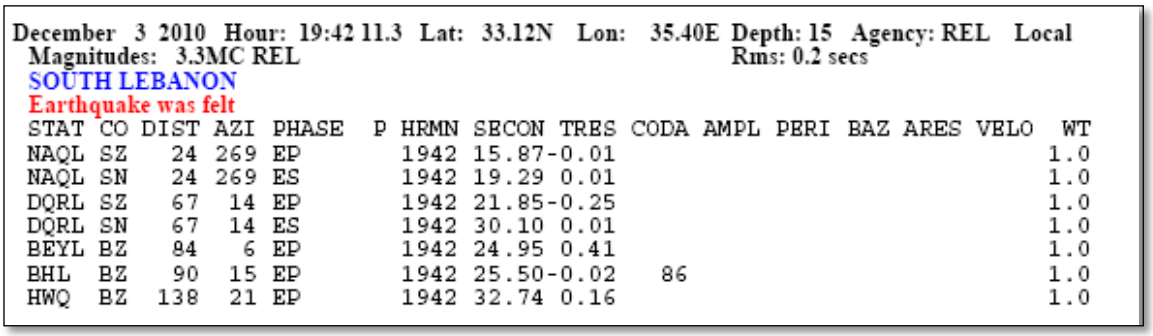

December 3 2010 Hour: 19:42 11.3 Lat: 33.12N Lon: 35.40E Depth: 15 Agency: REL Local
Magnitudes: 3.3MC REL Rms: 0.2 secs
SOUTH LEBANON
Earthquake was felt

STAT	CO	DIST	AZI	PHASE	P	HRMN	SECON	TRES	CODA	AMPL	PERI	BAZ	ARES	VELO	WT
NAQL	SZ	24	269	EP		1942	15.87	-0.01							1.0
NAQL	SN	24	269	ES		1942	19.29	0.01							1.0
DQRL	SZ	67	14	EP		1942	21.85	-0.25							1.0
DQRL	SN	67	14	ES		1942	30.10	0.01							1.0
BEYL	BZ	84	6	EP		1942	24.95	0.41							1.0
BHL	BZ	90	15	EP		1942	25.50	-0.02	86						1.0
HWQ	BZ	138	21	EP		1942	32.74	0.16							1.0

Figure 4.4: A sample event extracted from the December 2010 catalogue, showing how the data provided by GRAL is formatted.

The NCGR monthly catalogs present the information about each recorded earthquake separately. Figure 4.4 is a sample of a recorded earthquake extracted from the catalog of December 2010, which shows the format adopted in the NCGR catalogs. Data about each event includes its date, time of occurrence at the hypocenter, geographic coordinates, depth in Km, the area of occurrence (e.g. Local, Regional or Distant, South Lebanon, Beirut area…), magnitude (mainly coda magnitude M_C), the RMS and whether the tremor was felt or not (Fig. 4.4). Additional details about each

recording station are also listed. This information usually includes the phase of the wave picked for each station, the exact arrival time of the seismic wave at the recording seismic station and the estimated distance and azimuth of the event with respect to each station (Fig. 4.4).

4.4.2. The SCML Seismicity Pattern between 2006-2010

In this research we used the provisional bulletins provided by NCGR for the years 2006-2010 in order to create our database. We extracted all the local and regional events that happened during these five years. Those located within the southern central Mt. Lebanon between longitudes: E35°10'0"-E35°50'0" and latitudes: N33°30'0"-N34°0'0"are selected to create a specific catalog for this area (Fig. 4.5).

A total of 849 earthquakes in the magnitude range of $2.1 \leq M_C \leq 3.7$ were located within the study area between years 2006-2010 as located by the NCGR (Fig. 4.5). Their epicenters are distributed over all the area, but interestingly, a well aligned/dense group of earthquakes stands out in the seismicity of the SCML, extending from Zahle to Damour, in ~ENE-WSW direction, parallel to the strike of the DBF zone (Fig. 4.5). Accordingly we call it the DBF cluster.

Other earthquakes have epicenters loosely grouped in parts of the SCML (Fig. 4.5):

- A first group lies parallel to the Yammouneh Fault, on the eastern side of the Bekaa Valley, extending over ~25Km to the south from Zahle.

- A second group of loosely distributed events is spread between Beirut and Baskinta.

However the alignment of epicenters over the DBF is more pronounced and striking than the rest of the seismicity in this area.

In this section we first assess the accuracy of location of the SCML earthquakes located by the NCGR, then we investigate these spatial, temporal and magnitude distributions of the earthquakes within the DBF cluster, and we conclude on possible relationship between the seismicity and the geological structures of the area.

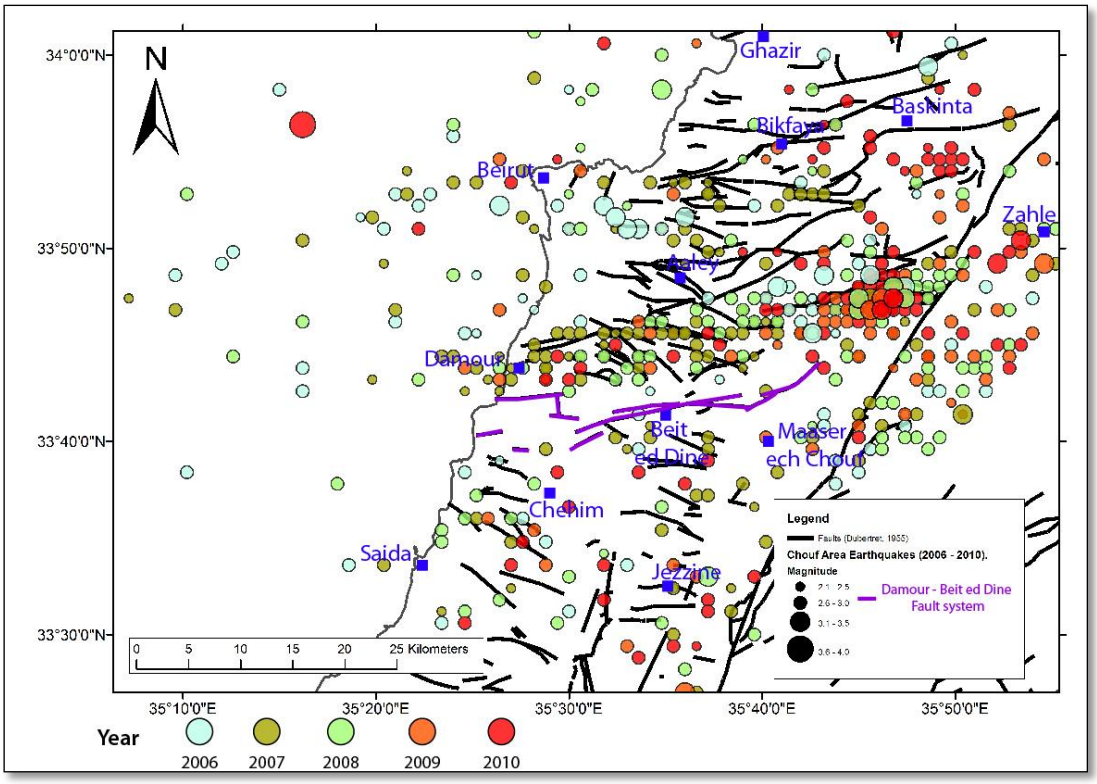

Figure 4.5: Earthquake map of the SCML for years 2006-2010 as recorded by GRAL/NCGR, showing the magnitudes of the events recorded (Faults are taken from Dubertret, 1955).

4.4.2.1. Assessing the Accuracy of Seismic Solutions as Given by NCGR

Two key elements -the velocity model used and the overall geometry of the GRAL seismic network- play major roles in the accuracy of the solutions. These two elements are discussed first in order to assess the reliability of the NCGR data in representing the real active seismic sources within the area. Additionally, we have used depth and RMS distributions for the 5 years SCML seismicity catalog to examine the reliability of this dataset.

4.4.2.1.1. The Velocity Model Adopted by NCGR

The Middle East region has a complex geological and tectonic setting not necessary reflected in the global velocity models used in locating earthquakes. Specific velocity models for the area are therefore required in order to reach better precision on earthquake locations (Gök et *al.*, 2012).

The NCGR uses a 1-D five plane parallel layer velocity model to locate local and regional events. This model adopted from the "Reducing Earthquake Losses in the Eastern Mediterranean Region" initiative (RELEMR) was developed specifically for the Eastern Mediterranean region, after a regional seismic calibration experiment, conducted in 1999. During this experimentation, five tons of buried explosives detonated in the Dead Sea, generated a magnitude 4.0 seismic event monitored at distances of 4000 Km from the source (USGS International Program - RELEMER - http://international.usgs.gov/projects/prjrelemr.htm).This calibration shot allowed estimation of the seismic velocity distribution in the crust of the Middle East.

The RELEMR1-D velocity model, takes in consideration the depth variation in the velocity of P- waves, and doesn't account for its lateral variation. It is summarized as follows (Table 4.5) in the bulletins provided by NCGR (NCGR provisional bulletin, 2006-2010):

Table 4.5: Velocity Model adopted by NCGR for locating local and regional earthquakes (NCGR, 2006 - 2010).

P-wave velocity (Km/sec)	**Depth to top of layer (Km)**
6.2	0.0
6.8	14.0
8.05	34.0
8.25	50.0
8.5	80.0

4.4.2.1.2. The Network Geometry and Density of GRAL

The NNE-SSW elongated shape of Lebanon imposed the NNE- SSW elongated geometry of GRAL. The stations of this small local seismic network are roughly aligned and randomly distributed, with the highest concentration in the southern part of the country, more precisely in southwest Lebanon (Fig. 4.6). Large areas north and east of the country have much smaller number of seismic stations covering them. Earthquakes in the southwestern part of the country -coinciding with the SCML- falling within the

densest part of seismic network are more likely to have better locations than elsewhere (Fig. 4.6).

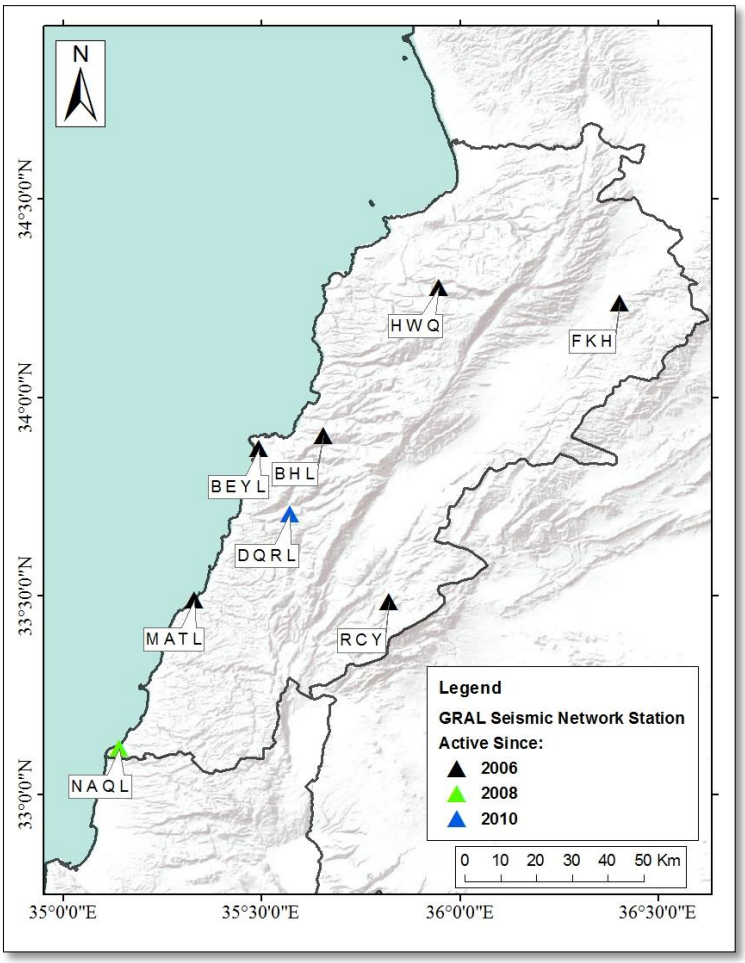

Figure 4.6: Map showing the seismic stations of the GRAL seismic network.

Because of the geometry of the network and the small magnitude of the earthquakes in the SCML area, the localization of these events by the GRAL network was done with data provided by 4-7 stations on average. Few events are located with data from more stations but never more than 10.

4.4.2.1.3. Depth Distribution Uncertainties

The depth distribution for the 2006-2010 SCML catalog are graphically shown on figure 4.7, where the variation of earthquake percentages are plotted versus depth at a 1Km increment.

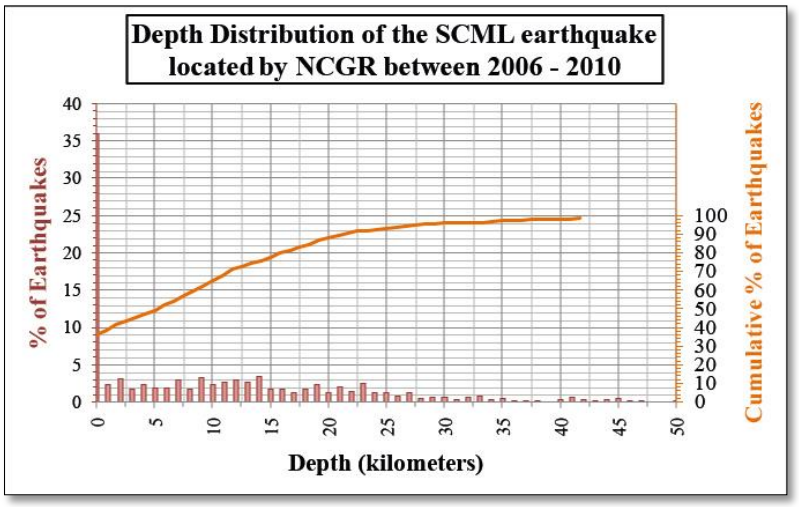

Figure 4.7: The depth distribution of the SCML earthquakes for the years of 2006-2010, as located by the NCGR. The histogram represents the percentage of earthquakes at depth (x); the orange line represents the cumulative number of earthquakes above a certain depth.

Earthquakes located at 0Km depth are the most frequently observed and constitute ~35% of the selected earthquake population. Their percentage is about 10 folds higher than the second most frequent events located at 14Km depth. At 1Km depth, the percentage of earthquakes falls rapidly 2.5% and remains in the range of 2 - 3.5% up to 14Km depth. At 15Km a less remarkable decrease in the events percentages is observed, starting another domain that ends at 27Km depth and where the percentage of earthquakes at each depth is between 1-2%, with the exception of 19Km and 23Km

depths, where values are slightly higher than 2%. Between 28Km and 35Km, this percentage never exceeds 1%. Below 35Km very few events are recorded.

The cumulative depth distribution of earthquakes shows an exponential increase with depth in the upper 32-33Km. A noticeable drop in number of events is seen at around 14-15Km depth. Below, the cumulative number of events displays a much slower increase and most (96% of) events happen in fact above 35-37Km depth in the crust.

Earthquakes are known to nucleate along fault planes at depths greater than 1.5-2Km (Yeats et *al.*, 1997). The 41.34% of the SCML events located by the NCGR are at depths ≤ 2Km (Fig. 4.7), and can be totally discarded from any seismotectonic analysis of the area.

4.4.2.1.4. The Residual Root Mean Square Error (RMS) of the Events Located by NCGR

The Root Mean Square (RMS) error is often adopted as a parameter to assess the accuracy of an earthquake's solution. Havskov & Ottemöller (2010) argue that for a small local seismic network, better hypocentral locations may be obtained for earthquakes with RMS ≤ 0.5s. In this study we adopt this value as a proxy to investigate the precision of the SCML earthquake solutions provided by the NCGR.

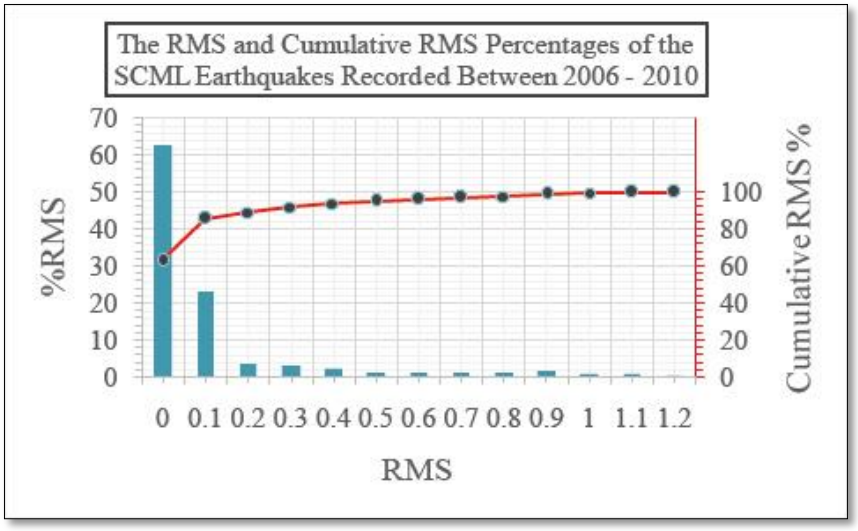

Figure 4.8: The RMS distribution for the southern central Mt. Lebanon earthquakes recorded between 2006 and 2010.

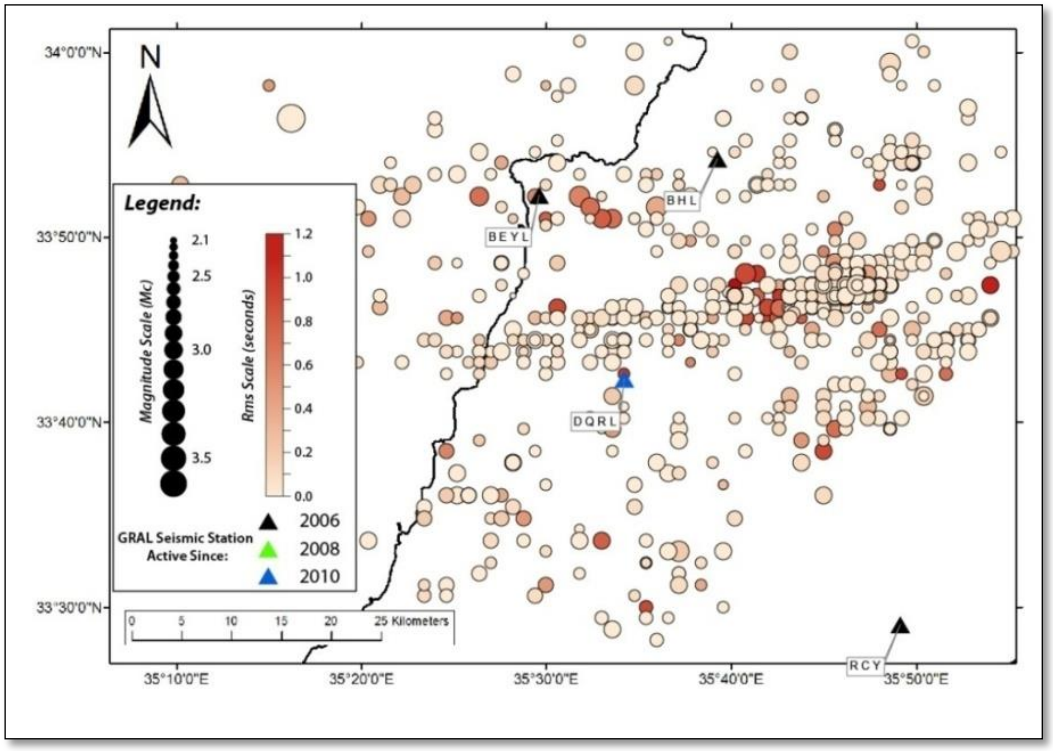

Figure 4.9: Instrumental seismicity map of the southern central Mt. Lebanon, for the years 2006-2010, showing the RMS/magnitude distributions.

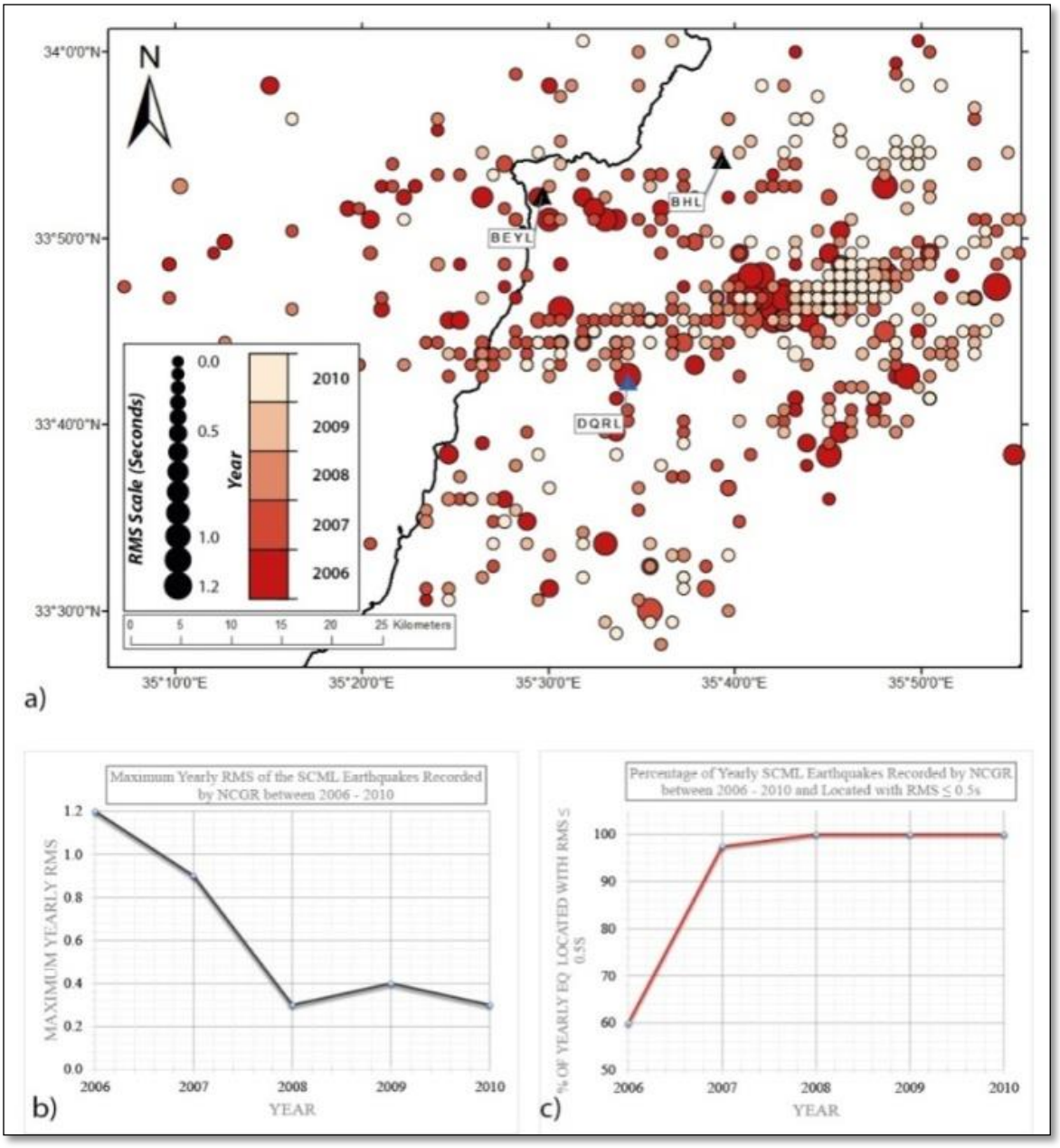

Figure 4.10: a) Map showing the geographic distribution of the yearly RMS residuals for events located in the SCML, between 2006-2010. b) Graph showing the variation of the maximum yearly RMS. c) Graph showing the yearly variation of the percentage of earthquakes with RMS ≤ 0.5s.

Out of the 849 earthquakes of the SCML (for years 2006-2010), 806 events are located with RMS ≤ 0.5s (Fig. 4.8), suggesting that around 95% of this population are reasonably well located. The 5% earthquakes with RMS > 0.5s fall in the eastern half (slightly toward the middle) of the DBF cluster and within Beirut area (Fig. 4.9).

Analysis of the RMS yearly distribution shows that the 2006 events have the largest RMS errors, (Fig. 4.10a), reaching a maximum of 1.2s (Fig. 4.10b). In fact during this year, 60% of the events are located with RMS ≤ 0.5s (Fig. 4.10c), suggesting a low precision of the localization process for that period. Over the following four years (2007-2010), an exponential decrease in the yearly maximum RMS error is observed with a minimum of 0.3-0.4s in the years 2008-2010 (Fig. 4.10b).

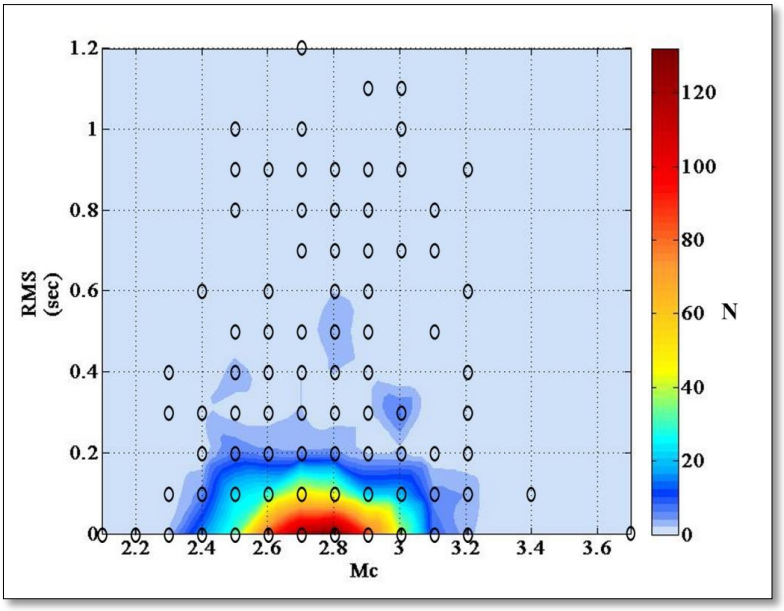

Figure 4.11: Plot showing the interpolation of event numbers (N) of RMS versus Magnitude values for the SCML earthquakes of 2006-2010. The hollow circles indicate data available for interpolation.

These high RMS values correspond to events with magnitudes $2.4 \leq M_C \leq 3.2$ (Figs. 4.9-4.11).As indicated on the graph plotting the event number (N) of the RMS versus the Magnitude values (Fig. 4.11), they are spread, in a more or less homogeneous manner over this magnitude range hosting ~99% of the SCML seismicity (838 out of 849 events) and reach their maximum (RMS = 1.2s) for $M_C = 2.7$ (Fig. 4.11). Thus for the 2006-2010 SCML catalog the accuracy of earthquake location seems to be unaffected by the magnitude of the recorded events.

With depth, on the other hand, these same high RMS values correspond to earthquakes located at depth $0Km \leq d \leq 21Km$ (Fig. 4.12). They constitute ~6% of the earthquakes shallower than 21Km, seem to be spread uniformly over this depth range, where 83% of the SCML seismicity is located (706 out 849 events), and reach their maximum value (RMS = 1.2s) at 0Km (Fig. 4.12). At greater depths ($d > 21Km$) a zone of low RMS values is observed, where this parameter never exceeds 0.5s (Fig. 4.12), with the exception of 1 event located at 67Km (constituting thus ~0.7% (1 out of 143 events) of the deep earthquake population). The depth decrease in the RMS values for the SCML earthquakes suggests a depth increase in the accuracy of their location, thus disagreeing with theoretical expectations. Nonetheless looking at the low RMS events ($RMS < 0.5s$) which constitute ~95% of the SCML earthquakes, we can notice that these spread over the entire depth range of the SCML events' depth distribution, which shows that majority of these recorded events are relatively well located independently from their depth.

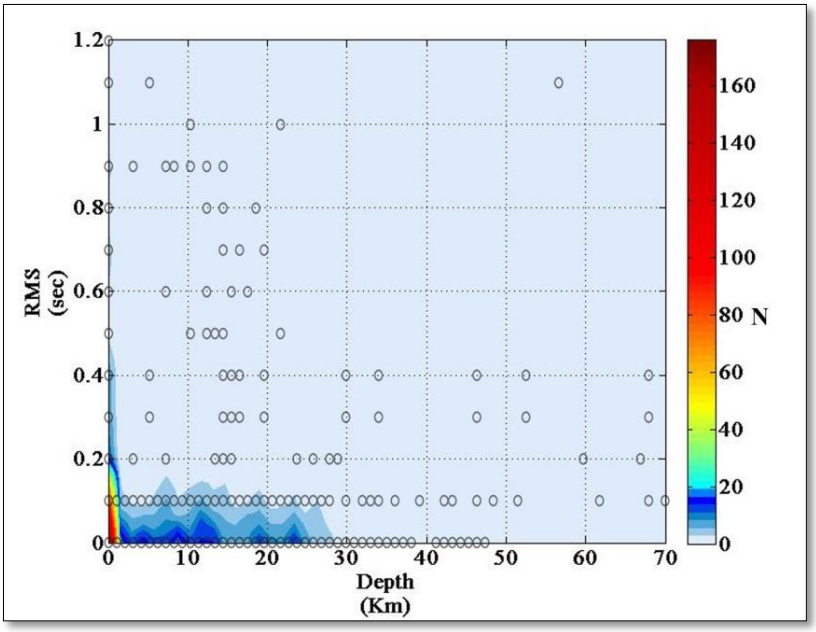

Figure 4.12: Plot showing the interpolation of event number (N) of RMS vs. Depth values for the SCML earthquakes of 2006-2010.The hollow circles represent the available data (X;Y) coordinates.

4.4.2.1.5. Inaccuracies Arising from the Data Format of the NCGR Catalog

The earthquake locations provided in the NCGR catalogs are in decimal degrees, shown with 2 decimal places, i.e. with (0.01 * decimal degree) accuracy. At the latitude of 33°, each 1° in longitude = 93453.18m and each 1°in latitude = 110904.44m. This adds another uncertainty on the location of plotted earthquakes since the 1% of a longitude degree corresponds to 934.53m and the 1% of a latitude degree is around 1109m, which suggests that each located event in the area falls in a rectangle 934.53m long and 1109m wide.

4.4.2.1.6. Discussion of the Accuracy of the SCML Earthquake Localization

The elongated geometry of the GRAL seismic network is unfavorable configuration for earthquake monitoring, and may lead to inaccuracies of located tremors in this country. A similar configuration seismic network, the CWB network of Taiwan, exhibits N-S elongated network geometry, at larger scale though, to the configuration of GRAL network in Lebanon. An assessment for the accuracy of earthquake locations reported by the Taiwanese network reveals that the CWB geometric configuration shifts the located quakes from their true place of nucleation into a zone of narrow azimuth from on the real earthquake location. This shift increases as the events get deeper (Tsai & Wu, 1996).

Hence inaccuracies most likely reside in the SCML seismicity dataset. These can be clearly depicted for the focal depths of the events solutions, where 41.34% of the earthquake population is at depths shallower than 2Km. We interpret such problematic locations to arise, most likely, from inaccuracies in the 1-D RELEMR velocity model adopted by NCGR.

Errors in the epicentral locations, even though they surely exist, are difficult to estimate. We have shown that the data format in the catalog alone contributes to around 1Km uncertainty in both longitude and latitude of events. More important effects on the accuracies of the epicentral solutions of the SCML earthquakes result from the network coverage and density. While the coverage in the SCML is relatively good with events happening within the extent of the network, the majority of events, however, are located using data provided by 4 to 7 stations, therefore not fulfilling the optimal conditions

suggested by Bondár et *al.* (2004) and Bai et *al.* (2006). Further investigation is needed to be able to quantitatively and qualitatively constrain these errors.

Analysis of the RMS of earthquake solutions suggests that in general 95% of the selected earthquakes are reasonably well located. The accuracy of the hypocentral solutions is time dependent: new seismic stations added to the GRAL network throughout the 5 year observation period improved its geometry and thus improved the accuracy of earthquake locations. In contrast no clear variations in the RMS values with depth and magnitude of the events were found, suggesting therefore the absence of any correlation between the accuracy of the location and these two entities.

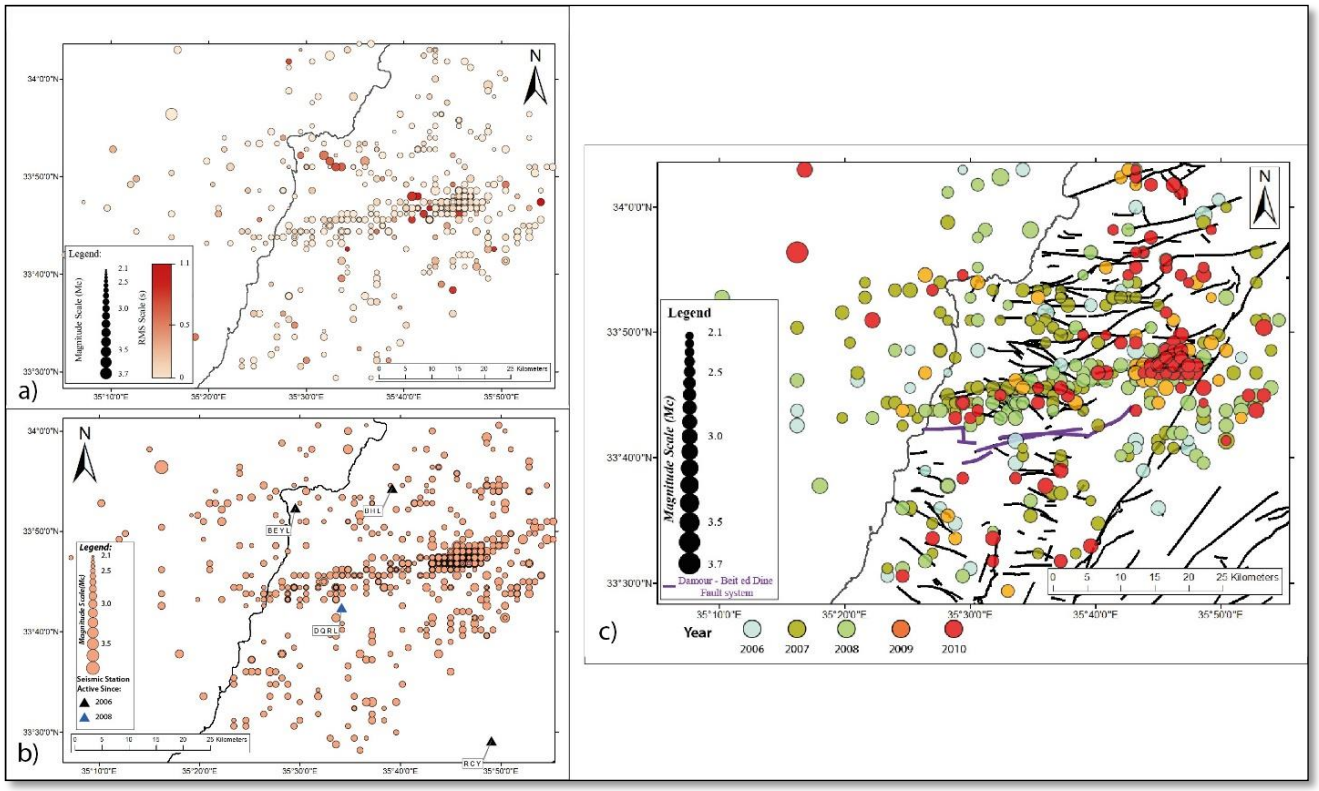

Figure 4.13: Maps showing the seismicity of the SCML for the year 2006-2010 after filtering: a) events shallower than 2Km. b) events located with RMS > 0.5s. c) events shallower than 2Km and located with RMS > 0.5s.

To better examine the effect of location inaccuracies on the seismicity pattern of the SCML, we filtered all the events assessed with low accuracy from our dataset by removing the earthquakes:

i. Located at depths shallower than 2Km, which represent ~41% of total number of events (Fig. 4.13a).

ii. Located with RMS residuals greater than 0.5s, which represent ~5% of total number of events (Fig. 4.13b).

iii. Located at depths shallower than 2Km and with RMS residuals greater than 0.5s, which represent ~44.5% of total number of events (Fig. 4.13c).

Although this process removes an important proportion of the SCML catalog's data -mostly contributed by filtering events shallower than 2Km -, no conspicuous change in the seismicity pattern of the studied area is observed. The most noticeable effect is the relative reduction in size of 2 small earthquake groups: east of the Yammouneh fault and east of Beirut (Fig. 4.13c compared to Fig 4.5). However, in none of the three cases the DBF cluster is affected, and remains visible as a dense ~ E-W elongated seismic pattern (Fig. 4.13a-b-c), suggesting that this trend cannot be an artifact of location inaccuracies.

To conclude the DBF cluster's density, orientation and proximity to the DBF zone implies a direct correlation between the fault's activity and this seismic pattern.

4.4.3. Analysis of the SCML Seismicity

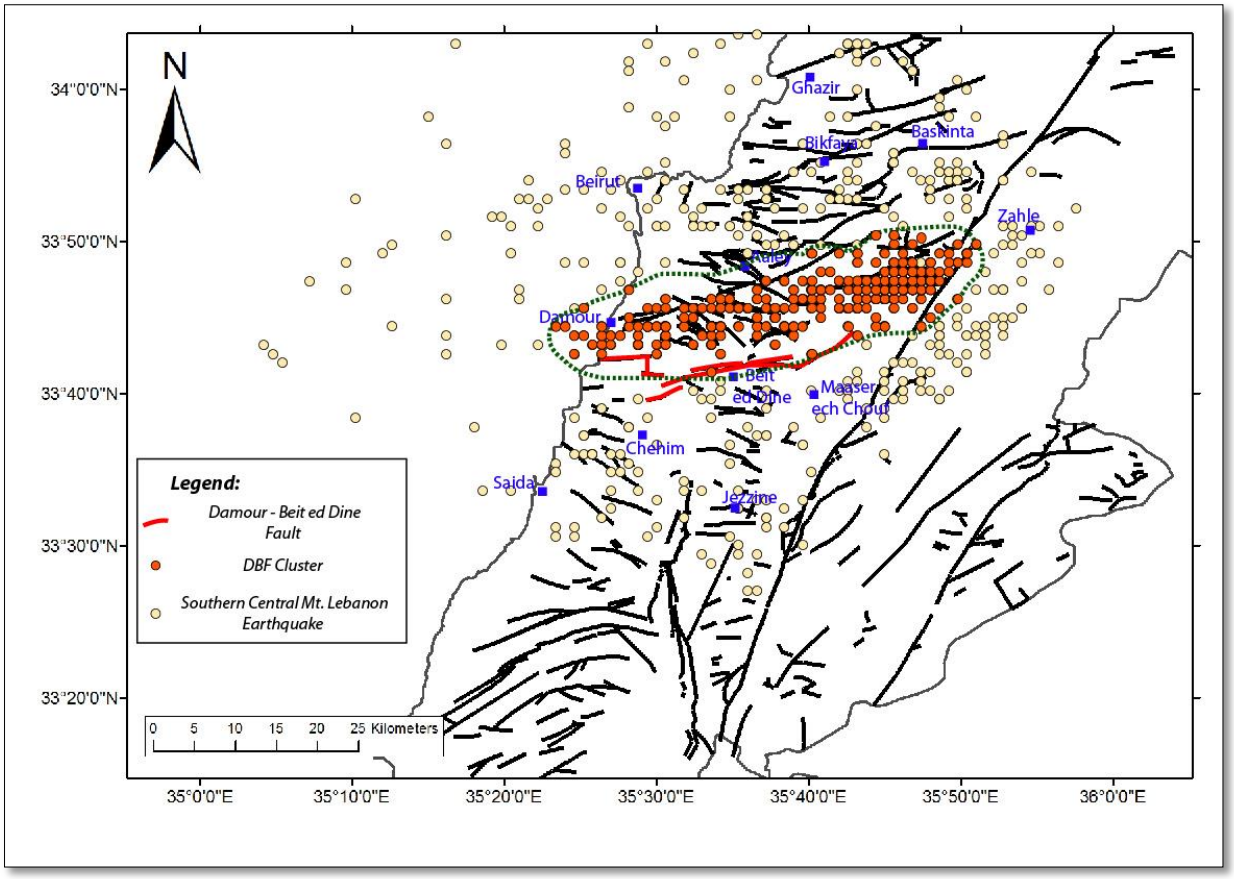

Figure 4.14: Map showing the visual selection of events from the DBF zone cluster. Note: Several algorithms (e.g. Gardner & Knopoff, 1974, Reasenberg, 1985…) allow to determin clustering mathematically, however they are not adobted here due to lack of tools.

The DBF seismic cluster is composed of a dense group of closely spaced earthquakes, distributed in a WSW-ENE oriented, 38 Km long and 3-4Km wide band - between Aaley and Beit ed Dine (Fig 4.14)- located 2.5 to 3km north of the mapped

fault surface trace. It terminates eastward along the Yammouneh Fault, and disappears offshore Damour (Fig. 4.14).

The events for this cluster were selected visually within an area of highest density of events, and extended over a buffer zone of 3km to roughly account for uncertainties in event location. 491 events corresponding to the DBF cluster are thus selected from within the regional seismicity of the SCML area (Fig. 4.14).

4.4.3.1. Time and Magnitude Distribution of DBF Cluster Events

These unfelt tremors had $2.1 \leq M_C \leq 3.4$ and occurred between 2006 and 2010. Available data from the GRAL network show that no significant seismic activity was observed in the area outside this 5 year period. For example only 12 events happened within this area in 2005.

The yearly distribution of the number of earthquakes between 2006 and 2010 (Fig. 4.15) shows a threefold increase in the number of earthquakes from 2006 (25 events) to 2007 (87events). This increase in seismic activity persists and slightly accentuates the following three years (2008, 2009 and 2010), with respectively 116, 99 and 131 recorded events (Fig. 4.15). In 2011, the number was also ~100 events, confined to the eastern tip of the DBF cluster, yet these were not included in our catalog and analysis, because the 2011 seismicity data was not available online until late 2014.

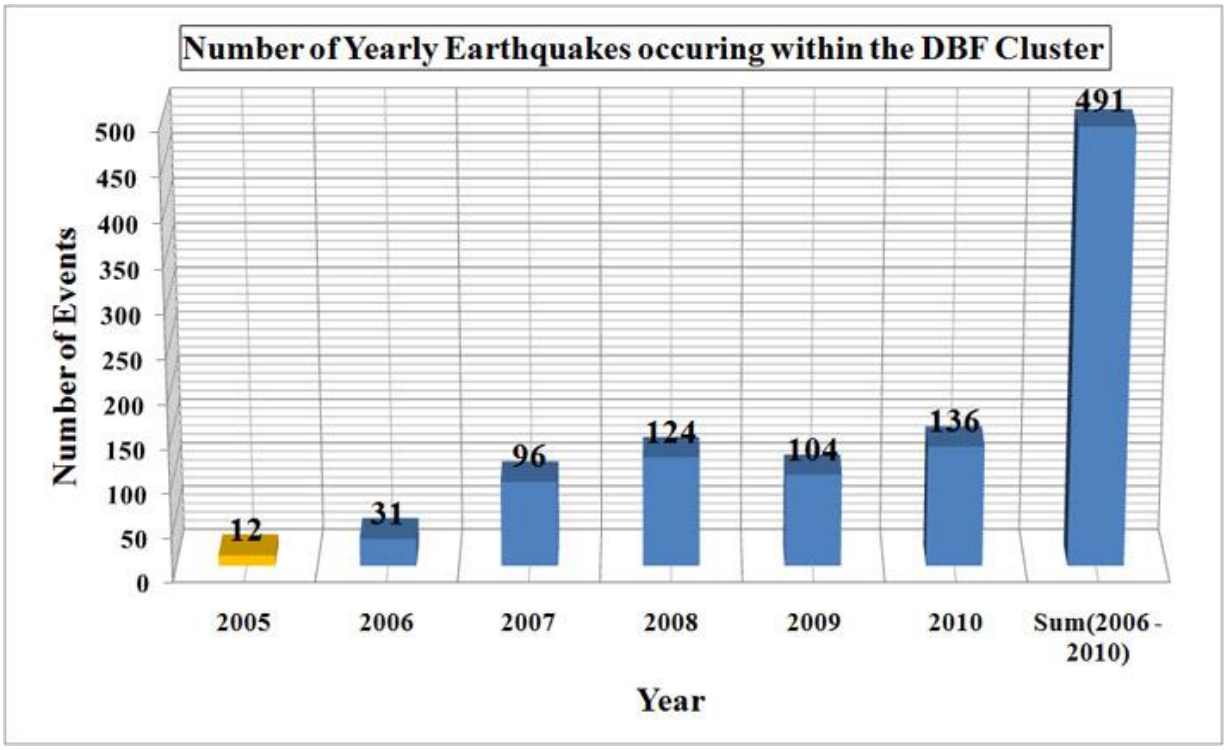

Figure 4.15: Histogram of the yearly distribution of earthquakes within the DBF cluster between 2005-2010. The year 2005 was also included to this diagram for comparison with the 5 years observation period.

The magnitude distribution for the 5 year period covered by the data is shown on figure 4.16a, along with the yearly magnitude distributions for each of these years (Fig. 4.16b-f).

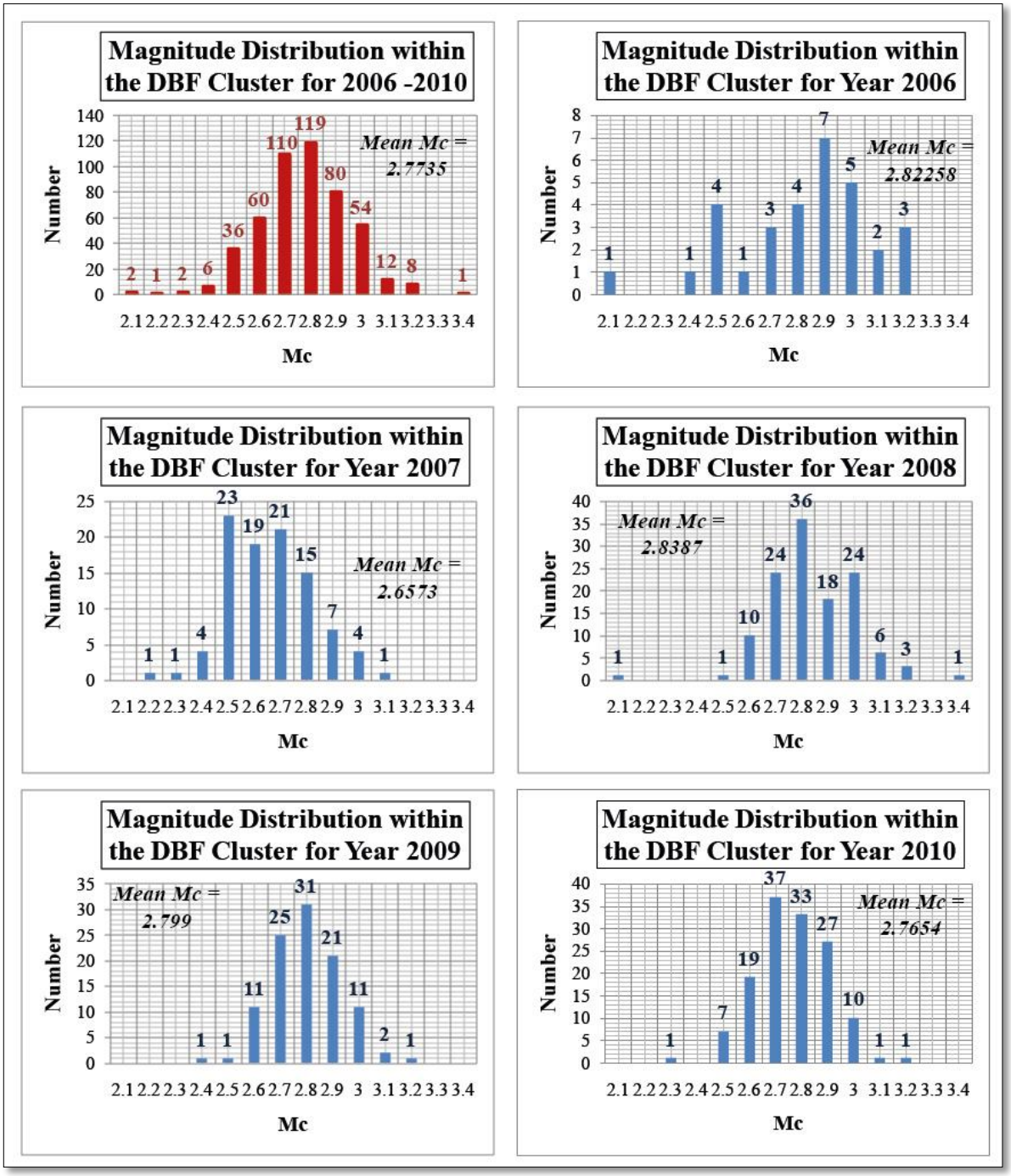

Figure 4.16: Magnitude distribution of the DBF cluster: a) For2006-2010. b) For year 2006. c) For year 2007. d) For year 2008. e) For year 2009. f) For year 2010.

4.4.3.2. The Depth Distribution of the SCML Earthquakes

We projected the SCML earthquakes recorded by NCGR between 2006 and 2010 along a line (d) perpendicular to the azimuth of the cluster alignment (Fig. 4.17a) and plotted their depth distribution (Fig. 4.17b).

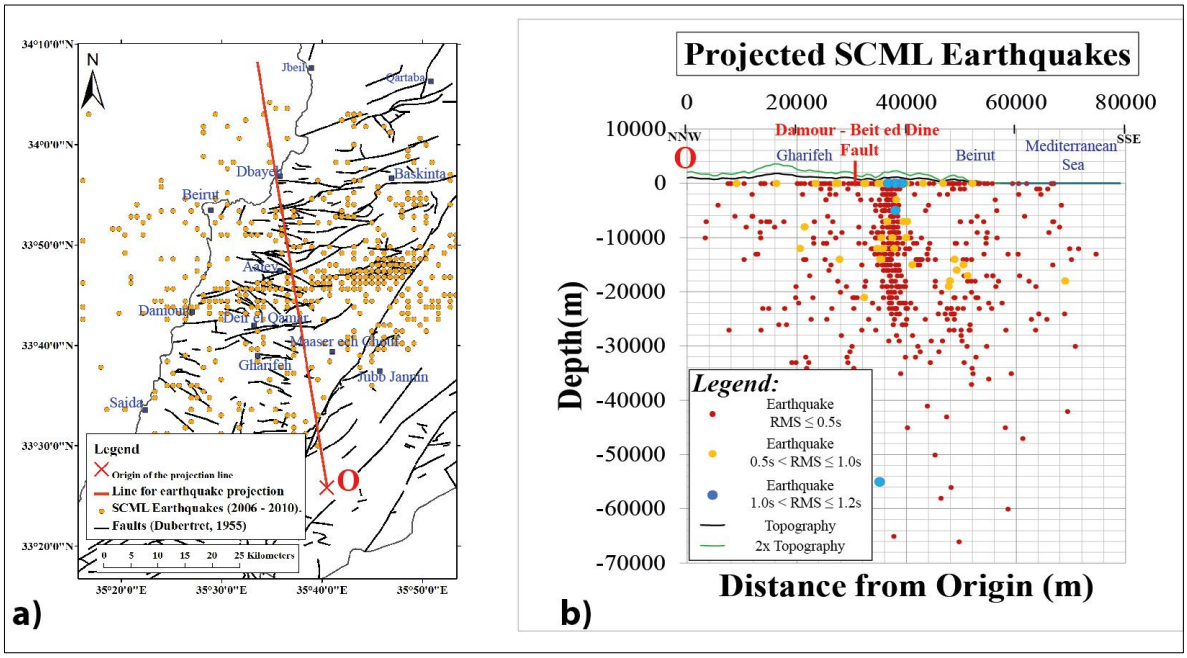

Figure 4.17: SCML projected earthquakes for the years of 2006-2010. a) A map showing the line of projection in red (eq: y = -6.082x + 250.4074). b) The depth plot along the line of projection.

On this depth plot, the events from the DBF cluster stand out from the surrounding seismicity of the area; they group over a vertical "slab" located between 0-30 Km depths. Beyond the ~30Km depth, the seismicity decreases greatly and the cluster disappears (Fig. 4.17b).

4.4.3.3. Discussion of the Geographic, Magnitude and Depth Distributions of the DBF Cluster

The pronounced seismicity within the DBF cluster kicks off along its western half during 2007 and continues in the following years (Figs. 4.5 and 4.15). In 2009 and 2010, the seismic activity becomes more localized in the eastern half of the DBF zone and continues through 2011. This locality change in the seismicity may probably related to spatial migration of strain release along the DBF.

The magnitude distribution analysis for the five year observation period (2006-2010) shows a normal distribution extending over $2.1 \leq M_C \leq 3.4$ with a mean M_C =2.77. The yearly magnitude distribution plots show similar bell curves extending over almost the same magnitude range and portraying similar mean magnitudes (Fig. 4.16).The increase in the seismicity rate of the DBF cluster in 2007 was not accompanied by an increase in the magnitudes of earthquakes.

The DBF cluster continuously mimicking the ~25Km long, mapped trace of the DBF zone on the surface and the 30km depth distribution over an almost vertical narrow zone, removes therefore any ambiguity on the origin of the DBF cluster. Earthquakes of this cluster seem to be releasing the tectonic stresses associated with the entire DBF tectonic activity. It also highlights the geologic importance of the DBF as a crustal scale fault zone.

That the DBF is a tectonically active structure has major implication on the seismic hazard of the area in particular. In fact, scaling laws (Wells & Coppersmith, 1994) suggest that a maximum M_W = 6.8 earthquake can be produced in case the 38Km

length DBF cluster ruptures in a single event (Fig. 4.18). In a more optimistic scenario, assuming that only the 25 Km long mapped fault trace of the DBF ruptures, it results in an M_W = 6.5 event. Both cases could result in important macroseismic consequences in the area given the special geology and morphology of the region. This explains the frequent large landslides and other morphotectonic features already described in the area. Consequently, the seismic hazard of the area must account for this structure as a potential seismic source.

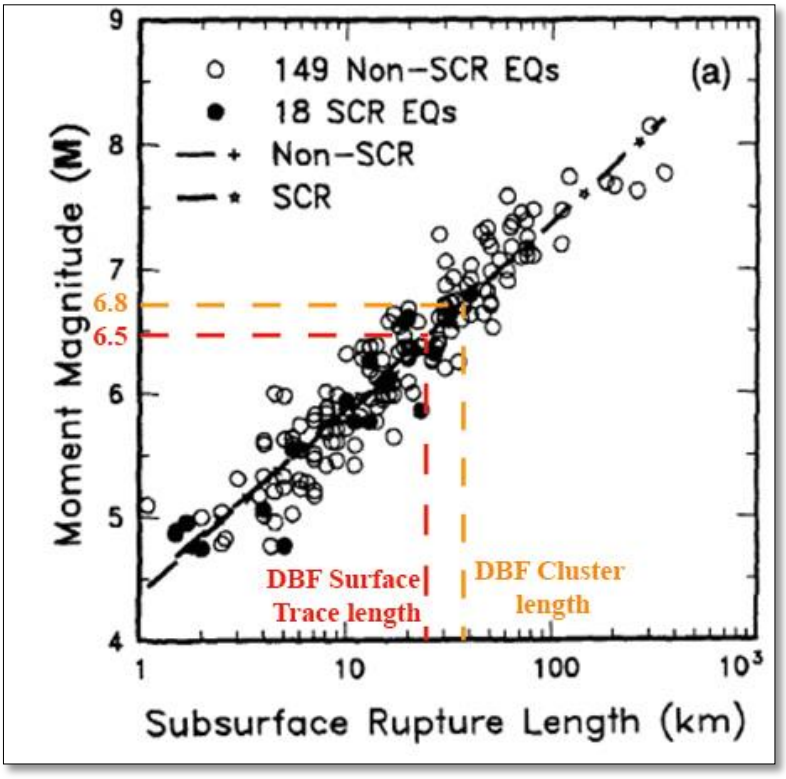

Figure 4.18: Graphs showing the Magnitude (M_W) vs. length of surface rupture relationships (modified from Wells & Coppersmith, 1994).

4.5. The Seismic Hazard of the Southern Central Mt. Lebanon Using the Seismicity Catalogs Data

4.5.1. Estimating the b-value from the SCML 2006-2010 Catalog

For seismic hazard assessment, we plotted the Gutenberg-Richter (GR) magnitude frequency relationship of the SCML for the five year observation period (Fig. 4.19). The obtained curve shows change in concavity and deviation from the expected linear trend of the GRMF function below Mc=2.9 (Fig. 4.19), for that reason we adopted this value as a completeness magnitude (MC) for the 5 year SCML earthquake catalog.

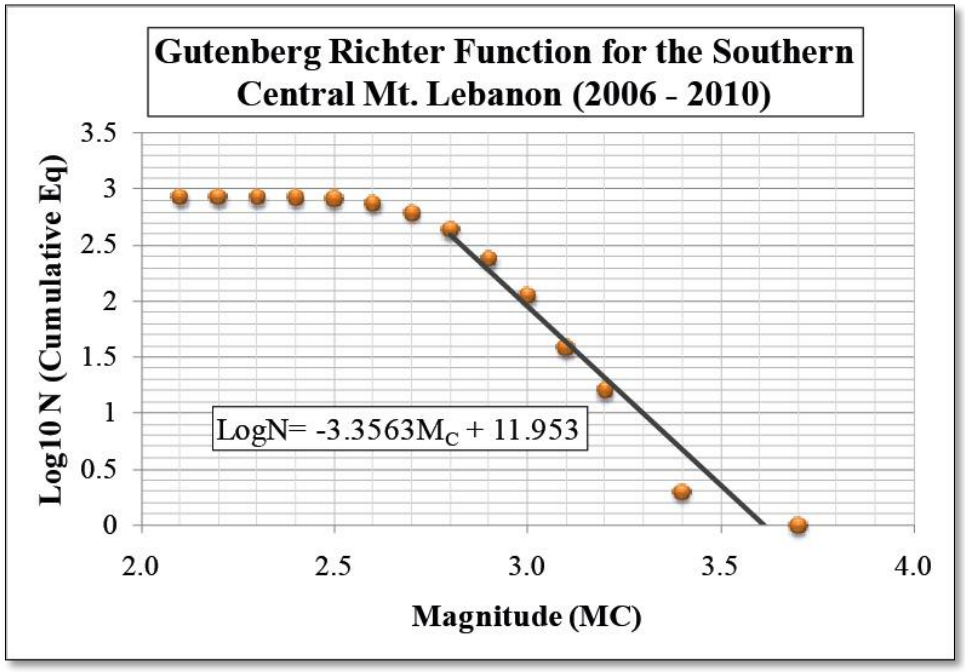

Figure 4.19: Frequency-Magnitude distribution of the southern central Mt. Lebanon.

From events with $M_C > 2.9$ belonging to the complete part of our catalog (Fig. 4.19) we deduced the following GR equation represented by the best fit linear function for this dataset:

$LogN = -3.3563M_C + 11.953$

with b = 3.3563and a = 11.953, for the southern central Mt. Lebanon, for the years of 2006 – 2010.

4.5.2. Discussion of the b-value Obtained from the 2006-2010 SCML Catalog

The b-value obtained for the southern central Mt. Lebanon is 3.3563. This value is significantly higher than expected normal b-values, which are supposed to be close to 1.

The SCML 2006-2010 catalog exhibits a uniform coda magnitude scale M_C, where the highest recorded magnitude is $M_C = 3.7$; at these small magnitudes there is no risk of magnitude saturation. Furthermore, the incomplete part of the data ($M_C < 2.9$) is removed from the Gutenberg-Richter linear fits.

Other important reliability criteria are lacking for this dataset. Mainly, the recurrence of major earthquakes in the southern central Mt. Lebanon (i.e. the Chehim 1956 M = 5.8 earthquake and the 1997 M = 5.3 Chouf earthquake) is not accounted for in the five year time period covered by this catalog. Furthermore, declustering of the SCML catalog is not applicable because of the absence of a noticeable main shock within this cluster series. In addition, an insufficient number of events (238) with magnitudes above the MC (~2.9) are available for the computation of the b-values. These events spread over a one unit magnitude range (2.1-3.7 Mc) only.

Subsequently the calculated b-value suggests that the SCML seismicity is dominated by small magnitude earthquakes advocating a negligible seismic hazard, which contradicts with the historical seismicity of the area.

4.5.3. Estimating the "b-value" of SCML from the 1956-2010 Catalog

To better assess the SCML seismic hazard we calculate a b-value of the study area for a longer time period. For this purpose we extend our SCML seismicity catalog to cover the 54 year time period between 1956 -the time of occurrence of the Chehim earthquake- and 2010. Data included in this catalog is extracted from the following sources:

- The Plassard & Kogoj (1981) data for events happening between 1956 and 1978,
- The IPRG network contribution to the ISC catalog between 1979 and 2002,
-The GRAL network contribution to the ISC catalog between 2003 and 2005
-The GRAL data between 2006 and 2010.

We were very selective in our earthquake extraction method in order to have a uniform Mc catalog. Yet, 90% of the selected data consisted of $M_{C;}$ the remaining 10% (mainly the IPRG contributed earthquakes) were available in M_L (local magnitude). Thus we converted the local magnitudes (M_C) to coda magnitudes (M_C) using regression relationship found by comparing Mc and Ml magnitudes (Fig. 4.20) when both available for events that occurred in Lebanon in the entire observation period (1956-2010):

$$M_C = 0.81M_L + 0.757$$

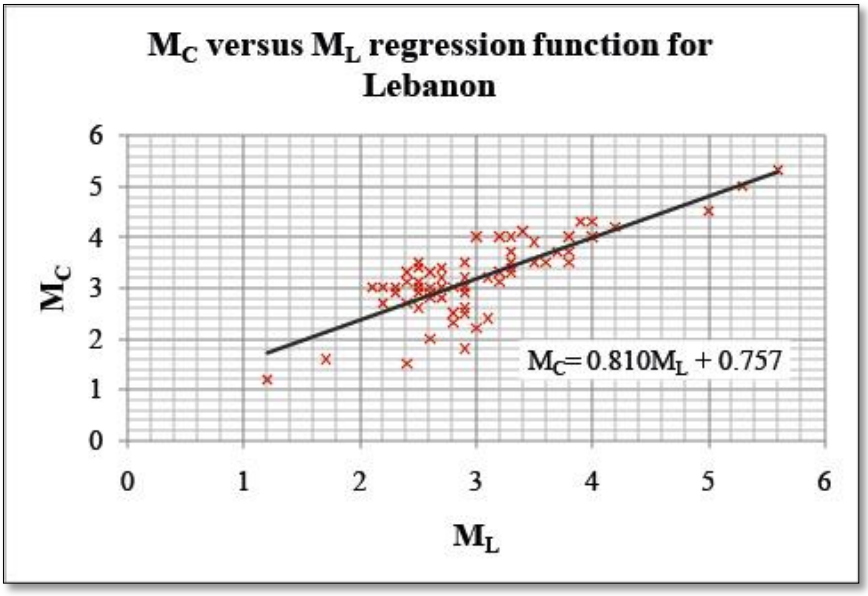

Figure 4.20: The linear relation between M_C and M_L for Lebanon calculated from earthquakes that happened between 1956 and 2010.

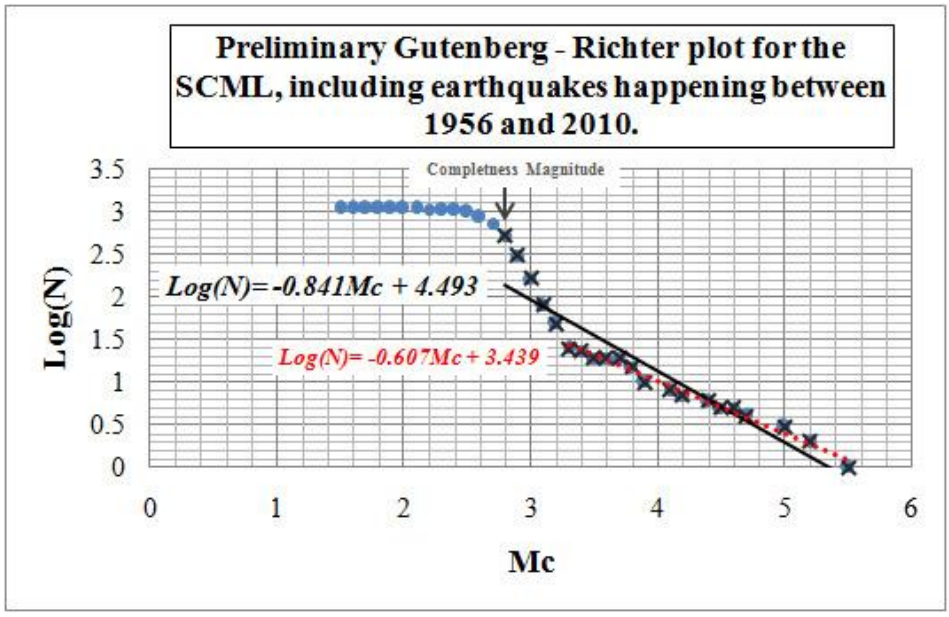

Figure 4.21: The preliminary Gutenberg-Richter plot for 1956-2010 observation period of the SCML. The black line is the best fit solution for the complete part of the dataset; the red line is the best fit solution for the events with $M_C \geq 3.2$.

The frequency-magnitude curve for the 54 year period has a completeness magnitude MC ~ 2.8 M_C. Subsequently the GR law is calculated for $M_C \geq 2.8$. The equation of the best fit line is (Fig. 4.21):

$Log(N) = -0.841M_C + 4.493$

Thus a = 4.493 and b = 0.841.

4.5.4. Discussion of the b-value Obtained from the 1956-2010 SCML Catalog

Compared with that of 2006-2010, the 1956-2010 SCML b-value is more conformable with the normally expected range for this parameter, and therefore more likely to be a better representative for seismic hazard of the area.

The obtained b-value of 0.841 is preliminary. Further processing steps are usually undertaken in order to improve the reliability of the hazard level: mainly declustering of the catalog. This task was not performed in our case for lack of time and technical tools. That said, the effect of declustering on the 1956-2010 SCML catalog can be intuitively anticipated. Declustering is the process by which time and space dependent events (usually foreshocks and aftershocks) are removed (Stark, 20122; Boyd, 2012). Clustering in this dataset occurs mostly in the range $2.1 \leq M_C \leq 3.2$ influenced by the seismicity of the DBF cluster, and less for greater magnitudes. This effect is reflected in the shape of the complete part ($2.8 \leq M_C \leq 5.5$) of the frequency-magnitude curve, where an abrupt decrease in the slope of the plot is noticeable at M_C = 3.2 (Fig. 4.21). Declustering the 54 year SCML earthquake catalog will reduce the frequency of events $2.1 \leq M_C < 3.2$, and yield a more homogeneous distribution for the complete part of this dataset, thus decreasing the slope b-value of the computed best fit

line for the1956-2010 SCML GR function closer toward the b-value (0.607) of the best fit line computed for $M_C \geq 3.2$ (Fig. 4.21).

Taken at its face value, this GR plot gives information about the seismic hazard of the SCML for a 54 year period. In fact, the maximum expected magnitude (M_{Cmax}) for the SCML estimated by considering Log (N) = 0, results in M_{Cmax} = 4.493/0.841 = 5.3. If data declustering is attempted as discussed above, a lower b-value is anticipated and translates into a higher value of M_{Cmax}. As presented here the GR relationship thus yields only a minimal assessment of the earthquake hazard in the SCML area.

Using events with Mw from EMSC network and corresponding Mc from GRAL, we calculated a conversion relationship from Mc to Mw, for the range $3.5 \leq M_C \leq 5.3$.:

$M_W = 1.247M_C - 1.608$ (Fig. 4.22) yielding an M_{Wmax} = 5.0

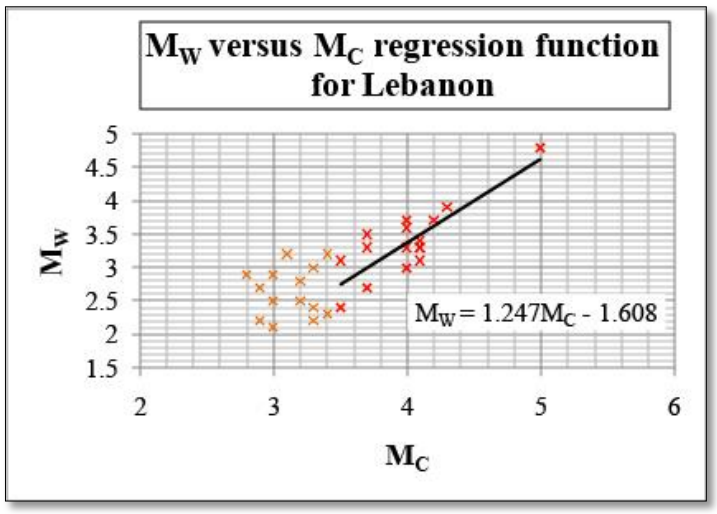

Figure 4.22: The linear relation between M_W and M_C derived from earthquakes with $3.5 \leq M_C \leq 5.3$ recorded by both the EMSC and GRAL.

Compared with the maximum moment magnitude (M_W = 6.3-6.8) expected in case of the entire rupture of the DBF in one single event (see section 4.4.3.3), the $M_{W\text{-}max}$ derived from the 1956-2010 SCML Gutenberg-Richter plot is significantly lower. Possibly, such discrepancy arises from the period of time covered by the selected catalog for the GR-relationship calculation, relatively shorter than the recurrence interval of large events on the DBF. Another possibility is that the segmented DBF does not rupture entirely in one single event, and the $M_{W\text{-}max}$ obtained by scaling laws of the entire length over-estimate the hazard.

Nonetheless, this work suggests that the SCML is susceptible to potentially strong and destructive earthquakes representing important seismic risk that urges the development of adequate preventive contingency plans.

4.6. Conclusion

Even though the record of historical seismicity for the SCML does not reveal any previously, well-identified seismic events on the DBF, the 2006-2010 instrumental seismicity data clearly signals the activity of this crustal fault thus endorsing the morphologic and structural observations presented in chapter 3.

The results of the GR frequency-magnitude relationship analysis for the SCML area suggest a b-value lower than 1, which indicates that it may be an area of high differential stress (Schorlemmer et *al.*, 2005), possibly hosting the nucleation of strong earthquakes in the future.

On the other hand the comparison of the maximum expected magnitudes calculated by both scaling laws and GR methods propose the disposition of the SCML to important seismic hazard.

CHAPTER 5

CONCLUSION

5.1. The Initiation of the DBF in Mesozoic Period

The inception age of the DBF and associated NW-SE faults within the SCML is indicated by their apparent vertical offset of Mesozoic stratigraphic units constrained in the field. The vertical displacement decreases upwards, indicating that the DBF and associated faults were active normal faults at least since the lower Aptian (Mreijat formation) up into the Mid-Cretaceous Cenomanian. Such normal offset is still expressed by the apparent throw of Mesozoic formations between the relatively higher block north of the DBF to that in the south. These structures controlled the paleo-bathymetry and syn-deposition of Lower Cretaceous formations within the area, as part of a larger region, dominated by extensional tectonics.

5.2. Cenozoic to Present Time Tectonics of the DBF

In the absence of stratigraphic units in the SCML, younger than the Mesozoic, the morphotectonic evidence gathered in the area enabled a better constrain of its recent tectonic deformation, associated with the Mid-Cenozoic to present transpression on the Lebanese Restraining Bend segment of the LFS.

During this Cenozoic episode, the left-lateral shear component on the LRB reactivated the DBF as a primary, dextral fault. Around 2Km of right-lateral offset are mapped along the DBF, and attributed to this tectonic phase.

The recent tectonic activity of the DBF is indicated by morphotectonic evidence such as fault scarps some of them with mirrors where striations conformable with oblique slip are still visible. Moreover deflection of drainages by folds and faults creating wind gaps and other special drainage geometries are to be taken on the account of the tectonic activity of the underlying structures associated with the DBF. Frequent landslides are also mapped in the area and are closely distributed around the active fault trace.

The recent and ongoing activity of the DBF is clearly indicated by the 2006-2010 seismic catalog of the SCML, where the seismicity of this structure stands out as a cluster of small magnitude events localized over the DBF zone. Analysis of the instrumental record of recent earthquakes along the DBF proves the deep, crustal extent of this structure. Furthermore, seismic activity maps of Lebanon show with no doubt an important decrease in the number of recorded events north of the DBF zone (www.cnrs.edu.lb). This difference can be tentatively attributed to the difference in the type of the underlying crusts, suggesting that the DBF is a major crustal boundary between clearly continental block in the south and thinned, or transitional crust in the north as discussed by previous authors (Walley, 2001; Carton et al ., 2009). Yet more detailed seismological and geophysical studies of the area are needed to confirm such hypothesis.

5.3. Primary and Secondary Bookshelf Faulting and Rotation in Central Mt. Lebanon

That the DBF is an active right-lateral fault with around ~2Km of shear, suggests that the other latitudinal faults located over the western flank of central Mt-Lebanon between Damour and Batroun are similar active structures. This set of latitudinal faults accommodates counter-clockwise bookshelf rotation along the western flank of Mt-

Lebanon (Freund & Tarling, 1979; Ron, 1987; Tapponnier et *al.*, 2004; Daëron, 2005). More detailed investigation of offset markers along these E-W faults is needed in order to quantify the entire amount of shear absorbed by the primary bookshelf mechanism.

In addition to the primary bookshelf faulting in the area, secondary, sinistral and clockwise bookshelf faulting was observed where overlapping E-W faults are mapped. This mechanism is related to the right-lateral shear on the E-W faults and thus is of the same age (late Miocene-present). It is responsible for the re-activation of the NW-SE faults north of the DBF only. In the SCML the secondary bookshelf mechanism rotated the northern NW-SE by 10˚-18˚ clockwise with respect to those to the south. It subsequently induced around 500m (maximum) of left-lateral offset that were mapped on northern NW-SE faults, while no horizontal offset is observed on the NW-SE counterparts south of DBF that presumably remained inactive during this period. Secondary block rotation is masking part of the total shear resulting in underestimated finite amounts of strike-slip displacement on the LRB.

5.4. Cenozoic Folding in the SCML Area

Finally, unlike previous studies where the structure of central Mt. Lebanon is described with normal faults and extensional structures only, our study presents evidence of active compressional structures that control the deformation style of the area. Folding is related to the compressive component of the Cenozoic transpression on the LRB, which is absorbed in the area by deep and blind flat-ramp geometry. This blind structure is indicated by the morphology of the terrain and expressed as asymmetrical fault-propagation folds close to the surface. The overall structure of the area is best represented by a series of

asymmetric, mostly west-vergent folds separating long wavelength warping of the covering Mesozoic formations.

That folding and uplift of the SCML are active is indicated by the wind gaps and the perched and abandoned alluvial deposits along the Damour River as well as by the deep incision of the rivers in the area. We estimate that at least 3% of shortening took place in the area in an E-W direction since Mid Cenozoic.

5.5. Seismic Hazard Associated with the DBF

The present-day tectonic activity within the SCML translates into potential seismic hazard for this area. The DBF is located at close distance from major cities in the country. It represents a significant seismic hazard to Beirut, Saida and Zahle cities, all of them located at less than 20km from the fault. Scaling laws used to estimate the hazard arising from the activity of the DBF alone suggest that this structure is capable of generating a maximum 6.5-6.8 Mw event.

A more comprehensive estimation of the SCML seismic hazard using the Gutenberg-Richter method suggests that this area is characterized by alow b-value of 0.81 and indicates that it is prone to the nucleation of future events with expected maximum magnitudes Mw~5.0. However this result does not take into consideration the presence of major active faults not far from the boundaries of SCML that would significantly add to the seismic hazard of the area if considered. This hazard is also significantly amplified by the weak lithologies cut by steep slopes in an area of important precipitation and runoff rates.

5.6. Recommendations and Improvements

Additional tasks and approaches that were not performed within this thesis will enable the refinement of its results and their application on larger level. They include:

- More detailed mapping of the eastern part of the DBF and its connection with the Yammouneh Fault.
- Dating the landslides along the DBF using radiometric, cosmogenic and/or other methods, to constrain the recurrence of mass movements in the area and presumably of causative earthquakes.
- Dynamic analysis of meso- and micro-scale structures in the SCML.
- Declustering of the seismic catalog would improve the quality and the reliability of the seismic hazard assessment.

We also recommend:

- Geophysical investigation of the crustal structure in the area.
- Improving the seismic network coverage around the E-W faults in order to closely monitor their seismic activity baseline level and understand their seismic behavior.
- Developing a local, 3D seismic velocity model that will help improve the localization of earthquakes in the country.
- Proposing contingency plans, founded on seismic risk models, which will improve the resiliency of the communities facing seismic hazards.
- Comparing and analyzing the structural setting of the E-W faults in western Lebanon with that of the deep Levantine Basin offshore, especially within the Mesozoic sequences, in order to better understand the evolution of the margin.

BIBLIOGRAPHY

Agliardi, F. (2012). Landslides: definitions, classification, causes. Czech Geological Survey-Geological Survey of Austria- UNIMIB. Educational project geological field trip and workshop. Koefels-Suedtirol-Matrei, 17-20 June 2012.

Ambraseys, N. (2001). Reassessment of earthquakes, 1900–1999, in the Eastern Mediterranean and the Middle East, Geophysical Journal International. Vol. 145, pp. 471–485.

Ambraseys, N. (2009). Earthquakes in the eastern Mediterranean and in the Middle East. Multidisciplinary study of seismicity up to 1900. Cambridge University Press; 1 edition.

Ambraseys, N. and Barazangi, M. (1989). The 1759 earthquake in the Bekaa valley: implications for earthquake hazard assessment in the Eastern Mediterranean region. Journal of Geophysical Research, Vol. 94, n. B4, pp. 4007–4013.

Ambraseys, N. and Melville, C.P. (1988). An analysis of the eastern Mediterranean earthquake of 20 May 1202. In History of Seismography and Earthquakes of the World, edited by Lee, W.K.H., Meyers, H. and Shimazaki, K., pp. 181–200. Academic Press, San Diego, CA.

Ambraseys, N. (1997). The earthquake of 1 January 1837 in southern Lebanon and northern Israel. Annali di Geofisica, Vol. XL, n. 4, pp. 923–935.

Amiran, D.H.K., Arieh, E., and Turcotte, T. (1994), Earthquakes in Israel and adjacent areas: Macroseismic observations since 100 B.C.E.: Israel Exploration Journal, Vol. 44, pp. 260–305

Amorèse, D., Grasso, J.R. and Rydelek, P.A. (2010). On varying b values with depth: results from computer-intensive tests for Southern California. Geophysical Journal International () , 1–??

Arnaud, R. (1969). Etude morphologique des plateaux côtiers du Liban-Sud (au Nord de Nahr el Aouali), thèse 3^{e} cycle, Beyrouth, 113p.

Avni, R., Bowman, D., Shapira, A. and Nur, A. (2002). Erroneous interpretation of historical documents related to the epicentre of the 1927 Jericho earthquake in the Holy Land. Journal of Seismology, Vol. 6 (4), pp. 469–476.

Bai, L., Wu, Z., Zhang, T. and Kawasaki, I. (2006).The effect of distribution of stations upon location error: Statistical tests based on the double-difference earthquake location algorithm and the bootstrap method. Earth Planets Space, Vol. 58, pp. e9–e12.

Ben-Menahem, A., (1991). Four thousand years of seismicity along the Dead Sea rift. Journal of Geophysical Research, Vol. 96, NO. B12, pp. 20195 – 20216.

Berberian, M. (1994). Natural hazards and the first earthquake catalogue of Iran, v.1, Historical Hazards in Iran Prior to 1900. IIEES, Tehran.

Beydoun, Z. R. (1977). "Petroleum prospects of Lebanon: re-evaluation." AAPG bulletin Vol. 61(1), pp. 43-64.

Beydoun, Z. R. (1997). Earthquakes in Lebanon: An overview. Lebanese Science Bulletin, Vol. 10, No.1.

Beydoun, Z.R. (1981). Some open questions relating to the petroleum prospects of Lebanon. Journal of Petroleum Geology, Vol. 3, pp. 303-314.

Billings, S.D., Sambridge, M.S. and Kennett, B.L.N. (1994). Errors in hypocenter location: picking, model and magnitude dependence. Bulletin of the Seismological Society of America, Vol. 84, No. 6, pp. 1978 – 1990.

Bolt, B. (1999). Earthquakes. Fourth Edition. ISBN 0-7167-3396X W. H. Freeman and Company.

Bondár, I., Myers, M., Engdahl, E. and Bergman, E.A. (2004).Epicentre accuracy based on seismic network criteria. Geophysical Journal International, Vol. 156, pp. 483–496.

Boyd, O. (2012). A visitation of earthquake catalog Declustering. USGS seismic hazard workshop for CEUS sources 22 – 23 Feb. February 2012.

Brew, G., Lupa, J., Brazangi, M., Sawaf, T., Al – Imam, A. and Zaza, T. (2001). Structure and tectonic development of the Ghab basin and the Dead Sea fault system, Syria, Journal of the Geological Society, London, Vol. 158, pp. 665–674.

Carton, H., Singh, S.C., Tapponier, P., Elias, A., Briais, A., Sursock, A., Jomma, R., King, G.C.P., Daëron, M., Jacques and E., Barrier, L. (2009). Seismic evidence for Neogene and active shortening offshore of Lebanon (Shalimar cruise). Journal of Geophysical Research, Vol.114, pp. B07407.

Chan, C.H., Wu, Y.M., Tseng, T.L., Lin, T.L. and Chen, C.C. (2012).Spatial and temporal evolution of b-values before large earthquakes in Taiwan. Tectonophysics 532-535 pp. 215–222.

Chorowicz, J., Dhont, D., Ammar, O., Rukieh, M. and Bilal, A., (2005). Tectonics of the Pliocene Homs basalts (Syria) and implications for the Dead Sea Fault zone activity, Journal of the Geological Society, London, Vol. 162, pp. 259–271.

CNRS (2006-2010). Provisional Seismological Bulletin from the National Seismic Network. January 2006-December 2010.

Courtillot, V., Armijo, R. and Tapponnier, P. (1987). The Sinai triple junction revisited. Tectonophysics, Vol. 141, pp. 181–190

Daëron, M. (2005). Rôle, cinématique et comportement sismique à longterme de la faille de Yammoûneh, Thèse de doctorat, 178 pp., Instut De Physique du Globe de Paris, Paris.

Daëron, M., L. Benedetti, P. Tapponnier, A. Sursock, and Finkel, R. (2004), Constraints on the post (25-ka slip rate of the Yammouneh fault (Lebanon) using in-situ cosmogenic Cl^{36} dating of offset limestone-clast fans, Earth Planet Science Letters, Vol. 227, pp. 105– 119.

Darawcheh, R., Sbeinati, M.R., Margottini, C. and Paolini, S. (2000). The 9 July 551 AD Beirut earthquake, Eastern Mediterranean region. Journal of Earthquake Engineering, Vol. 4, n. 4, pp. 403–414.

Dubertret, L., (1945). Carte geologique au 50000. Feuille de Djezzine. Notice explicative.

Dubertret, L., 1949. Carte geologique au 50000. Feuille de Saida. Notice explicative.

Dubertret, L., (1955). Carte géologique du Liban au 1/200 000 - Note explicative de la carte géologique du Liban au 1/200 000.

Durand, V., Bouchon, M., Karabulut, H., Marsan, D., Schmittbuhl, J., Bouin, M., Aktar, M., and Daniel, G. (2010). Seismic interaction and delayed triggering along the North Anatolian Fault. Geophysical Research Letters, Vol. 37, L18310.

Dziewonski, A.M., Woodward, R.L. (1992). Acoustic imaging at the planetary scale. In: Emert, H., Harjes, H.P. (Eds.), Acoustical Imaging, Vol. 19, pp. 785–797.

Elias, A. (2006), Le chevauchement de Tripoli-Saida: Croissance du Mont Liban et risque sismique, Thèse de doctorat, 230 pp., Instut de Physique Du Globe de Paris, Paris.

Elias, A., Tapponier, P., Singh, S.C., King, G.C.P., Briais, A., Daëron, M., Carton, S., Sursock, A., Jacques, E., Jomaa, R. and Klinger, Y. (2007). Active thrusting offshore Mount Lebanon: source of the tsunamigenic A.D. 551 Beirut-Tripoli earthquake. Geology, Vol. 35, pp. 755-758.

Enescu, B. and Ito, K. (2003). Values of b and p: their variations and relation to physical processes for earthquakes in Japan. Annuals of Disaster Prevention Research Institute, Kyoto University. No.46 B.

Eyal, M., Eyal, Y., Bartov, Y. and Steinitz, G. (1981). The tectonic development of the western margin of the Gulf of Elat (Aqaba) rift. Tectonophysics, Vol. 80, pp. 39-66.

Felzer, K.R. (2006). Calculating the Gutenberg-Richter b value. American Geophysical Union, Fall Meeting 2006, abstract #S42C-08.

Freund, R. and Tarling, D.H. (1979). Preliminary Mesozoic paleomagnetic results from Israel and inferences for a microplate structure in the Lebanon. Tectonophysics, Vol. 60, pp. 189-205.

Freund, R. (1965). A model of the structural development of Israel and adjacent areas since Upper Cretaceous times. Geological Magazine, Vol. 102, pp. 189–20.

Freund, R., Garfunkel, Z., Zak, I., Goldberg, I., Weisbrod, T. and Derin, B. (1970). The shear along the Dead Sea rift. Philosophical Transactions of the Royal Society of London, Vol. 267, pp. 107-130.

Gardner, J.K. and Knopoff, L. (1974). Is the sequence of earthquakes in southern California, with aftershocks removed, poissonian? Bulletin of the Seismological Society of America, Vol. 64, No. 5.

Garfunkel, Z., Zak, I. and Freund, R. (1981). Active faulting in the Dead Sea rift. Tectonophysics, Vol. 80, pp. 1–26.

Girdler, R.W. (1990). The Dead Sea transform fault system. Tectonophysics, Vol. 180, pp. 1–13.

Gitterman, Y., Pinsky, V., Shapira, A., Ergin, M., Gurbuz, C. and Solomi, K. (2005). Improvement in detection, location and identification of small events through joint data analysis by seismic observations in the Middle East/Eastern Mediterranean Region, Final Report DTRA01-00-C-0119, DOD USA.

Gök, R., Herzog, S., Nakanishi, K., Pasyanos, M. E., Mellors, R. J., Rodgers, A. J., Harris, D. B. and Vergino E. S. (2012). Lithospheric models of the Middle East to improve seismic source parameter determination/event location accuracy. Lawrence Livermore National Laboratory1 and the National Nuclear Security Administration2 Sponsored by the National Nuclear Security Administration and the U.S. Department of State Award Nos. DE-AC52-07NA27344/24.2.3.2 and DOS_SIAA-11-AVC/NMA-1.

Gomez, F., Karam, G., Khawlie, M., McClusky, S., Vernant, P., Reilinger, R., Jaafar, R., Tabet, C., Khair, K. and Barazangi, M. (2007). Global Positioning System measurements of strain accumulation and slip transfer through the restraining bend along the Dead Sea fault system in Lebanon. Geophysical Journal International, Vol. 168, pp. 1021–1028.

Guidoboni, E., A. Comastri and G. Traina (1994). Catalogue of Ancient Earthquakes in the Mediterranean area up to the 10th century, Vol. 1, 504 pp.

Guidoboni, E., Bernardini, F., Comastri, A. and Boschi, E. (2004). The large earthquake on 29 June 1170 (Syria, Lebanon, and central southern Turkey). Journal of Geophysical Research, Vol. 109, No. B07304

Hancock, P.L., Atiya, M.S. (1979). Tectonic significance of mesofracture systems associated with the Lebanese segments of the Dead Sea Transform Fault. Journal of Structural Geology, Vol. 1, pp. 143–153.

Havskov, J. and Ottemöller, L. (2010). Routine data processing in earthquake seismology. Springer Dordrecht Heidelberg London New York.ISBN 978-90-481-8696-9 e-ISBN 978-90-481-8697-6DOI 10.1007/978-90-481-8697-6.

Heybroek, F. (1942). La géologie d'une partie du Liban Sud. Leidsche Geol. Medit., 12, 251- 470.

Jaafar, R. (2008). GPS Measurements of Present day crustal deformation within the Lebanese Restraining Bend along the Dead Sea Transform. A Thesis presented to the Faculty of the Graduate School at the University of Missouri-Columbia in Partial Fulfillment of the Requirements for the Degree Master of Science.

Joffe, S., and Garfunkel, Z. (1987). Plate kinematics of the circum Red Sea: A re-evaluation, Tectonophysics, Vol. 141, pp. 5– 22.

Kanaori, Y., Endo, Y., Yairi, K. and Kawakami, S.I. (1990): A nested fault system with block rotation caused by left-lateral faulting, the Neodani and Atera faults, central Japan. Tectonophysics, Vol. 177, pp. 401-418.

Kim, K.H., Chiu, J.M., Pujol, J. and Chen, K.C. (2005). Earthquake relocations, fault zone geometry and constraints on lateral velocity variations using the joint hypocenter determination method in the Taiwan area. Earth Planets Space, Vol. 57, pp. 809–823.

Kulhaneck, O. (2005). Seminar on *b*-value. Department of Geophysics, Charles University, Prague December 10-19, 2005.

Le Beon, M., Klinger, Y., Amrat, A.Q., Agnon, A., Dorbath, L., Baer, G., Ruegg, J.C., Charade, O. and Mayyas, O. (2008). Slip rate and locking depth from GPS profiles across the southern Dead Sea Transform, Journal of Geophysical Research., Vol. 113, No. B11403.

Lienert, B. R. (1997). Assessment of Earthquake Location Accuracy and Confidence Region Estimates Using Known Nuclear Tests. Bulletin of the Seismological Society of America, Vol. 87, No. 5, pp. 1150-1157.

Lienert, B. R. and Havskov (1995). A computer program for locating earthquakes both globally and locally, Seismological Research Letters, Vol. 66, pp. 26-40.

Lienert, B. Berg, E. and Frazer, L. (1986). Hypocenter: an earthquake location method using centered, scaled, and adaptively leastsquares, Bulletin of the Seismological Society of America, Vol. 76, pp. 771-783.

Lowrie, W. (2007). Fundemantals of Geophysics. Cambridge University Press.

Mandl, G. (1987). Tectonic deformation by rotating parallel faults: the "bookshelf" mechanism. Tectonophysics, Vol. 141, pp. 277-316.

Marco, S., Hartal, M., Hazan, N., Lev, L. and Stein, M. (2003). Archaeology, history and geology of the A.D. 749 earthquake, Dead Sea transform. Geology, Vol. 31, pp. 665–668.

Marzocchi, W. and Sandri, L. (2003).A review and new insights on the estimation of the *b*-value and its uncertainties. Annals of Geophysics, Vol. 46, N. 6.

Matsuda, T. (1974). Surface faults associated with Nobi (Mino-Owari) Earthquake of 1891, Japan. Bulletin of the Earthquake Research Institute, Vol. 14, pp. 85-126.

Meghraoui, M., Gomez, F., Sbeinati, R., Van der Woerd, J., Mouty, M., Darkal, A., Radwan, Y., Layyous, I., Al Najjar, H., Darawcheh, R., Hijazi, F., Al-Ghazzi, R. and Barazangi, M. (2003), Evidence for 830 years of seismic quiescence from palaeoseismology, archaeoseismology and historical seismicity along the Dead Sea fault in Syria, Earth Planet Science Letters, Vol. 210, pp. 35–52.

Meirova, T. and Hofstetter, R. (2012).Observations of seismic activity in Southern Lebanon. Journal of Seismology. DOI 10.1007/s10950-012-9343-2.

Mitra, S. (1990). Fault-propagation folds: geometry, kinematic evolution and hydrocarbon traps. The American Association of Petroleum Geologists Bulletin, V.74, No. 6 (1990), P. 921-945.

Moghabghab, N. (2000). "تاريخ اللأمير حيدر الشهابي, نزهة الزمان في تاريخ جبل لبنان." الجزء الثاني, من وفاة أحمد المعني الى ولاية الأمير بشير عمر الكبير.,

Mogi, K. (1962). Magnitude-frequency relation for elastic shocks accompanying fractures of various materials and some related problems in earthquakes, Bulletin of Earthquake Research Instute, University of Tokyo, Vol. 40, pp. 831-853.

Murphy, J., Goldman, M., Fuis, G., Rymer, M., Sickler, R., Miller, S., Butcher, L., Ricketts, J., Criley, C., Stock, J., Hole, J. and Chavez, G. (2010). Seismic calibration shots conducted in 2009 in the Imperial Valley, Southern California, for the Salton Seismic Imaging Project (SSIP). U.S. Department of the Interior, U.S. Geological Survey. Open-File Report 2010–1295.

Nemer, N., Meghraoui, M. and Khair, K. (2008). The Rachaya-Serghaya fault system (Lebanon): Evidence of coseismic ruptures, and the AD 1759 earthquake sequence. Journal of Geophysical Research, Vol. 113, No. B05312.

Nemer, T., and M. Meghraoui (2006). Evidence of coseismic ruptures along the Roum fault (Lebanon): A possible source for the AD 1837 earthquake. Journal of Structural Geology, Vol. 28, pp. 1483-1495.

Nuannin, P., Kulhanek, O. and Persson, L. (2005). Spatial and temporal b value anomalies preceding the devastating off coast of NW Sumatra earthquake of December 26, 2004. Geophysical Research Letters, Vol. 32, No. L11307.

Okal, E. A. and Romanowicz, B. A. (1994). On the variation of *b*-value with earthquake size.Physics id the Earth and Planetary Interiors, Vol. 87, pp. 55-76.

Ollier. C.D. (1985). Glossary of morphotectonics. 2nd edition. Bureau of Mineral Resources, Geology and Geophysics, Australia. Record 1985/30.

Olsson, R., (1998). An estimation of the maximum *b*-value in the Gutenberg - Richter relation. Geodynamics, Vol. 27, pp. 547-552.

Perucca, L., Rothis, M. and Vargas, H. (2014). Morphotectonic and neotectonic control on river pattern in the Sierra de la Cantera piedmont, Central Precordillera, province of San Juan, Argentina. Geomorphology, Vol. 204, pp. 673–682.

Plassard, J. and Kogoj, B. (1981). La Séismicité du Liban.

Quennell, A.M. (1958). The structural and geomorphic evolution of the Dead Sea rift. Quarterly Journal of the Geological Society of London, Vol. 114, pp. 2-24.

Quennell, A.M. (1959). Tectonics of the Dead Sea rift. In Proceedings of the 20th International Geological Congress, Mexico, pp. 385–403.

Reasenberg, P. (1985). Second-order moment of central California seismicity. 1969–1982, Journal of Geophysical Research, Vol. 90, pp. 5479-5495.

Reches, Z. and Hoexter, D.F. (1981). Holocene seismic and tectonic activity in the Dead Sea area. Tectonophysics, Vol. 80, pp. 235-254

Reicherter, K., Hoffmann, N., Lindhorst, K., Krastel, S., Fernandez-Steeger, T., Grutzner, C. and Wiatr, T. (2011). Active basins and neotectonics: morphotectonics of the Lake Ohrid Basin (FYROM and Albania). Zeitschrift der Deutschen Gesellschaft für Geowissenscaften, Vol. 162, pp. 217-234.

Richter, C. (1935). An instrumental earthquake magnitude scale. Bulletin of the Seismological Society of America. Vol. 25, No. 1.

Ron, H. (1987). Deformation along the Yammuneh, the restraining bend of the Dead Sea transform: paleomagnetic data and kinematic implications. Tectonics, Vol. 9, pp. 1421–1432.

Sanlaville, P, (1977). Etude géomorphologique de la région littorale du Liban. Publications de l'Université Libanaise (section des étudesgéographiques).

Sbeinati, M.R., Darawcheh, R. and Mouty, M. (2005). The historical earthquakes of Syria: an analysis of large and moderate earthquakes from 1365 BC to 1900 AD. Annali di Geophysica 48 (3), 347-435, 2005.

Scholz, C.H. (1968): The frequency-magnitude relation of microfracturing in rock and its relation to earthquakes, Bulletin of the Seismological Society of America, Vol. 58, pp. 399-415.

Schönholzer, S. (2009).Assessing the solution quality of the earthquake location problem. Semesterarbeit HS 2008. Department of Earth Sciences ETH Zurich.

Schorlemmer, D., Wiemer, S. and Wyss, M. (2005).Variations in earthquake-size distribution across different stress regimes. Nature, Vol. 437.

Shapira, A., Hoffstetter, R., Abdallah, A.F., Dabbeek, J. and Hays, W. (2000 – 2007). Earthquake hazard assessments for building codes final report, April 2000 - March 2007 Proposal Number: M18-057 Grant No. PCE-G-00-99-00038.

Stark, P. (2011). Earthquake clustering and declustering. Institut de Physique du Globe de Paris.

Stein, S. and Wysession, M. (2004).An introduction to seismology, earthquakes and earth structures.

Storchak, D., Hanka, W., Dewey, J., Sato, H. and Musson, R. (2007). IASPEI - International Association of Seismology and Physics of the Earth'sInterior, SS001 6110 – 6248. Symposium Seismic Observations and Interpretation.IUGG XXIV General Assembly July 2-13, 2007 Perugia, Italy.

Suppe, J. (1983). Geometry and kinematics of fault-bend folding. American Journal of Science, Vol. 283, pp. 684-721.

Tan, O., Cengiz Tapirdamaz, C. and Yoruk, A. (2008). The earthquake catalogues for Turkey. Turkish Journal of Earth Sciences, Vol. 17, pp. 405-418.

Tapponnier, P., Daëron, M., Sursock, A., Jomaa, R., Briais, A., Carton, H., Singh, S.C., Elias, A., King, G. and Jacques, E. (2004). Passive-active margin inversion along the Levant plate boundary: subduction birth and growth of Mt Lebanon. In Eos Transactions, American Geophysical Union, Vol. 85, Abstract T52B-05.

Tsai, Y.B. and Wu, H.H. (1996).A Study of the Errors in Locating Earthquakes due to the Geometry of the Taiwan Network. Note and Correspondance, Vol. 8, No. 3, pp. 355-370.

USGS International Program – RELEMER (international.usgs.gov/projects/prjrelemr.htm).

Walley C.D., Ed. (2001). The Lebanon passive margin and the evolution of the Levantine Neo-Tethys. Peri-Tethys Memoir 6: Peri-Tethyan Rift/Wrench basins and passive margins., Mémoires du Museum National d'Histoire Naturelle.

Walley, C. D. (1988). A revision of the Lower Cretaceous stratigraphy of Lebanon. Geologische Rundschau, Vol. 72, pp. 377-388.

Walley, C. D. (1997). The lithostratigraphy of Lebanon: A review, Lebanese Science Bulletin, Vol. 10:1.

Walley, C. D. (2000). Mesozoic and Cenozoic paleogeographic maps of the Lebanon area. In G. Stampfli, G Borel, W. Cavazza, J. Mosar and P.A. Ziegler, The Paleotectonic Atlas of the Peritethyan Domain: European Geophysical Society CD-ROM.

Walley, C.D. (1998). Some outstanding issues in the geology of Lebanon and their importance in the tectonic evolution of the Levantine region. Tectonophysics, Vol. 298, pp. 37-62.

Warren, N.W. and Latham, G.V. (1970): An experimental study of thermally induced microfracturing and its relation to volcanic seismicity. Journal of Geophysical Research, Vol. 75, pp. 4455-4464.

Wells, D. and Coppersmith, K. (1994). New empirical relationships among magnitude, rupture length, rupture Width, rupture area, and surface displacement. Bulletin of the Seismological Society of America, Vol. 84, No. 4, pp. 974-1002.

Westaway, R. (1994). Present-day kinematics of the Middle East and Eastern Mediterranean. Journal of Geophysical Research, Vol. 99, NO. B6, pp. 12071-12090.

Woessner, J. and Wiemer, S. (2005). Assessing the quality of earthquake catalogues: estimating the magnitude of completeness and its uncertainty. Bulletin of Seismological Society of America, Vol. 95, No. 2, pp. 684-698.

Wyss, M. and Stefansson, R. (2006). Nucleation points of recent mainshocks in southern Iceland, mapped by *b*-values. Bulletin of the Seismological Society of America, Vol. 96, No. 2, pp. 599–608.

Wyss, M., Schorlemmer, D. and Wiemer, S. (2000). Mapping asperities by minima of local recurrence time: San Jacinto-Elsinore fault zones. Journal of Geophysical Research, Vol.105, NO. B4, pp. 7829-7844.

Yamada, N. (1978). Tracing the Atera Fault, central Japan, part 1. From Ena Tunnel to Tsukechi. Geology News, Vol. 283, pp. 37-49.

Yang, W. and Hauksson, Y. (2011).Evidence for vertical partitioning of strike-slip and compressional tectonics from seismicity, focal mechanisms, and stress drops in the east Los Angeles basin area, California. Bulletin of the Seismological Society of America, Vol. 101, No. 3, pp. 964–974.

Yeats, R. S., Sieh, K. and Allen, C. R. (1997).The geology of earthquakes. Oxford University Press.

Zalipin, I. and Ben-Zion, Y. (2013). Earthquake clusters in southern California: Identification and stability. Journal of Geophysical Research. In Review.

Zumoffen, G. (1926). Géologie du Liban. Paris: Barrère.